A PyrOil-GEM Process for Bio-LNG Production

Techno-Economic Process Analysis combining Bio-Oil Gasification, Intermittent Electrolysis of Sea Water, and Sorption-Enhanced Methanation

Laurens G. Braskamp

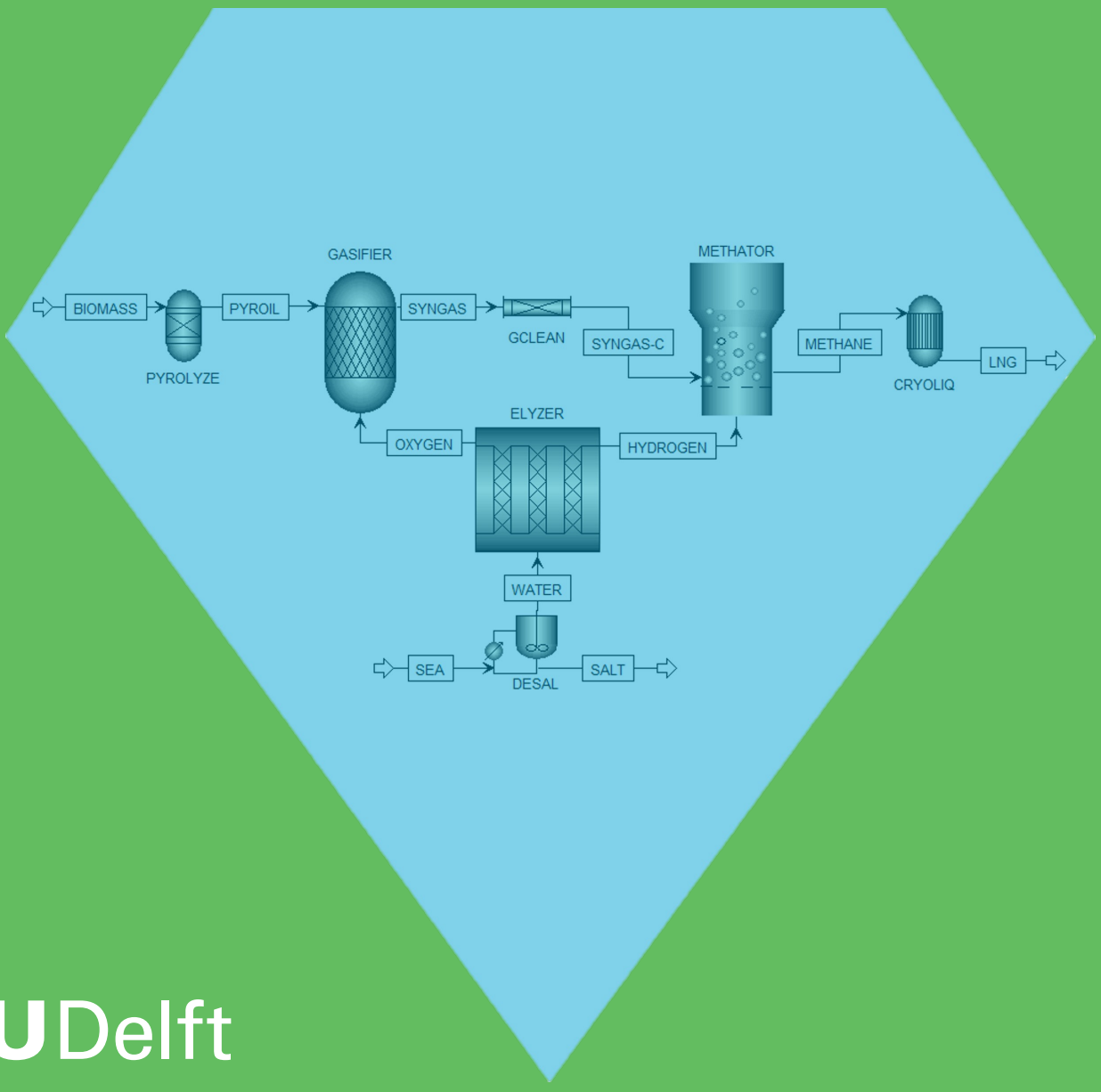

TU Delft

A PyrOil-GEM Process for Bio-LNG Production

Techno-Economic Process Analysis combining Bio-Oil Gasification, Intermittent Electrolysis of Sea Water, and Sorption-Enhanced Methanation

Thesis Report

by

Laurens G. Braskamp

to obtain the degree of Master of Science
in Sustainable Energy Technology
at Delft University of Technology
to be defended publicly on March 24, 2025 at 14:00

Thesis committee:

Chair:	Prof.dr.ir. W. de Jong	ME (P&E)
Supervisors:	Dr.ir. M. Ramdin	ME (P&E)
	Dr.ir. M.d.M. Pérez-Fortes	TPM (E&I)
Place:	Department of Process & Energy	
	Faculty of Mechanical Engineering	
Project Duration:	December 2023 – February 2025	
Student number:	4411064	

An electronic version of this thesis is available at `https://repository.tudelft.nl/`.

Faculty of Mechanical Engineering · Delft University of Technology

Preface

Uit-*erst*-eindelijk.

Voor u ligt het slotakkoord van mijn net iets meer dan een decennium in Delft. Jaren waarin veel is gebeurd. Jaren ook die een met dit verslag afgesloten levensfase vormen.

In het voorjaar van 2020 arriveerde CoVID-19 in Nederland, met lockdowns en enkel online onderwijs tot gevolg. Voor mij was (en nog altijd is) fysiek aanwezig zijn echter een onmisbare voorwaarde voor studievoortgang, dus heeft de coronapandemie alleen mij al zeker een jaar vertraging opgeleverd. In de jaren daarna had ik vervolgens lang niet altijd voldoende vakken overig om een weekrooster mee te vullen. Zodoende was ik pas na tweemaal nominale studieduur toe aan het laatste onderdeel: deze scriptie.

Daarmee was mijn medische malaise nog niet voorbij. Afgelopen zomer vond mij een *amyotrofische neuralgie* in de rechterschouder. Eenmaal onder voldoende pijnstilling was daar allicht nog mee te werken, maar letterlijk alles anders is oneindig veel moeilijker met één arm. Fysiotherapie heeft vervolgens geholpen bij het herstel, maar nam ook maandenlang dagen uit mijn week.

Desalniettemin is dit thesisrapport getuige van een succesvol scriptieonderzoek. Een proefschrift van mijn hand, dat er echter niet zou zijn geweest zonder eenieder die zich in de afgelopen jaren met mij en mijn voorgang hebben bemoeid.

Dankwoord
Het is mij dan ook niet minder dan gepast om mijn erkentelijkheid uit te spreken jegens allen die, om wat voor reden dan ook, onmisbaar zijn geweest in het tot stand komen van deze scriptie. Een aantal wil ik hier bij name noemen.

Allereerst Wiebren, die bijna anderhalf jaar soms vrijwel dagelijks tijd voor mij heeft willen inruimen. Dank tevens voor de vele zijsporen over welke verschillende van onze meetings wisten te zwerven zonder te ontsporen.

Ik dank René van Swaaij, opleidingsdirecteur van SET, voor zijn inspanningen om mij en een thesisproject te koppelen. Dit verslag was er niet geweest zonder zijn connectiviteit.

Ik dank Paula, de studieadviseur, en Marije, mijn ambulant begeleider, voor de moeiten die ik hen heb aangedaan de afgelopen anderhalf jaar, en met hen hun voorgangers – Leonie, Charlotte, Nick, en iedereen bij Jados/Stumass – die zich gedurende dit mijn Delfts decennium hebben bekommerd om mijn studievoortgang. Zonder jullie allemaal weet ik niet of ik ooit op dit punt gekomen zou zijn.

I'd like to acknowledge – in English – the people of the Department of Precision and Microsystems Engineering (PME), Ahmed, Daria, George, Giulio, Hava, Jurga, Ruben, Santiago, Serena, and Stavros, whose office was moved about a year ago now into the room where I had just found an empty workspace, for never making a problem of my presence, and for the conversations we had every now and again.

Verder wil ik al mijn docenten binnen SET bedanken; in het bijzonder Linda Kamp, Ruud van Ommen, en Laura Ramírez, die bovengemiddeld veel te stellen hebben gehad met mijn desorganisatie tijdens en in de nasleep van de coronapandemie.

Bovenal God zij dank, want Hij is goed geweest, en oneindig is Zijn goedertierenheid.

Delft, 11 maart 2025
Laurens G. Braskamp

Abstract

Transitioning the global energy system from finite fossil fuels towards renewable energy resources is probably the most pressing issue of the 21st century. To mitigate the variability in typical sustainable electricity generation technologies, such as solar and wind power, on-demand generation methods are needed, powered by renewable sources such as biomass. As biomass may be converted into conventional types of fuel, methane (CH_4) for example, it could additionally help minimize the financial investment needed to complete the energy transition.

This thesis designs and analyzes a process for making Liquefied Natural Gas (LNG) from Dutch domestic biomass resources, modeled in *Aspen Plus* process simulation software. Specifically, the process design combines gasification of biomass pyrolysis oil, desalination and electrolysis of sea water, and Sorption-Enhanced Methanation, as well as cryogenic liquefaction to produce bio-LNG, a renewable liquid fuel. This bio-LNG may then be used to generate electricity, to fuel heavy road traffic, or whatever application might be found for it.

Based on a 6 kg/s intake of wood pyrolysis oil, nearly 12 t/h LNG can be produced, in addition to useful side products such as sea salt and drinking water. Economic evaluation yields a project NPV of nearly €4 billion, and an IRR of 36.7%. Furthermore, the LCOM of this process is lower than several biomass-to-X processes, at €190/MWh.

Contents

Nomenclature

Abbreviations

AC	Average Cost, M€/y
AE(C)	Alkaline Electrolysis (Cell)
ar	As Received
BCM	Billion Cubic Meters (STP), 10^9 Nm³
BFB	Bubbling Fluidized Bed reactor
BtG	Biomass to Gas often specifically methane
BtL	Biomass to Liquid as MeOH, DME, or FT fuels
BTX	Benzene, C_6H_6, Toluene, C_7H_8, and Xylenes, C_8H_{10}
CAPEX	Capital Expenditure, M€
CCE	Carbon Conversion Efficiency, %
CCS	Carbon Capture and Storage / Sequestration
CCU	Carbon Capture and Utilization
CEPCI	Chemical Engineering Plant Cost Index
CFB	Circulating Fluidized Bed reactor
CFD	Computational Fluid Dynamics
CNG	Compressed Natural Gas
daf	Dried & Ash-Free
DEA	Diethanolamine, $NH(C_2H_4OH)_2$
DIFB	Dual Interconnected Fluidized Beds reactor
DME	Dimethylether, $(CH_3)_2O$
EF	Entrained Flow reactor
EG	Ethylene glycol, $C_2H_4(OH)_2$
ER	Equivalence Ratio, $1/\lambda$, sometimes λ
EY	Energy Yield, %
FB	Fluidized Bed reactor
FC	Fixed Carbon
FICFB	Fast Internally Circulating Fluidized Bed reactor
FT	Fischer-Tropsch synthesis/synthesized
FxB	Fixed Bed reactor
GHG	Greenhouse Gas
HER	Hydrogen Evolution Reaction
HHV	Higher Heating Value, kJ/mol (product water is liquid)
IRR	Internal Rate of Return, %
KPI	Key Performance Indicator
LCOM	Levelized Cost of Manufacturing, €/kg, €/L, or €/MWh
LHV	Lower Heating Value, kJ/mol (product water is gas)
LNG	Liquefied Natural Gas
MD	Membrane Distillation
MDC	Membrane Distillation & Crystallization
MDEA	Methyldiethanolamine, $N(CH_3)(C_2H_4OH)_2$
MEA	Monoethanolamine, $NH_2(C_2H_4OH)$
MeOH	Methanol, CH_3OH
MR	Membrane Reactor
NG	Natural Gas; Methane, CH_4
Nm³	Normal Cubic Meter, gas volume at STP
NPV	Net Present Value, M€
O&M	Operation and Maintenance Cost, M€/y
OER	Oxygen Evolution Reaction
OPEX	Operational Expenditure, M€/y
PEM(EC)	Proton Exchange Membrane (Electrolysis Cell)

PM	Particulate Matter
PtL	Power-to-Liquid
Pyroil	(Biomass) Pyrolysis Oil
RC-MR	Rankine Cycle with Mixed Refrigerant
RES	Renewable Energy Source(s)
RKS	Redlich-Kwong-Soave Equation of State
SBR	Steam-to-Biomass Ratio
SEC	Specific Energy Consumption, kWh/kg H_2
SEM	Sorption-Enhanced Methanation
SNG	Synthetic (or Substitute) Natural Gas
SOE(C)	Solid Oxide Electrolysis (Cell)
STP	Standard Temperature and Pressure, 25°C (293.15 K) & 1 atm
VM	Volatile Matter
WGS	Water Gas Shift (reaction)

Constants

R	Universal Gas Constant 8.314 J/(mol K)

Latin Symbols

A	Area, m²
C_i	Cost estimate for unit i, M€
E^0_{cell}	Electrochemical Cell Potential, V
ΔH_f	Enthalpy of Formation, kJ/mol
ΔH^0_r	Standard Enthalpy of Reaction, kJ/mol
M_i	Atomic or Molecular Mass of i, g/mol
$\dot{m}^j_i$	Mass flow of i in(to) stream or process unit j, kg/h
$\dot{n}_i$	Molar flow of i, mol/h
P	Pressure, bar
P_{El}	Electrical Power, W
q	Heat flow, W
S_i	Size (production or processing capacity) of unit i
T	Temperature, °C
t	Time, s, h, or yr
W	Wobbe index, MJ/m³
y_i	Molar fraction of species i

Greek Symbols

η	Conversion Efficiency, %
λ	Stoichiometric Oxygen Ratio
ρ	Density, kg/m³

List of Figures

List of Tables

1

Introduction

Section 1.1 shortly explores the principal problem human civilization is currently facing, and the threat it poses to energy security. Section 1.2 establishes the framework of research that is being done to investigate potential solutions mitigating the impacts and addressing the causes of this problem. Within this framework, Section 1.3 poses the main research question of this thesis, as well as its constituent subquestions. Section 1.4 finally outlines the structure of this thesis, and discusses the methodology used.

1.1. Climate & Energy

The year 2023 concluded as the hottest and wettest year recorded in the Netherlands since the Royal Dutch Meteorological Institute (KNMI) began measurements in the first decade of the 20th century [1, 2], and the following 2024 then tied its temperature record at 11.8°C [3]; the yearly average temperature measurements are graphed in Figure 1.1. Breaking weather records like these has become a trend in the last years: even on the European record, the three warmest years have all occurred since 2020, and all of the top ten since 2007, according to the 2023 report by EU programme Copernicus and the World Meteorological Organization (WMO) [4, 5].

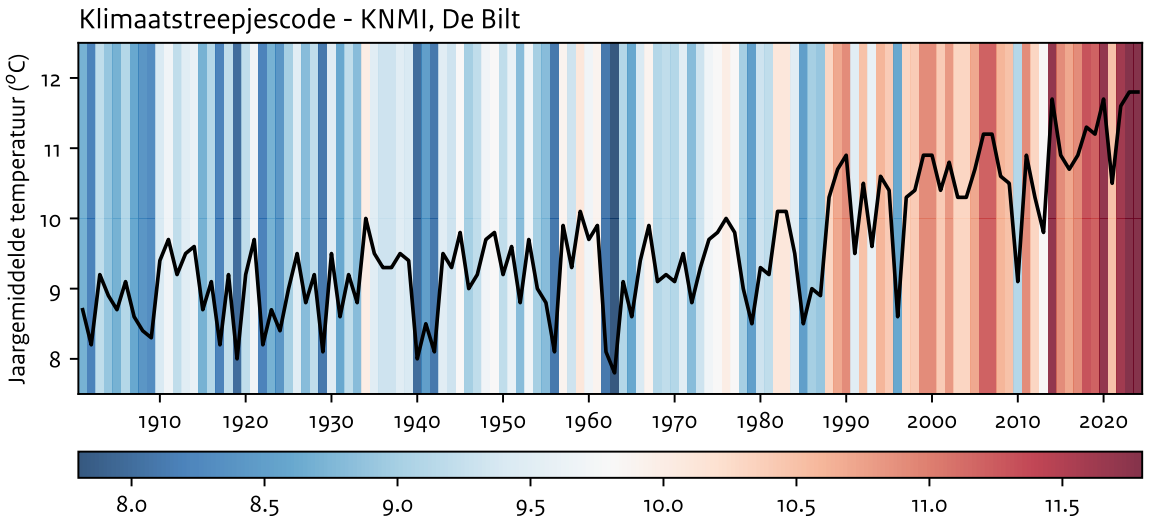

Figure 1.1: Climate Bar Code: Yearly average temperature (°C) in the Netherlands from 1901 – 2024, as measured at the primary KNMI weather station in De Bilt [2, 3].

The primary cause of these climate changes is virtually certainly human activity: greenhouse gas (GHG) emissions resulting from the use of fossil fuel resources, which have been exploited since the Industrial Revolution to satisfy the increasing demand for energy from human behavior [6]. The most important GHGs in these anthropogenic emissions are carbon dioxide (CO_2), methane (CH_4) and nitrous oxide (N_2O).

1.1.1. History of Carboniferous Fuels

Considering their chemical qualities, it is hardly surprising that hydrocarbons and carbohydrates have forever been used as fuels and as energy storage by humanity and nature alike. In comparison with other fuels, as done in Table 1.1, carboniferous chemicals feature generally superior energy densities, with respect to both their weight and to the volume they occupy. The gases, due to the thousandfold lower density of their state of matter, have volumetric energy densities some orders of magnitude smaller, for which they compensate by being easily compressed and pumped through a distribution pipeline network.

Table 1.1: Energy Density comparison of various fuels.

Fuel	Gravimetric Energy Density (MJ/kg)	Volumetric Energy Density (MJ/L)	Ref.
Wood, dry	16.2	6.5 – 9.7	[7]
Coal, bituminous	30.2 – 32.5	33.2 – 58.5	[8]
Oil, crude	44.9	38.7	[7]
Methane, STP	55.5	0.0365	[9]
LNG	49.9	20.5	This work
Gasoline	46.4	34.2	[7]
Diesel	45.6	38.6	[7]
Propane, STP	50.3	0.0250	[9]
Glucose	15.6	23.9	[9]
Ethanol	29.8	22.8	[9]
Hydrogen, STP	141.8	0.0127	[9]
Battery, Li-ion	0.875	2.43	[10]

Having been used on a small scale for centuries, coal was the preferred fuel for the steam engine during the Industrial Revolution halfway the 18th century. Thus, coal became the primary energy resource for trains and ships, as well as for the production of iron and steel. Gasification of coal yielded town gas, which was used in the early 19th century for street lights. When electricity took over energy supply for lighting, coal moved to electricity generation: the first practical coal power station was developed by Thomas Edison, and started providing electricity to New York City households in 1882 [11].

During the 1960s, oil overtook coal as the largest primary energy source [11]. The three fossil fuels have dominated energy supply to this day: in 2022, oil provided 31.6% of primary energy, followed by 26.7% for coal, and 23.5% for natural gas; together amounting to 81.8% of global primary energy [12].

1.1.2. Problems with Fossil Fuels

There are, however, two distinct disadvantages to the use of fossil carbon-based fuels: their impact on the climate and living conditions of the planet, and their limited supply.

As stated before, the primary combustion product of every carbonaceous fuel, carbon dioxide (CO_2), is the main vehicle of human-induced climate change. The use of fossil fuels immediately implies that tons of carbon that laid sequestered in Earth's crust for centuries have now been and are still being released into the atmosphere as GHGs. Those cumulative emissions then cause the rising trend in Figure 1.1, as well as numerous side-effects on the planetary climate, threatening and endangering living conditions and living standards the world over.

Additionally, the amount of fossil fuels available is limited: 2020 estimates in the Statistical Review of Energy indicate that oil and gas reserves will be depleted in about 50 years, and coal in some 140 years [12, 13]. Although the estimated oil and gas reserves have been around 50 years for 40 years now due to technological innovation and new fields being found, these reserves will inadvertently turn out to be finite, and new energy sources need to be developed and integrated as soon as possible to allow for a orderly transition.

1.2. Research Framework

Two things are required to repair the impact that industrialization has made on the planetary climate. Firstly, the causes of climate change should be addressed: the sources of the energy needed cannot have any net CO_2 emissions associated with them – in other words, the energy system must be defossilized. This could be assisted by reducing the overall demand for energy; considering, however, that the world population is still growing and economically developing, global energy demand will likely not decrease in the coming decades.

Secondly, the industrial carbon emissions should be taken out of the atmosphere to undo the damage that still is reversible. The carbon could be sequestered in the biosphere, fixing more carbon in living people, animals and plants, or in rocks, converting oxides to carbonates. It is also possible to store CO_2 in empty gas fields, as in the Porthos project [14, 15, 16]. Technologies for Carbon Capture and Storage (CCS) or Carbon Capture and Utilization (CCU) are beyond the scope of this thesis.

This thesis is concerned with defossilization of the energy system. Such transition only needs to be made once if the finite fossil energy sources are substituted by Renewable Energy Resources (RES). Now, the only energy source that might qualify as inexhaustible on the timescale of life on Earth is the sun; however, directly using light to drive (bio)chemical processes is limited in scope – photosynthesis is the most prominent example. Therefore, the energy needs to be converted into a more usable form, which then can be transported, stored, and used. Consequently, not only direct sunlight is considered a renewable source of energy, so are all its derivatives – natural and artificial. Thus, RES include solar PV, wind, oceanic tides and river flows, as well as the electricity, fuels and heat generated by these resources.

1.2.1. Challenges for Sustainable Energy Systems

Converting the world's current energy system based on fossil sources like coal, oil, and natural gas into a sustainable energy system based on renewable sources like solar and wind is a complex but urgent challenge with technological, economic, and political facets. Among the first techno-economic questions that needs to be addressed in designing a sustainable energy system, is what energy carrier(s) will be used instead of the fossil fuels. Two very different energy carriers that could take over the dominant position of fossil fuels in a sustainable energy system are *electricity* and *hydrogen*.

Both these energy carriers have advantageous and disadvantageous qualities, all of which need to be taken into consideration when designing a concept for a renewable energy system. Specifically, there are two structural inequalities that a RES-powered energy system has to solve: the mismatch between supply and demand in *time*, and the mismatch between supply and demand in *space*.

Energy Storage

Temporal inequality between the supply of and demand for energy occurs on two timescales: short-term (up to several days), and long-term (seasonal). This mismatch in time is addressed by energy *storage*, to which both timescales set different constraints.

Electricity is typically stored in batteries, which are commonly found in portable devices like mobile phones. On those smaller scales, battery storage works perfectly fine; on large scale, however, it has significant problems. Because the energy density of a battery is severely limited (see Table 1.1), batteries for an entire energy system need to be enormous, which results in highly expensive facilities that also need constant cooling.

Hydrogen gas can be absorbed into and diffuse through various common storage container materials, causing mechanical stress and ultimately failure [17]. Two common ways to combat this embrittlement exist: either the gas tank can be coated with or even made of materials that are more resistant to hydrogen embrittlement (aluminium is often used), or the hydrogen can be chemically bound to another material, forming metal hydrides [18], ammonia, or methane.

Energy Transport

Spatial inequality between the supply of and demand for energy is more structural in nature: energy end-use is not necessarily located where the sun shines most of the time or where the wind blows most consistently, nor even where fossil reserves are found. This mismatch in space is addressed by energy *transport*: physically moving energy carriers from generator to user.

For electricity transport, transmission and distribution grids exist in many, even substantially less developed parts of the world. High penetration of mobile phone usage, which implies widespread adoption of rechargeable batteries, necessitates infrastructure that can provide the power to recharge those batteries. Even in wealthy countries, however, the grid currently cannot accommodate the electrification of the entire energy system – it was never designed to do so.

Hydrogen transport has to work around embrittlement, which might necessitate a total renovation of the natural gas grid. Additionally, in order to achieve a reasonable volumetric energy density, it needs to be pressurized further than common hydrocarbon gases.

Infrastructure Investment
In order to facilitate the storage and transport of quantities of sustainable energy sufficient to replace all fossil fuel use, substantial investment is needed in the production, storage, and transport facilities of renewable energy carriers. As alluded to before, the current electricity grid is already inadequate to facilitate full electrification (just for the Netherlands, see [19, 20, 21]), and hydrogen transport requires a complete rebuild of the gas distribution infrastructure.

If, however, an energy carrier could be interjected for which the necessary storage and transport infrastructure already exists, the energy system transformation can be executed more gradually and organically. The sole requirement for such intermediary energy carrier is a net-zero carbon emission over its production and use.

1.2.2. The Case for Biomass

If its acquisition is properly managed, biomass is a fully renewable energy carrier. While growing, biomass fixes carbon by photosynthesis, which, once released by consumption, can be re-sequestered by the next generation of plant life. In addition to serving as a carbon sink, biomass can be used as fuel directly (like firewood), or converted into more energy-dense chemicals, as well as specialty materials.

Biofuel Storage & Transport
Once converted into familiar chemical substances, such as ethanol or methane, storage and transport of biofuels is no different from how their fossil counterparts are handled already. It can be stored in the tanks and vessels that are used now for fossil fuels, and from there be distributed by the same tankers and pipelines. Hence, no separate infrastructure needs to be constructed, no personnel retrained, and no new regulations introduced.

On top of these, as any chemical fuel, production and consumption of biofuels are not affected by the weather. It can thus reliably be called upon whenever it is needed. There are a few RES that similarly can provide power on demand, most notably hydroelectricity; the potential in exploitation of such sources is, however, geographically limited, whereas biomass can grow and be cultivated wherever people live, with only very rare exceptions.

Biofuel Synergy with RES Energy Systems
These qualities offer important advantages upon integration into a renewable energy system. Exactly because biofuels can supply electricity on-demand – unlike solar PV and wind power – they make an excellent complement to solar and wind, stepping in to generate electricity in adverse weather conditions, and just as easily stepping aside when the intermittent sources produce plenty. This synergy stabilizes the electricity grid, providing enhanced energy security to the people connected.

Besides, biomass-derived synthetic fuels in sectors where high energy density is crucial, like mobility. In particular, heavy vehicles and heavy-duty equipment such as trucks, buses, airplanes, cargo ships and emergency service vehicles are not a good fit for electrification, but would run perfectly fine on biodiesel, FT-gasoline, or synthetic methane. So, biofuels could prove crucial for the transport sector of a RES-powered energy system.

1.3. Research Questions

With all aforementioned considerations in mind then, the following Research Question is formulated:

How could a techno-economically feasible production process be designed for Synthetic Natural Gas based on Sorption-Enhanced Methanation of syngas ($H_2/CO/CO_2$) generated by Biomass Pyrolysis Oil gasification and conditioned by sustainable hydrogen from water electrolysis with intermittent supply of renewable electricity in the Netherlands by 2050?

In order to address this question, the following subquestions need to be answered:

1. *Biomass Availability*: How much renewable biomass sourced from the Netherlands can sustainably be used, and in what form should it be supplied?
2. *Methanation*: Why should methane be produced, in what form, and what is the benefit of sorption enhancement (SEM) to do so?
3. *Gasification*: Considering the requirements of the SEM process and the nature of the biomass available, what gasifier should be used, and what product gas cleaning is necessary?
4. *Electrolysis*: What is the benefit of including water electrolysis in this process, and how can it help stabilize a RES-powered electricity grid?
5. *Energy integration*: How much can heat integration improve the efficiencies of both the gasifier-methanator and electrolyzer sub-units? How can the system negotiate electricity intermittency?
6. *Economic analysis*: Would the resulting process design be economically feasible, and if not, under what conditions could it become so?

1.4. Thesis Methodology & Outline

This thesis largely follows the process design approach set out by Douglas, whose decision procedure has the following levels [22]:

1. Selection of *modus operandi*: batch or continous process;
2. Input-Output Structure of the flowsheet;
3. Recycle Structure of the flowsheet, and reactor considerations;
4. Separation System Specification, for
    a. Vapor Recovery System;
    b. Liquid Recovery System;
5. Heat Exchanger Network.

Considering the size of the Dutch energy system, a continuous process is appropriate. The economic analyses that terminate each of the five steps are aggregated in a penultimate chapter.

In order to facilitate comparison with possible alternative biofuel production processes, a number of Key Performance Indicators (KPIs) will be calculated in the final chapters.

The structure of the thesis is then as follows.

Chapter 2 reviews academic literature on the components of the proposed process design: syngas methanators, biomass and bio-oil gasifiers with their necessary gas cleaning, and water electrolyzers. Based on that information, the equipment types to be used are selected.

Chapter 3 establishes a basis of design, and estimates the sizes and qualities of feed, product, and waste streams associated with all process units.

Chapter 4 translates that basis of design into a mathematical process model in *Aspen Plus*, resulting in a mass flow sheet for the proposed facility.

Chapter 5 improves on that flow sheet by optimizing the heat exchanger network, aiming for maximum energy efficiency, and assesses the technical performance indicators of the resulting design.

Chapter 6 analyzes the economic performance indicators of the plant proposal, and tests their sensitivity to their most important parameters.

Chapter 7 finally summarizes the conclusions reached throughout this thesis, and from these makes recommendations for future research and further investigation.

2

Literature Review

This chapter reviews academic literature on the subprocesses of the proposed bio-oil to methane process design, which is sketched in Figure 2.1. Section 2.1 looks into the background and history of, as well as the latest developments in syngas methanation. Section 2.2 then explores the current status of bio-oil gasification, and investigates the necessary gas cleaning. Next, Section 2.3 addresses the reasons and methods for including water electrolysis in the process. Finally, Section 2.4 concludes the literature review with some closing remarks.

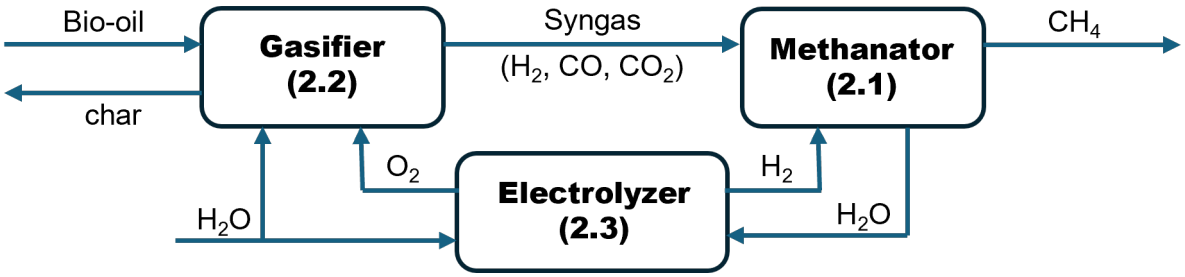

Figure 2.1: "PyrOil-GEM": Bio-oil Gasification and Methanation Process.

2.1. Syngas Methanation

In 1902, Frenchmen Paul Sabatier and Jean-Baptiste Senderens discovered that nickel catalyzes the methanation of CO_x [23, 24]:

$$CO + 3\,H_2 \rightleftharpoons CH_4 + H_2O \qquad \Delta H_r^0 = -206\ \text{kJ/mol} \tag{2.1}$$

$$CO_2 + 4\,H_2 \rightleftharpoons CH_4 + 2\,H_2O \qquad \Delta H_r^0 = -165\ \text{kJ/mol} \tag{2.2}$$

Methanation is performed at temperatures in the range of 520-770 K (about 250 – 500°C), slightly higher than FT synthesis, and at pressures in the range of 20 – 70 bar [25].

Relevant side-reactions are the Water-Gas Shift (WGS, reaction 2.3), which makes up the difference between the Sabatier reactions, and the Boudouard reaction (2.4), which forms solid carbon depositions that can be intermediary species in the methanation reaction, as well as a blockade preventing the catalyst from operating as intended [24]:

$$CO + H_2O \rightleftharpoons CO_2 + H_2 \qquad \Delta H_r^0 = -41\ \text{kJ/mol} \tag{2.3}$$

$$2\,CO \rightleftharpoons C(s) + CO_2 \qquad \Delta H_r^0 = -173\ \text{kJ/mol} \tag{2.4}$$

Methanation was originally employed to remove traces of CO from hydrogen streams in ammonia synthesis plants. After the second World War, the process came to be applied for the production of SNG, often fueled by coal gasification. Over those years, several process designs have been conceived [24].

Recently, separation enhancement began being applied to the methanation process: by removing the coproduct water from the reaction, the equilibrium is shifted towards the products. Thus, better conversion can be achieved under thermodynamically moderate conditions. This manipulation of Le Châtelier's principle can be performed in two ways: by seperation with a membrane, or by sorption [26, 27, 28, 29].

The historical development of methanation technology is reviewed in Section 2.1.1; then, Section 2.1.2 explores the modern developments in Sorption-Enhanced Methanation (SEM).

2.1.1. Methanator History

Historically, coal was the main feedstock for methanation. Two main reactor concepts have been found suitable: either a series of Fixed-Bed reactors with coolers in between and/or recycles, or a Fluidized Bed [24, 25]. Three process designs for coal gasification and methanation that have been conceived in the past century are still in use today: the Lurgi, Topsøe, and Linde processes, all Fixed-Bed designs.

Coal Methanation Technology

Until the 1970s, the Lurgi coal gasification process was the only commercial method to make grid-grade SNG. It contains two adiabatic fixed bed reactors with internal recycle, and runs at an adiabatic temperature of 450°C. After pilot plants in South Africa and Austria, the first and only coal gasification & SNG plant in the world, the Great Plains Synfuels Plant, was commissioned in 1984 in Beulah, ND (US); it has been operated to this day by the Dakota Gasification Company, with 98.7% availability over 20 years [24].

In the 1970s and 80s, Danish engineer Haldor Topsøe invented the TREMP: Topsøe's Recycle Energy-efficient Methanation Process. Its methanator features three adiabatic fixed bed reactors with recycle, in which temperatures range from 250 to 700°C, and pressures up to 30 bar. After thousands of hours of demonstration runs with the '79 and '81 test facilities, the research project of which the TREMP had been part, was terminated. Topsøe's eponymous company does, however, still provide the process today [24].

German company Linde AG developed a methanation process with an adiabatic and an isothermal fixed bed reactor. However, little is known about its performance producing SNG, and the design is nowadays used for MeOH synthesis [24].

Various Fluidized Bed methanators have also been under investigation at several times and places, most notably by the Bureau of Mines (1950s) and the Bi-Gas project (1960s-70s) in the US, and the 1975-86 Comflux process development in Germany [24].

Biomass Methanation Research

In the last decades, SNG production processes, now fueled by biomass, have regained research attention, and new technology has been developed accordingly.

In Alkmaar, the Netherlands, a 4 MW_{th} demonstration plant was planned, based on the MILENA gasifier, OLGA tar remover, and ESME methanation units, all developed from 2002 onwards by the Energy research Centre of the Netherlands (ECN), part of TNO since 2018, and collaborators [24, 30].

The Center for Solar Energy and Hydrogen Research (ZSW) in Stuttgart, Germany is investigating a molten salt cooled multitubular fixed bed methanator with commercial nickel catalyst. It runs on producer gas made by their Absorption-Enhanced gasification/Reforming (AER) dual FB gasifier, which produces a hydrogen-rich biogas by low-temperature gasification [24, 31].

In Güssing, Austria, a 1 MW_{SNG} Process Development Unit (PDU) was built in collaboration with the Swiss Paul Scherrer Institute (PSI) and TU Vienna by their industrial partners. It consists of a Fast Internally Circulating Fluidized Bed (FICFB) gasifier, developed at TU Vienna, and a Comflux FB methanator [24].

2.1.2. Sorption Enhancement

About a decade ago, the Sorption-Enhanced Reaction Process (SERP) [32] started being applied to methanation [26, 27]; thus, Sorption-Enhanced Methanation (SEM) was conceived. A literature overview on SEM is provided in Table 2.1.

Borgschulte *et al.* gave a proof of concept in 2013. They characterized and analyzed a Ni-exchanged zeolite 5A as catalyst and sorbent, and confirmed the CO_2 methanation reaction mechanism [26].

Table 2.1: Overview of Experimental SEM Literature.

Reactor	Catalyst	Sorbent	Func.*	T (°C)	P (bar)	Ref.
FxB	Ni	Zeolite 5A	Bi (exch.)	100 – 230	1.2	[26]
FxB	Ni	Zeolite 4A	Mono	150 – 450	5 – 60	[28]
FxB	Ni & Ru	Zeolites 5A & 13X	Bi (evap.)	240 – 440	1	[33, 34]
FxB	Ni/CeO_2	Zeolite 13X	Bi (evap.)	240 – 400	1	[33, 35]
FxB	Rh	Zeolite 5A	Mono	200 – 300	1	[36]
DIFB	Ni	CaO		250 – 350	1	[37]
FxB	Ni	Zeolite 13X	Bi	300	1	[38]
FxB	$NiAl_2O_3$	Zeolite 3A	Mono	200 – 250	1	[39]

***Note:** Functionality; *i.e.*, are catalyst and sorbent separate, monofunctional particles, or have they been combined (and how) into a bifunctional particle.
Exch. = ion exchanged; evap. = evaporative impregnation.

Walspurger *et al.* demonstrated that SEM enables the synthesis of grid-grade methane at pressures below 10 bar, saving 40% on energy expenses for compression. They achieve full H_2 conversion using a non-specific commercial Ni-based catalyst and zeolite 4A as sorbent, at temperatures between 250 and 350°C [28].

Delmelle *et al.* designed and analyzed Ni/5A and Ni/13X catalyst-sorbent particles for CO_2 methanation. Both catalysts produced pure methane at 300°C; compared to Ni/5A however, Ni/13X demonstrated superior water uptake capacity leading to triple the operating time, which is attributed to its larger pore size (9 Å for Ni/13X, 5 Å for Ni/5A). In addition, Ni/13X showed such improved performance when regenerated under oxidizing atmosphere, which could be used to counteract deactivation by coke or sulfur [40].

Catarina Faria *et al.* computationally investigated the influence of the *in situ* water removal fraction R on the reactor performance, with $R = 0$ for a reference reactor, $0 < R < 0.99$ simulating a membrane reactor (MR), and $R \geq 0.99$ indicating a sorption-enhanced reactor. They find that the optimal value for R, although variable with operation conditions, never exceeds 0.6, because the reaction favors making coke beyond that point [29].
In their final comparison, Catarina Faria *et al.* discuss more details for operating sorption- and membrane-based reactors. In their analysis, a MR allows for continuous operation while an optimized fraction of the water produced is continuously removed. A (fixed-bed, implicitly) sorption reactor meanwhile, they argue, needs to be constructed and operated as a pair: while the one reactor is performing methanation, the other has to be regenerated with inert gas, draining the adsorbed water. As a result, they prefer the MR, even though both its capital and operational costs are higher than those of a SEM reactor [29].

The coking issue is extensively addressed by Massa, Coppola and Scala, who have calculated the limits of carbon deposition for both fixed and fluidized bed methanators. They conclude that the formation of carbon is avoidable if the methanator is provided with excess hydrogen in both fixed and fluidized bed reactors; moreover, that dual fluidized beds are capable of processing stoichiometric feed without coke formation [41].

Coppola *et al.* also introduced the Dual Interconnected Fluidized Beds (DIFB) with chemical looping as a methanator concept, and analyzed its performance with CaO and an attrition-resistant zeolite 3A as sorbents. They find that the sorption capacity of CaO decays with the number of adsorption-desorption cycles, due to it reacting with CO_2, forming calcium carbonate. The zeolite showed a more stable performance, and a significantly weaker tendency to adsorb CO_2 [42, 43].
In a recent modeling study, Coppola and coworkers conclude that CaO sorbent is best used in a hydrogen-lean environment [37], which makes it practically incompatible with the conditions required to prevent the formation of solid carbon.

Wei *et al.* examined the effects of catalyst preparation and composition on the methanation process. First, they synthesized and characterized Ni-impregnated zeolites 5A and 13X from nickel citrate, acetate, and nitrate precursors; they found that the 13X-supported catalysts outperformed the 5A-based ones due

to better precursor penetration into the zeolite structure, and that the citrate precursor gave better catalyst dispersion, resulting in better performance [33, 44].
Then, the introduction of Ru in both zeolites was evaluated, for which 5A and 13X zeolites were loaded with nickel and/or ruthenium in Ni:Ru molar ratios of 1:0, 6.9:1, 1.7:1, and 0:1. Again, the 13X-supported catalysts yielded better results than the 5A catalysts; additionally, no improvement in conversion was made by the presence of ruthenium [33, 34].
Next, the possible promotion by ceria (CeO_2) in Ni/13X was investigated. The composition 5% Ni, 2.5% Ce (Ni:Ce molar ratio equal to 1:0.21) proved very active and highly selective for methane [33, 35].

Bareschino *et al.* have modeled a SEM process with Ni on zeolite 13X as bifunctional catalyst. Among other things, they found axial and radial temperature distributions in excess of 100°C, and identified the reaction rate as limiting [38].

In conclusion, the main challenges that SEM faces – discontinuity from adsorption-desorption cycles, imbalance between water sorption and coke formation, limited scalability, and severe temperature gradients – are essentially all features of the fixed bed reactor.
Fluidized beds, on the other hand, have excellent temperature distribution, scale up well, and, when employing a coupled pair of them (one adsorbing and one desorbing), allow continuous operation: the bed cycle rate controls the water removal fraction, keeping carbon deposition under control [41]. If conditions can be found that minimize catalyst and sorbent attrition – like the unexplained ”attrition-resilient” zeolite of [43] – fluidized beds hold great potential for SEM.

2.1.3. Post-processing

There are three possible post-processing procedures resulting in three different distribution options for end products: the H-gas grid, compression, or liquefaction.

Gas Grid

Over relatively short distances, the existing natural gas grid is the most practical way to export SNG. In 2015, the Wobbe index W of the H-gas grid had to be within the range of 47 – 55.7 MJ/m³ (25/0), when the recommendation was made by DNV GL to narrow that range down to 51 – 55.7 MJ/m³ (25/0); pure methane, for reference, has W = 53.47 MJ/m³ [45].

Compressed Natural Gas

Compressed Natural Gas (CNG), in a pressure range of 200 – 250 bar, is an intermediate solution: for short distances, pipe lines are the superior option; over long distances, LNG offers logistical advantages over CNG. Where, however, no LNG infrastructure (yet) exists, CNG is transported in bulk on carriers.

Liquefied Natural Gas

For long distance traffic and transport, Liquefied Natural Gas (LNG) is the preferred state: because it is a liquid, it has the highest volumetric energy density of all options. To liquefy natural gas, it is cryogenically cooled to a temperature of –162°C at atmospheric pressure, or –120°C at 10 bar.

An additional benefit of liquefaction is purification: any carbon dioxide in the gas stream solidifies around –78°C at ambient pressure; meanwhile, nitrogen (atmospheric boiling point –196°C), hydrogen gas (–253°C) and even carbon monoxide (–192°C) remain in the gas phase.

2.2. Pyrolysis Oil Gasification

Gasification is a thermochemical process that employs heat and a stream of gas, usually air, steam, oxygen, or a combination thereof, to convert a solid or liquid fuel into a combustible gas which is called ’raw syngas’. It has been used since at least the 19th century on carboniferous feedstocks like coal, wood, peat, and later also oil. Only in recent decades, due to growing sustainability concerns, renewable biomass streams such as agricultural, forestry and food wastes, have started to be considered potential feedstocks for gasification [25].

Gasification reactions are subdivided into two subsequent processes. The first step is devolatilization: thermal decomposition of the feedstock, producing char (solids, including carbon), tars (C_nH_m), and permanent gases.

In the second step, these intermediates react further with each other, producing more gases. The most significant of these gasification reactions are [25]:

$$\mathrm{C} + \mathrm{O_2} \rightarrow \mathrm{CO_2} \qquad \Delta H_r^0 = -394\ \mathrm{kJ/mol} \tag{2.5}$$
$$\mathrm{C} + 0.5\,\mathrm{O_2} \rightarrow \mathrm{CO} \qquad \Delta H_r^0 = -111\ \mathrm{kJ/mol} \tag{2.6}$$
$$\mathrm{C} + \mathrm{H_2O} \rightleftharpoons \mathrm{CO} + \mathrm{H_2} \qquad \Delta H_r^0 = 131\ \mathrm{kJ/mol} \tag{2.7}$$
$$\mathrm{C} + \mathrm{CO_2} \rightleftharpoons 2\,\mathrm{CO} \qquad \Delta H_r^0 = 173\ \mathrm{kJ/mol} \tag{2.8}$$
$$\mathrm{C} + 2\,\mathrm{H_2} \rightleftharpoons \mathrm{CH_4} \qquad \Delta H_r^0 = -75\ \mathrm{kJ/mol} \tag{2.9}$$
$$\mathrm{CO} + 0.5\,\mathrm{O_2} \rightleftharpoons \mathrm{CO_2} \qquad \Delta H_r^0 = -283\ \mathrm{kJ/mol} \tag{2.10}$$
$$\mathrm{H_2} + 0.5\,\mathrm{O_2} \rightarrow \mathrm{H_2O} \qquad \Delta H_r^0 = -242\ \mathrm{kJ/mol} \tag{2.11}$$
$$\mathrm{CO} + \mathrm{H_2O} \rightleftharpoons \mathrm{CO_2} + \mathrm{H_2} \qquad \Delta H_r^0 = -41\ \mathrm{kJ/mol} \tag{2.12}$$
$$\mathrm{CH_4} + \mathrm{H_2O} \rightleftharpoons \mathrm{CO} + 3\,\mathrm{H_2} \qquad \Delta H_r^0 = 206\ \mathrm{kJ/mol} \tag{2.13}$$

$$\mathrm{C_nH_m} + \mathrm{n\,H_2O} \rightarrow \mathrm{n\,CO} + (\mathrm{n} + \mathrm{m}/2)\ \mathrm{H_2} \tag{2.14}$$
$$\mathrm{C_nH_m} + \mathrm{n\,CO_2} \rightleftharpoons \mathrm{n\,CO} + \mathrm{m}/2\,\mathrm{H_2} \tag{2.15}$$
$$\mathrm{C_nH_m} \rightleftharpoons \mathrm{n\,C} + \mathrm{m}/2\,\mathrm{H_2} \tag{2.16}$$
$$\mathrm{C_nH_m} + (4\mathrm{n} - \mathrm{m})/2\,\mathrm{H_2} \rightarrow \mathrm{n\,CH_4} \tag{2.17}$$

Considering the often poor energy density of raw biomass, it is energetically wasteful to first collect raw biomass at a central location and only then start converting it into more energy dense forms; a superior strategy would be to preprocess the feedstock decentrally, and take the intermediate to a central, large-scale plant.

Therefore, parallel to suggestions in literature [46, 47, 48, 49, 50], the gasifier-methanator plant under design here will take in pyrolysis oil as feed. This bio-oil can be produced in small batches across the biomass acquisition area, from where it is to be transported in larger quantities to the centrally located, large-scale facility. The design for these small-scale pyrolyzers lies outside the scope of this thesis.

Section 2.2.1 reviews the most commonly found reactor types for the gasification of biomass, and of pyrolysis oil specifically. Then, Section 2.2.2 discusses the needed post-processing of the syngas product.

Table 2.2: Overview of some Biomass Gasification Literature.

Type	Agent	Feed	Feed rate	P (bar)	Ref.
FxB	O_2	Pine & spruce chips, crushed; Forest residues, dried & crushed; Bark, dried & crushed	1 MW_{th}	1	[51]
FxB	O_2/H_2O	Wood, dried; Wood, straw & sewage sludge	1.0 – 1.3 kg/s	1 & 20	[52]
BFB	Air, H_2O/Air	Spruce wood, pellets	3 – 5 kg/h	1	[53, 54, 55]
BFB	H_2O	Wood & wheat straw, pellets	30 kW_{th}	1	[56]
CFB	O_2/H_2O	Pine & spruce pellets	9.1 – 11.3 g/s	2 – 2.5	[57]
CFB	O_2/H_2O	Bark, beech, miscantus, pine, & rice straw, dried	1800 kg/h	1	[58]
DIFB	O_2/H_2O	Lignocellulosic	100 MW_{LHV}	1	[59]
FICFB	H_2O/Air	Wood chips	20 MW_{th}	1	[60, 61]
EF	O_2	unspec., dried, torrified, & ground	unspec.	n.a.	[62]

2.2.1. Gasification Reactors

Various reactor designs have been tried and tested over the years, so that today, there are three main reactor concepts that are considered suitable to use as gasifiers: Fixed Bed, Fluidized Bed, and Entrained Flow reactors [25]. These and their most important variations will be shortly evaluated. A literature overview on gasification of biomass is provided in Table 2.2.

Fixed Bed Gasifiers

Fixed Bed (FxB) gasifiers exist in various designs and sizes up to single-digit MW_{th}. Comparatively, however, their mass and heat transfer characteristics are poor, which make them not feasible for large-scale gasification [25]. Occasionally, they are subject of small-scale gasification studies [51, 52].

Fluidized Bed Gasifiers

Fluidized Bed (FB) gasifiers are found from mid- to large-scale capacities (tens to hundreds MW_{th}), typically operating at temperatures about 700 – 900°C and pressures up to 7 MPa [25]. Three variations are frequently found in biomass gasification literature: the Bubbling Fluidized Bed (BFB), the Circulating Fluidized Bed (CFB), and the Dual Interconnected Fluidized Bed (DIFB). Sketches of a BFB and CFB are shown in Figure 2.2, and an exemplary DIFB is depicted in Figure 2.3.

Bubbling Fluidized Beds (BFBs) derived their identifier from the bubbles the fluidizing gas forms in the dense bed zone, with typical gas velocities ranging from 0.5 – 2 m/s. Carbon conversion efficiencies of well over 90% can be achieved [25, 53, 54, 55].
Bareschino *et al.* operated a catalytic BFB from previous works in their group [54, 55] on commercial spruce wood pallets to investigate, among other things, the potential benefits of including steam in the gasification agent. They found that the inclusion of steam does indeed improve the H_2/C ratio, which in turn lowers the demand for additional hydrogen in syngas conditioning for the methanator [53].

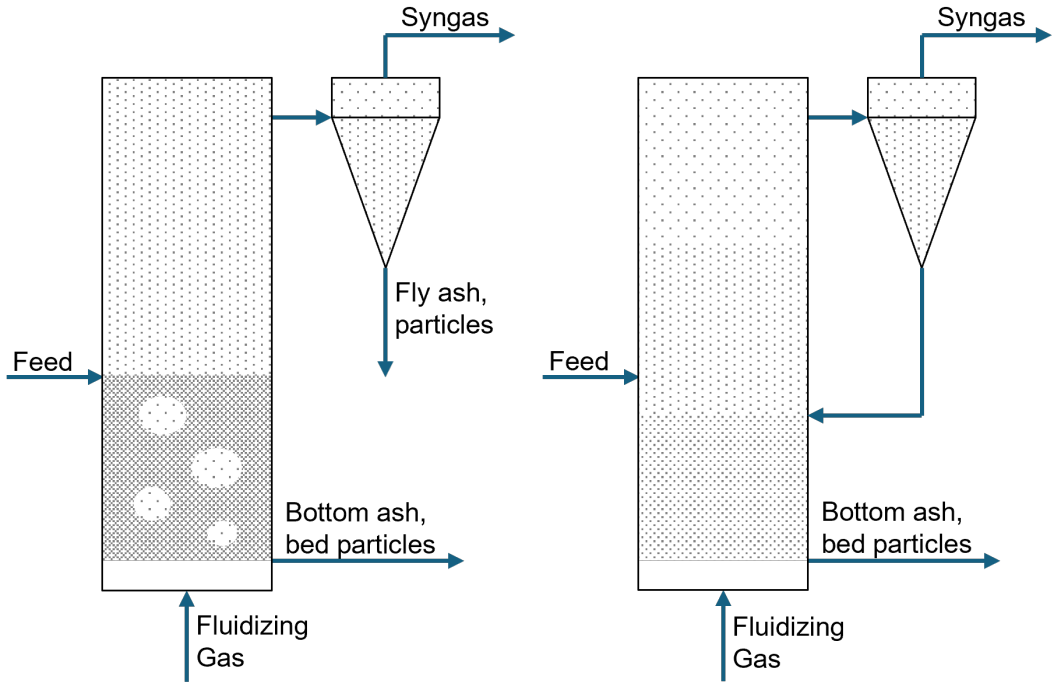

Figure 2.2: Sketches of BFB (left) and CFB (right) gasifiers with cyclones.

Circulating Fluidized Beds (CFBs) are similar to BFBs, but feature higher fluidizing gas velocities. Consequently, bed particles get entrained in the gas flow, and need to be separated by a cyclone and returned to the bed. Due to this recycling of bed materials, CFBs typically achieve carbon conversion efficiencies in excess of 95%, and their product gas has a significant dust content [25, 58].
Giglio *et al.* modeled a CFB in their process integration study, following suggestions in literature [24, 63, 64] that CFBs are suitable for large-scale application in synthetic fuel production. They fed it bark,

beech, miscanthus, pine, and rice straw at temperatures between 780 and 850°C, finding similar product gas compositions for the four woody biomasses, and near-equal amounts of CO and H_2O from the rice straw [58].

Dual Interconnected Fluidized Bed (DIFB) gasifiers consist of two fluidized beds: one is a gasifier, and the other functions as char combustor, generating the heat for the gasifier [25, 59, 65]. An evolution from this concept is the aforementioned Fast Internally Circulating Fluidized Bed (FICFB), developed at TU Vienna. Currently, one is being employed in their semi-commercial PDU in Güssing [24, 60, 61].

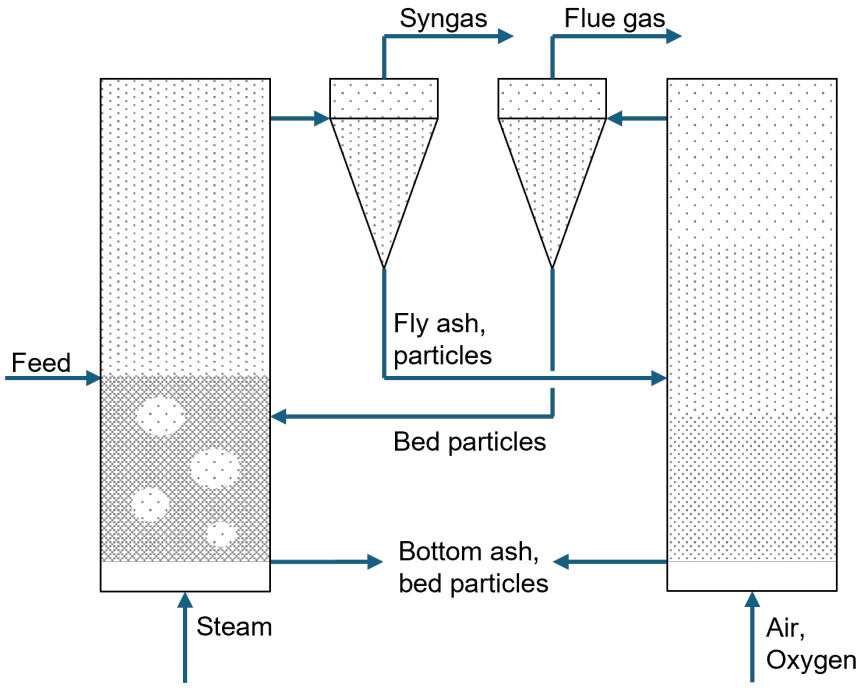

Figure 2.3: Sketch of a DIFB gasifier with cyclones; featuring a BFB gasifier (left) and a CFB char combustor (right).

For bio-oil gasification, however, fluidized beds are not as common [46]. Latifi *et al.* have experimented with an interesting novel design, the Jiggle Bed Reactor (JBR), a batch setup of µL size [66]. Ghezelchi and Wu performed extensive CFD calculations on a more conventional fluidized bed gasifier [67].

Recently, Cortazar *et al.* employed a Conical Spouted Bed (CSB) reactor to study pyrolysis oil gasification between 800 and 900°C. With increasing temperature, they achieved a 70% reduction in tar yields, an improvement in carbon conversion efficiency to 96.3%, and an increase in gas yield [49]. A short literature overview of pyrolysis oil gasification is given in Table 2.3.

Table 2.3: Overview of Pyrolysis Oil Gasification Literature.

Type	Agent	Feed (source)	Feed rate	P (bar)	Ref.
JBR*	Air	Pyroil (hardwood & birch)	4 µL batch	1	[66]
FB	Air, H_2O	Pyroil (*comp.*)	0.16 – 0.25 kg/h	1	[67]
CSB*	H_2O	Pyroil (pine wood)	0.75 g/min	1	[49]
EF	H_2O/Air	Pyroil (rice husks)	9 kg/h	1	[68]
EF	O_2/Air	EG & EG with char	12.5 kg/h	1	[48]
EF	O_2	Pyroil (pine wood & wheat straw)	80 kg/h	40	[69]
EF	Air	Pyroil (pine wood)	1000 kg/h	1	[50]

*__JBR__: Jiggle Bed Reactor; __CSB__: Conical Spouted Bed reactor.

Entrained Flow Gasifiers

Entrained Flow (EF) gasifiers have been specifically designed for large-scale application (tens to several hundreds MW_{th}) at high temperatures (about 1200 – 1500°C). They are capable of converting a range of fuels, fluid or solid – although the latter needs to be fed as finely ground powder or as slurry [25].

Due to their relatively strict feedstock size requirements, EF gasifiers are rarely found processing solid biomass, like the simulation study by Bernical *et al.*[62]; on the other hand, literature on EF gasification of pyrolysis oil, which can be sprayed in droplets of any size, is not uncommon [46, 48, 50, 68, 69]. A graphical representation of an EF gasifier is shown in Figure 2.4.

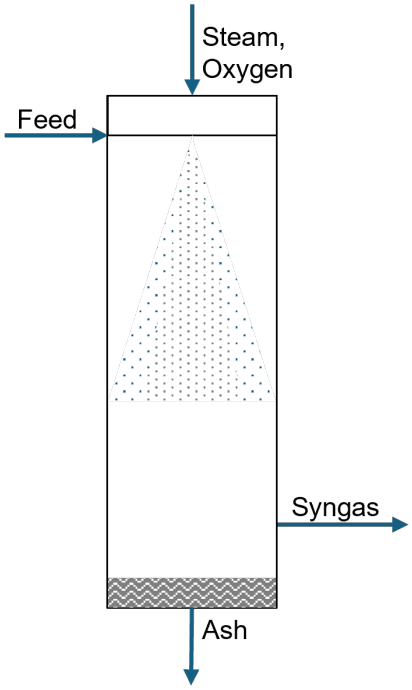

Figure 2.4: Sketch of a EF gasifier.

Leijenhorst *et al.* tested the feedstock flexibility of the Pressurized Entrained flow Biomass Gasifier (PEBG) at the Energy Technology Center (ETC) in Piteå, Sweden. To that end, they prepared pyrolysis oils from two different sources, namely pine wood and wheat straw; a water phase was evaporated from the oils to obtain a more homogeneous product. Both oils were gasified at 4 bar and about 1250°C, yielding syngas of similar quality, but a substantial sulfur content was found in the straw-derived oil [69].

Zheng *et al.* investigated the potential benefits of including steam in the gasifying agent. Their results agreed with Bareschino *et al.* [53] that the inclusion of steam improves the H_2/CO ratio. They also measured only minute quantities of tar in the product gas (which is consistent with EF gasifiers), and noticed significant amounts of N_2 and CO_2, which they recommend to be removed before hydrogenation [68]. Now, nitrogen gas should be nearly absent unless air (80% N_2) is used in the gasifier, and CO_2 is still useful for methanation (Eq. 2.2).

Fradet *et al.* investigated gasification of a slurry of biochar and ethylene glycol (EG) as surrogate pyrolysis oil, developing a CFD model that proved in good agreement with experimental results. Additionally, they listed three major reasons for preferring EF gasification over FB and FxB technologies [48]:

1. *Feedstock flexibility*: In addition to being indifferent to the physical form of the fuel, as mentioned above, a fuel HHV of a mere 10 MJ/kg suffices for EFs;
2. *Throughput capacity*: When EFs are pressurized to about 50 bar, conversion times are short, and reactors remain compact, yet reaching capacities over a GW_{th};
3. *Output quality*: The raw syngas from an EF gasifier is virtually tar-free, so less exit gas cleaning is required, and carbon conversion is almost complete (>99%).

Buelvas *et al.* performed energy and exergy analyses on a computational comparison between direct gasification of biomass and indirect gasification of pyrolysis oil from that same biomass. At 1000°C and ER = 0.4, they find direct gasification more efficient: 62% against 53% energy efficiency, and 65% versus 61% exergy efficiency. Yet they recognize that the indirect process offers ”crucial logistic advantages” [50]. As noted in Section 2.2, these logistic benefits are exactly the reasoning behind the design philosophy of decentralized pyrolysis – which produces a feedstock with increased energy density, and thus decreased transport volume – followed by large, central gasification and methanation, taking maximum advantage of economies of scale [46, 47, 48, 49, 50].

A comprehensive comparison of advantages and drawbacks of the different large-scale gasification reactors is provided in Table 2.4.

Table 2.4: Comparison of Large-scale Gasification Reactor Technology. Adapted from [25, Table 10.5] for liquid bio-oil feed.

	BFB	CFB	DIFB	EF
Advantages	High volumetric capacity	Easy scale-up	Temparature distribution	Very high capacity
	Temperature distribution	Medium operating temperature (about 850°C)	Oxygen not required	Very low tar and CO_2
				Exit gas temperature
Disadvantages	Limited operating temperature due to ash melting	Corrosion and attrition problems	More tar due to lower bed temperature	Complex operational control
	High tar and fine-particle content in gas	Potential for agglomeration	Difficult to operate under pressure	Higher exergy loss
	Possibility of high-C content in fly-ash	High dust content in product gas	Limited scalability	

2.2.2. Product Gas Cleaning

The raw syngas that exits the gasifier, is not yet suitable for use in methanation; it needs to be cleaned to remove pollutants and impurities. Which contaminants are present and in what quantities, is highly dependent on the gasifier type and conditions; the main categories are [70, 71, 72]:

- *Particulate matter* (PM) like dust, bed particles, entrained char, and other solids. Because of the abrasion that PM can cause on every single piece of equipment in the process, like turbines, compressors, and synthesis catalysts, it is imperative to virtually eliminate all PM from the gasifier exit stream before any other cleaning, conditioning, or synthesis process;
- *Tars*, condensable hydrocarbons with molecular weights higher than benzene (C_6H_6), sometimes including, but generally excluding BTX (benzene, toluene, and the three xylenes). Tar will condense downstream, plugging and fouling pipes and other equipment, so any tar that has formed in the gasifier needs to be dealt with before the temperature drops below about 400°C;
- *Sulfur species*, most commonly compounds like H_2S, SO_2 and COS, which are catalyst poisons;
- *Chlorine compounds*, usually present as HCl or alkali salts, that poison catalysts and corrode equipment;
- *Bound Nitrogen species*, primarily ammonia (NH_3) but HCN too, which are also poisonous to nickel catalysts;
- *Alkali elements*, primarily sodium and potassium salts, the condensing vapors of which block gas nozzles, cause fouling on turbine blades, and agglomerate fluidized bed particles.

There are two process sequences for gas cleaning: the more conventional *Cold gas cleaning*, which is subdivided in wet and dry cleaning methods, depending on whether or not liquids are involved; and the more energy-efficient *Hot gas cleaning*, which primarily consists of thermal and catalytic treatments [70, 71, 72].

It is desirable to arrange the gas cleaning processes in descending order of temperature wherever possible, to prevent wasting energy on repetitive cooling and heating cycles. As a result, the exact order in which the pollutant categories mentioned above are addressed, differs between the high- and low-temperature pathways [70].

Cold Gas Cleaning
Cyclones are particularly excellent at removing coarse particles from a gas flow, because they employ centrifugal and gravitational forces to separate by mass. Cyclones can be used at high temperatures (up to 900°C [71]), but are most common in middle- and low-temperature processes to protect their structural integrity [70, 71, 72].

The most common tar remover is a scrubber, which dissolves the tar in water or an organic solvent, simultaneously catching the finest particles that came through the cyclone. Water scrubbers are also suitable to remove contaminant gases like NH_3, HCl, H_2S and SO_2, because all these gases are highly soluble in water [70, 71, 72]. At slightly higher temperatures (300 – 100°C), occasionally deemed warm gas cleaning, sits the OLGA oil gas scrubber for tar removal from ECN/TNO [30, 70, 71, 72].

Amine scrubbers or packed beds, using solvents like MEA, DEA or MDEA, are well-suited for the capture of acidic gases, H_2S and CO_2 in particular. COS has to be hydrogenated to H_2S first, because it degrades the solvent. Another option for H_2S removal is an activated carbon and ZnO filter, with nitrogen and chloride compounds being removed thereafter by a water scrubber [70, 71, 72].

Alkali metals primarily exist in water-soluble salts in most biomasses; hence, a water wash or acid leach is sufficient to remove them from the syngas. [70, 71, 72]

Hot Gas Cleaning
Filtration is a more common choice than cyclones for particle removal at high temperatures. For hot gas cleaning, ceramic or metallic filters are applied, preferably in the form of *candles*, long tubes (1 – 3 m long, 60 – 150 mm across) that are closed at one end, hanging in the freeboard of the gasifier or in their own vessel. It is also possible to equip these candles with catalytic elements, so that for example catalytic reforming can take place on the filter [73]. Near perfect particle filtration has been demonstrated at temperatures of 800 – 900°C [73, 74, 75, 76, 77].

For tar, dolomite, olivine, iron oxides and nickel are all proven catalysts for cracking and reforming, improving the carbon conversion to syngas. Zeolites and nickel, especially when supported by MnO_3 and Al_2O_3, can revert ammonia into inert N_2 and H_2 around 800 – 850°C. [70, 71, 72]

When the sulfur, chlorine, and alkali compounds will react with filtration materials, adsorption-regeneration couples of FxB reactors are needed to continuously remove them from the syngas stream. At 900°C, alkali chlorides react with aluminosilicates such as bauxite, kaolinite and natural zeolite, releasing HCl. This process is, however, irreversible; therefore, unless a compelling use-case for the resulting rock exists, this pathway is little desirable [70, 78].

In the presence of nickel or zinc oxide, COS will readily be hydrogenated to H_2S in a hydrogen-rich environment [79]; subsequently, H_2S reacts with ZnO in the 400 – 600°C range, producing ZnS and water [80, 81, 82, 83]. ZnO can be regenerated from ZnS under steam or oxygen atmosphere at temperatures between 548 and 609°C, and the resulting hydrogen sulfide or sulfur dioxide could be used externally in the production of sulfuric acid or gypsum [84].

Kurkela *et al.* performed a 215 hour test of a pressurized CFB gasifier and hot gas filter. They report excellent filtration of Na, K, and Cl on ceramic filter candles at temperatures of 530–560°C [57, 70].

Chlorine sorption in the 350 – 600°C range was computationally investigated by Stemmler and Müller. They conclude that $NaHCO_3$ is a suitable chloride sorbent below 550°C, and K_2CO_3 below 600°C [70, 78].

2.3. Water Electrolysis

Electrolysis, which means 'decomposition by electricity', became the primary synthesis process for hydrogen gas from water by the end of the 19th century, supplying the ammonia and fertilizer industries. In the first half of the 20th century, however, more cost-competitive hydrogen production processes, namely coal gasification and steam methane reforming, forced electrolysis into niche applications [85]. Today, moving away from the use of such fossil resources, electrolysis is once again the preferred method for producing hydrogen.

The motivation for including water electrolysis in a BtG process design is discussed in Section 2.3.1, and the current state of technology is reviewed in Section 2.3.2. Then, Section 2.3.3 will introduce two multifunctional electrolyzer concepts.

2.3.1. Added Value of Water Electrolysis

Recent publications about research on BtG [51, 52, 53, 58, 63, 86] and biomass-to-liquid (BtL) [62, 87] processes include electrolysis of water or steam in their designs, or mention the addition of hydrogen gas as an improvement [65]. The primary reason is the needed increase of the hydrogen/carbon balance.

Whereas most desired products are hydrogen-rich (for example, methane and MeOH feature H_2/C ratios of 2, DME has 1.5), biomass is comparatively poor in hydrogen content (often with $H_2/C < 1$), and its oxygen and nitrogen contents also consume hydrogen to form water and ammonia. This implicates that the availability of hydrogen is a limiting factor in fuel synthesis reactions, carbon conversion efficiencies are thus low, and solid carbon may form and inhibit the catalyst from functioning (coking). There are three non-exclusive approaches to solve these problems.

The Water Gas Shift (WGS) equilibrium reaction (Eq. 2.3) is a common syngas conditioning reaction, which can convert the water formed in the gasifier into hydrogen gas [62, 53, 58]. However, because the H_2/C ratio of biomass is significantly suboptimal, the WGS reaction alone can never supply all the hydrogen needed for full carbon conversion [53].

It is possible to produce a hydrogen-richer syngas by including steam in the gasification process. Bareschino *et al.* find that this results in a decreased demand for additional hydrogen gas, as well as an increase in carbon conversion efficiency [53].

The most recent method to improve the H_2/C ratio is supplying the clean syngas with additional hydrogen gas, and electrolysis is the most sustainable way to synthesize the hydrogen gas required [51, 52, 53, 58, 62, 63, 86, 87]. Adding hydrogen in this stage also nullifies the need for the WGS [53].

The other product of water electrolysis is oxygen. It is safe to release this into the environment; however, many of the studies that include electrolysis for hydrogen recognize that this stream, including its potential heat and pressure, can be used in the gasification unit [51, 52, 58, 62, 63, 86, 87]. This is economically more beneficial than cryogenically separating the oxygen from air, and technologically more desirable than gasification with air (see Section 2.2.1 on [68]).

2.3.2. Electrolysis Technology

Electrolyzers are typically classified by electrolyte into three categories: alkaline, acidic, and solid oxide [85]. These will be shortly characterized; a summary of their development statuses is provided in Table 2.5.

Table 2.5: Development Status (2016) and process parameters of Electrolysis Technologies [85].

Technology		Status	T (°C)	P (bar)	SEC (kWh/kg H_2)
Alkaline	Large-scale	Commercial	70 – 90	1 – 25	48 – 60
	High-pressure	Commercial	70 – 90	< 690	56 – 60
	Advanced	Pre-commercial	80 – 140	< 120	42 – 48
Acidic	PEM	Commercial	25 – 80*	< 400	40 – 60
Solid Oxide		Prototype	900 – 1000	< 30	28 – 39

***Note:** Original table read 80-150°C, but these values are mentioned in the text. Compare [52], whose PEM operates between 50 and 70°C.

Alkaline Electrolysis
Alkaline Electrolysis Cells (AECs) utilize an alkali hydroxyl-carrier as electrolyte; the most common being NaOH and KOH solutions. AE half-reactions are as follows:

$$\begin{aligned} 2\,H_2O + 2\,e^- &\rightarrow H_2(g) + 2\,OH^- \\ 2\,OH^- &\rightarrow H_2O + 0.5\,O_2(g) + 2\,e^- \end{aligned} \tag{2.18}$$

As a catalyst, a flat plane of carbon steel-coated with nickel is typical, while Co, Pt (both electrodes), Fe, Zn, Pb, Pd, Au (cathode), Ir, Ru, Rh, and TiO_2 (anode) are also in use. The simple geometry and not necessarily expensive materials make that AECs can be easily and cost-effectively scaled [85].

In literature, Bernical *et al.* compared H_2/CO ratio adjustment for FTS by WGS, AE and High-Temperature Steam Electrolysis – which, considering the temperatures involved being 1000–1200 K (727–927°C), must involve a SOEC. Both electrolysis technologies reached equivalent carbon conversion efficiency (61%), but AE is found inferior to HTSE in both secondary and equivalent primary energy conversion efficiency [62].

Clausen *et al.* prefered using an AEC because both PEM and SOEC were then (2010) still in development and might take years to economically compete with AECs on large scale; yet they conceded that both newer technologies had already achieved higher efficiencies [87].

Acidic Electrolysis
Acidic Electrolysis mobilizes protons as charge carriers in the electrolyte. Its half-reactions are

$$\begin{aligned} 2\,H^+ + 2\,e^- &\rightarrow H_2(g) \\ H_2O &\rightarrow 2\,H^+ + 0.5\,O_2(g) + 2\,e^- \end{aligned} \tag{2.19}$$

The only mature technology on this principle uses a Proton Exchange Membrane (PEM) as electrolyte, the most well-known of which is Nafion. PEMECs also need to use platinum group metals for their electrodes because of the highly acidic environment; Pt itself as well as Ru and Ir oxides are used [85].

In recent publications, Bareschino *et al.* modeled a PEM stack without much discussion [53]. Anghilante *et al.* compared the performance of a PEMEC to a SOEC in a gasification process, finding that SOECs achieve a process efficiency over 15 percentage points higher than PEMECs, due to the SOEC being fed steam recovered from the methanation unit. Specifically, based on the HHV of the end products, for the production of SNG they achieved plant efficiencies of 81.9% with SOEC versus 64.9% with PEM; for CNG production (250 bar), 81.0% using a SOEC against 64.4% using a PEM [52].

Solid Oxide Electrolysis
Solid Oxide Electrolysis Cells (SOECs) operate at significantly elevated temperatures and use a non-porous solid metal oxide as electrolyte, that conducts oxide anions (O^{2-}). SOE features the half-reactions

$$\begin{aligned} H_2O + 2\,e^- &\rightarrow H_2(g) + O^{2-} \\ 2\,O^{2-} &\rightarrow O_2(g) + 4\,e^- \end{aligned} \tag{2.20}$$

Because of the temperature and acidity requirements, SOEC electrodes are made from highly specialized materials. The cathode is composed of porous yttrium-stabilized zirconia (YSZ) doped with nickel and/or cerium, and the anode is constructed from lanthanum and manganese oxides doped with strontium (LMS), $La_{0.8}MnO_3Sr_{0.2}$ [85].

The majority of the recent research opted for SOECs [51, 52, 58, 62, 86], which is technologically justifiable; SOECs feature higher efficiencies than AECs [62, 87], superior heat integration to PEMs [52], and lower specific energy cost for hydrogen production than both (Table 2.5 [85]).

2.3.3. Multifunctional Electrolyzer Concepts

In the last couple of years, several innovative multifunctional concepts to utilize electrolyzers have been conceived. Two will be highlighted here: the integrated battery-electrolyzer ('Battolyser') developed at TU Delft, and a desalinator-electrolyzer for salt water electrolysis ('SeaHydrogen') proposed by Wageningen University.

Battolyser
It has been a well-known flaw of Ni–Fe batteries that, when overcharged, they produce an explosive mixture of hydrogen and oxygen gas. Within the Battolyser, however, this electrolysis process is no longer a bug, but has been made a feature.

Combining the requirements for both a Ni–Fe battery and an alkaline electrolyzer, which were already composed of the same functional materials, the Battolyser will operate as electricity storage when charged,

$$\begin{aligned} \mathrm{Fe(OH)_2} + 2\,\mathrm{e^-} &\rightleftharpoons \mathrm{Fe} + 2\,\mathrm{OH^-} \\ \mathrm{Ni(OH)_2} + \mathrm{OH^-} &\rightleftharpoons \mathrm{NiOOH} + \mathrm{H_2O} + \mathrm{e^-} \end{aligned} \tag{2.21}$$

until, nearing full charge, fuel production for long-term storage begins by alkaline electrolysis (Eq. 2.18), with the produced Fe catalyzing the hydrogen evolution reaction (HER), and NiOOH the oxygen evolution reaction (OER). Additionally, the device has proven to be thermodynamically stable, flexible switching between operating modes, and highly energy efficient (80–90%) while maintaining a high utilization [88].

In 2018, the company *Battolyser Systems* was incorporated to commercialize the technology [89]. In October 2023, it reached a €40 million financing deal with the European Investment Bank (EIB) to scale up its production facilities in Rotterdam [90], and the first systems are planned for delivery this year.

SeaHydrogen
Concerned with the growing pressure on limited drinking water resources by population, agriculture, and electrolysis for clean fuel, a recent report from Wageningen University & Research (WUR) proposes a novel approach to use overly abundant sea water for hydrogen production: *ZeeWaterstof*, a contraction of *zeewater* (sea water) and *waterstof* (hydrogen).

The idea of this 'SeaHydrogen' concept, as illustrated in Figure 2.5, is valorizing the waste heat from electrolysis to run a membrane distillation device, which in turn produces the desalinated water from which the electrolyzer synthesizes hydrogen. Excess water is fit for consumption and other uses, leftover waste heat could further be used to recover minerals (primarily salt, NaCl) from the sea water, and eventually to produce electricity [91].

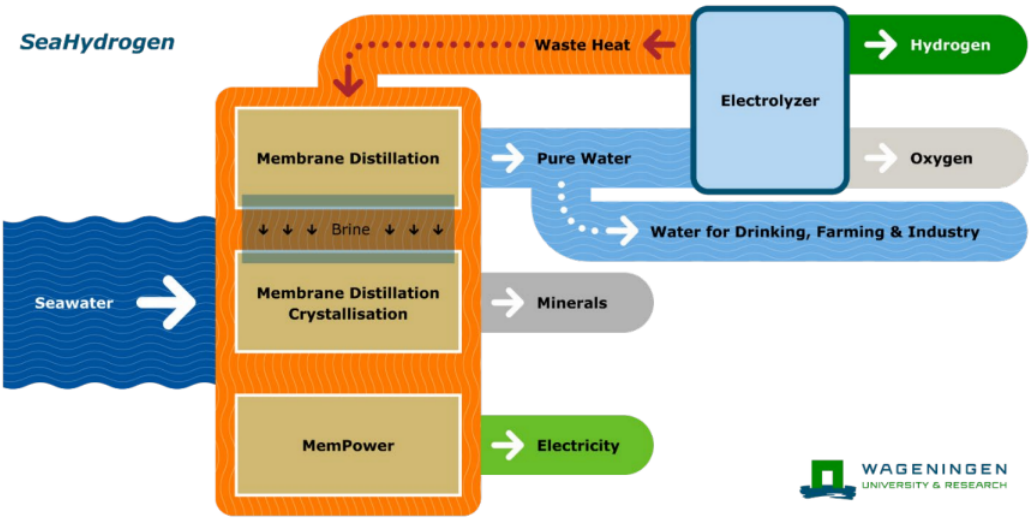

Figure 2.5: Schematic of the SeaHydrogen proposal [91].

A 50 kW pilot has demonstrated the first step in October and November 2021 on the island of Texel: it operated about 1,000 hours, producing a kilogram of hydrogen per hour using a PEMEC, and three times the amount of ultra-pure water (UPW) required for the electrolyzer [91].

2.4. Conclusion

From this review, a couple of conclusions can be drawn that impact the set-up of the process design; based on which, the process units to be used were selected.

Electricity Intermittency
Firstly, in order to negotiate the intermittency of primary renewable energy sources (solar and wind), the electrolyzer needs to be decoupled from the gasifier and methanator. This results in two subsystems: a gasification-methanation subprocess which operates continuously, and an electrolysis subprocess that is allowed intermittent operation to take maximum advantage of electricity supply peaks. This division also implicates the necessity of a storage buffer for all material flows between both subunits: hydrogen and oxygen gases, as well as recovered water.

Alternatively, as Pozzo *et al.* indicated, nuclear power could be used as a carbon-neutral continuous electricity source [51]. There is ongoing discussion in the Netherlands whether or not to add one or even several nuclear power generator(s); however, public opinion on nuclear power is quite fickle, which makes it impossible to reliably assess if additional nuclear energy facilities will be present by 2050, or not. Off-shore wind turbines on the North Sea are significantly less controversial, although even those cause some people worries about their impact on marine life.

Heat Integration
Secondarily, heat recovery and reuse is likely to significantly impact the energy efficiency of both the subprocesses and of the plant as a whole. In order to prevent the storage facilities for the intermittently produced gases from dissipating potentially useful heat, that energy needs to be recovered first, for example by generating steam, before they can be stored; similarly, heat recovered throughout the gasifier-methanator subunit could preheat those same gases before use in the subprocess.

2.4.1. Process Units Selection

Having considered all options that emerged from the academic literature review with all their advantages and drawbacks, the following technologies were selected to feature in the process design.

The **Entrained Flow Gasifier** was chosen to perform gasification on the bio-pyroil, because of its qualitative advantages and proven compatibility with pyrolysis oil feed. Considering its high exit gas temperature, a **Hot Gas Cleaning** strategy will subsequently be applied.

A **Dual Interconnected Fluidized Beds Methanator** shall be designed to harness the benefits that FBs can bring to methanation. After that, **Liquefaction** was selected as the preferred post-processing strategy despite the higher associated energy cost (and thus lower process efficiency) as compared to the other options [52]; the logistical benefits of having all necessary infrastructure for storage and grid-injection of LNG next-door is deemed decisive. A portion of the produced LNG will be reserved for own trucks, offsetting the climate impact of company logistics.

Because the electrolysis unit will have to negotiate an intermittent electricity supply, neither a SOEC [51] nor a PEMEC [92, 93] can guarantee long-term stability. In contrast, an **Alkaline Electrolyzer** has little problems handling such conditions. In fact, as discussed in Section 2.3.3, a **Battolyzer** is even capable of smoothing out the power supply intermittency by discharging the battery when supply is low, and recharging during supply peaks.
Within the context of this thesis, this possibility will remain theoretical; however, trading electricity between supply peaks and demand peaks is a possible future expansion of facility functionality.

Additionally, in order not to negatively impact the drinking water availability, the electrolyzer rest heat will be used to desalinate sea water conform the **SeaHydrogen** concept. Given that the operation temperature of an AEC is similar or slightly higher than that of a PEM as used in the original paper [91], the electrolysis unit should have sufficient heat available to drive the desalination.

3

Basis of Design

From the knowledge and data acquired in the literature review, this chapter formulates a design basis for the multifunctional biorefinery. Section 3.1 addresses the location where the facility is to be built. Section 3.2 then explores how much renewable biomass feedstock may be available for pyrolysis within reasonable distance from the facility's location, and how it should be transported to it. Section 3.3 discusses the gasifier, scaled for the amount of pyrolysis oil available, and the necessary gas cleaning steps. Section 3.4 subsequently designs the methanator with its dehydration bed. Finally, Section 3.6 sizes the electrolyzer to supply the hydrogen needed to maximize carbon conversion to methane.

3.1. Location for Facilities

In the Netherlands, there is likely no better place to build up a bio-based business than the Port of Rotterdam. It already features an extensive (petro-)chemical industry cluster and accompanying infrastructure, as well as the largest renewable industry cluster in the world. Also, Rotterdam is a European biofuel hub, and aims to be Europe's hydrogen hub too [15].

Additionally, considering the infrastructure that is already in place, from roads and highways, railways, and inland waterways to pipelines for platform chemicals and the electricity and heat grids, resource and product logistics will require little additional investment for stable operation.

3.2. Sourcing Biomass

Biomass acquisition for pyrolysis and gasification will be spatially limited to the Netherlands. This should allow sufficient supervision to ensure sustainable harvest and collection.

Section 3.2.1 assesses the availability of the most important sources of biomass in the Netherlands, and selects which will be used in the context of this thesis. Section 3.2.2 then considers the logistics of transporting the bio-pyroil to the process facilities in Rotterdam, and the products away from there. Finally, Section 3.2.3 analyzes the selected feedstock and discusses its conversion into pyrolysis oil.

3.2.1. Availability of Dutch Biomass Resources

Within the context of the 2019 Dutch Climate Agreement, reports and reviews were devised by various advisory institutions to the national government to assess the current and potential availability of and applications for several types of biomass in the Netherlands [94, 95, 96, 97].

Three potential sources of biomass will be evaluated to select which one(s) will be considered in this work: forestry, agriculture, and regional waste collection.

Forestry

Wood is possibly the most typical biomass, and as such has been used in many gasification studies (see Tables 2.2 and 2.3). Woody biomass is easy to transport and process, and tends to contain relatively little amounts of sulfur and alkali contaminants. In their bioresources road map, the Corbey commission estimates the 2030 availability of wood in the Netherlands to be about 1.4 Mt (dry) in forestry residues [96].

Agriculture
Agricultural biomass can be categorized in two distinct fractions: crop residues (most importantly straw) and manure. Manure is by far the larger of these two, amounting to almost 8 Mt (dry), some 80% of which is produced by cows. However, manure is generally very wet, and thus unsuitable for pyrolysis; fermentation is considered a better processing procedure to valorize manure [96].

Plant residues from agriculture and (greenhouse) horticulture, like straw, are better suited to pyrolysis. Such herbaceous biomass typically contains significant amounts of ash, sulfur, phosphorus, calcium and potassium. Availability estimates for 2030 by the Corbey commission are 2.5 Mt (dry) in agricultural residues, and 0.175 Mt (dry) in horticultural residues [96].

Regional Waste
Regional waste streams comprise the most diverse collection of potential biomass resources. Firstly, there is municipal green waste, known as *GFT* (*Groente-, Fruit-, en Tuinafval*, Vegetable, Fruit, and Garden Waste); although the collection is well organized, this stream is too diverse, not constant, and highly variable in quality, making it fairly difficult to process [96].

Then, maintenance of public green produces a mix of pruning wood and mowed grass, most of which is currently composted. This relatively wet biomass stream, the size of which is estimated to be 1.8 Mt (dry) in 2030, could be mixed in with other streams for biorefining [96].

There is also a wood stream coming from demolitions and renovations, the quality of which varies from essentially clean to contaminated, for example, with paint residues. Most of this wood is currently used for energy production. Its 2030 availability is estimated to be 1.6 Mt (dry) [96].

Selection of Pyrolysis Feed
Considering the availability and proven performance in gasification and pyrolysis studies, the combined wood resources – 1.4 Mt from forestry and 1.6 Mt demolition wood – were selected to serve as feedstock for this thesis' process design. Supposing that a market share of 10% is obtainable and suitable for the process, a yearly raw feed of 0.3 Mt (dry) or 300 million kg of wood is assumed.

This wood is pyrolyzed outside the scope of this thesis, which typically yields about 60 – 65 mass-percent of liquids (both organics and water), 15 – 25% of permanent gases, and 15 – 20% of char [69, 98]. Therefore, assuming the lower limit of selectivity towards liquids, the facilities will have to be designed to process an annual 180 thousand tons of pyrolysis oil, equivalent to 20.5 ton per hour or 5.7 kg/s.

For future scale-up, two possible strategies for the necessary acquisition of extra biomass could be pursued. Firstly, a larger share of the wood supply could be obtained for the associated costs. Secondly, the pyrolysis feed could be diversified, provided that the needed investments in equipment (especially gas cleaning) are offset by the comparative savings made by purchasing mowed verge grass or agricultural plant residues instead of supplementary wood.

3.2.2. Logistics
There are two aspects to logistics: how to bring the necessary supplies to the process facility, and how to take the products away from it. Therefore, the arrival of bio-pyroil, sea water, and electricity will be shortly discussed, followed by the departure of methane, salt, and pollutants from the gas cleaning sequence.

Pyroil Collection
The wood pyrolysis plants are assumed to be spaced relatively equally over most of the Netherlands; higher concentrations are expected around the Veluwe and Utrechtse Heuvelrug as these are the areas with the most forests, and hence the largest amounts of available wood, as can be seen in Figure 3.1.

Two means of transport are considered. Firstly, for pyrolysis plants located on navigable waterways, inland shipping is the obvious choice. Barges can ferry tanks full of pyrolysis oil to Rotterdam, and return empty tanks to the pyrolysis plants for refill.

If no navigable water is close enough, trucks will be used to either cover the distance to the nearest inland port, or drive the tanks themselves to Rotterdam. In order to offset the carbon emissions associated with these transports, part of the produced bio-SNG shall be used – either further compressed (CNG) or liquefied (LNG) – to fuel the trucks and barges.

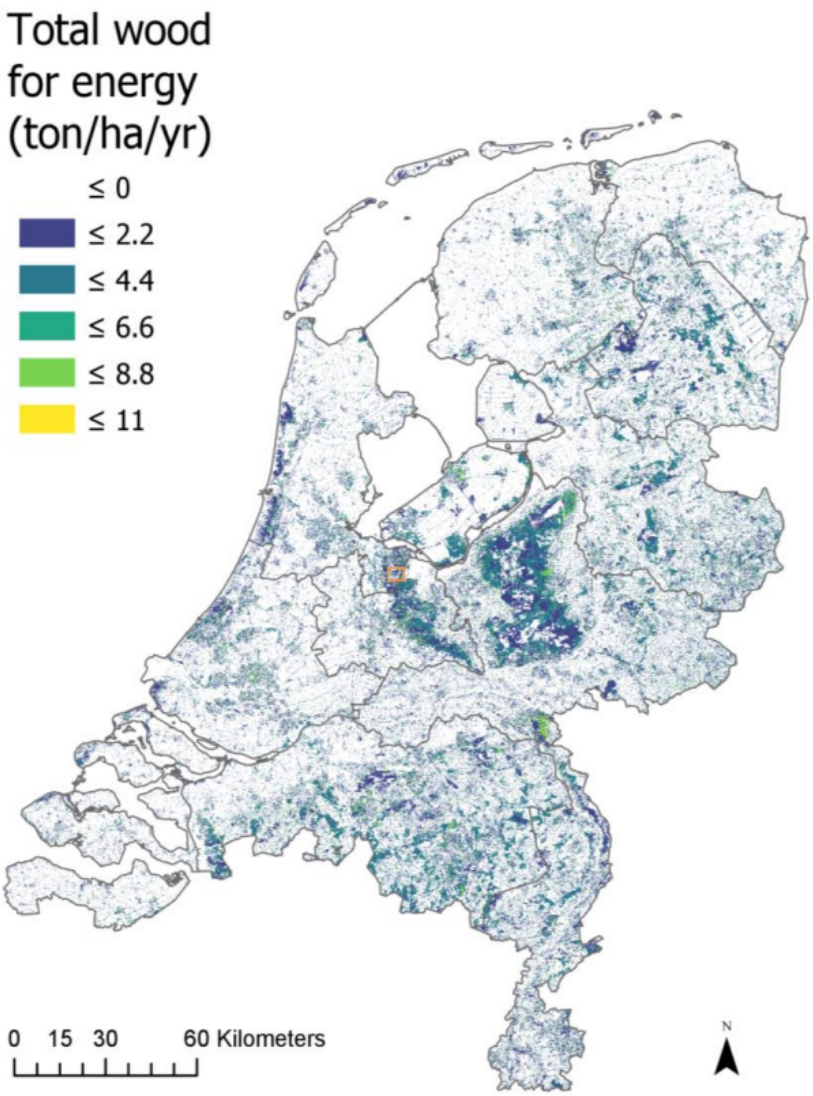

Figure 3.1: Spatial distribution of wood supply for energy applications in the Netherlands [99].

Sea Water Intake
The sea water is assumed to be clean and free of living organisms (fish, weeds, algae, etc.) and of rocks, sand and other debris. Salinity is calculated from the 28-day average of the chloride (Cl^-) concentration measured at Hoek van Holland (which sits at the sea entrance of the Rotterdam port) at –2.5 meters NAP. The measurement readings are published online by Rijkswaterstaat [100]. From this chlorinity reading, total salinity can be calculated by multiplying it by a factor of 1.80655 [101], accounting not only for sodium (Na^+), but for all ions in sea water, mainly sulfate (SO_4^{2-}), magnesium (Mg^{2+}), calcium (Ca^{2+}), potassium (K^+), and bicarbonate (HCO_3^-).

Electricity Supply
The Rotterdam port connects to several off-shore wind parks on the North Sea; hence, acquiring sufficient renewable electricity to power the electrolyzer should pose no problems. Because the electrolysis subprocess will be designed and sized to negotiate the intermittency, no additional power supply is needed. The subprocess unit will nevertheless be connected to the grid, in order to facilitate the supply of electricity to it – whenever needed – by discharging the battery.

Methane Distribution
Considering that it is technologically possible to synthesize nearly pure methane, the SNG can be supplied to the high-calorific gas (so-called *H-gas*) network – which, in time, is planned to be the only gas quality in the grid [45]. Tanks containing LNG could depart the facility on trucks, trains, and/or barges.

Sea Salt
From the desalination unit, crystallized sea salt constitutes a side product of the methanation process. Because the salt production is a mere consequence of the process design instead of its purpose, any price the salt sells for is a profit; therefore, it can be marketed at the price point of mineral table salt. Alternatively, external parties may want to refine the salt in order to recover particular minerals.

Gas Cleaning derived Streams
Two types of residual streams originate in the gas cleaning sequence. Firstly, there are the filter cakes, which contain whatever mineral ashes and tars will be produced by the gasifier, as well as particles from adsorption beds and condensed alkali hydroxides. The complex chemistry of these filter cakes is beyond scope of this thesis.

Secondarily, sulfur is recovered from regenerating the ZnO filter, either as H_2S (if regeneration is done with steam) or as SO_2 (with oxygen). Both of these are suitable feedstock for the Claus process, which produces elemental sulfur. This sulfur in turn can be used for the synthesis of sulfuric acid, gypsum, and several other chemicals.

3.2.3. Analysis of Feed
The proximate and ultimate analyses of pyrolysis oil are distinctly different from those of raw biomass. Noticeably absent from the sources is a chlorine content. Leijenhorst [102] rarely found a detectable HCl content in gasified wood-sourced pyrolysis oils. In fact, several investigations into the release of chlorine in pyrolysis indicate that the majority of chlorine – initially (up to about 600°C) as HCl, later (> 800°C) primarily as KCl and NaCl – is found in the gas fraction after pyrolysis [103, 104, 105, 106, 107, 108]. Combining this information with the typically low Cl contents of wood species, chlorine will be assumed absent from the pyrolysis oil; traces that might be in the syngas should be eliminated by the ZnO filter bed. Table 3.1 gives an overview of the results for proximate and ultimate analyses of pyrolysis oils derived from different types of wood.

Table 3.1: Proximate and Ultimate Analyses of selected Wood Pyrolysis Oils.

Wood PO	Pine	White Oak	Birch	Oak	Pine	Spruce	Poplar	'Wood'
Ref:	[69]	[98]	[66]	[46]	[46]	[46]	[46]	[46, 109, 110]
Water (wt-% ar)	21.1	16.1	49.85	25	22	22.4	19.6	15 – 30
Ash (wt-% dry)	0.09	0.50	–	0.02	0.1	0.0034	0.98	0.01 – 0.3
ρ (kg/L)	1.2	1.21	–	1.17	1.18	1.22	–	1.05 – 1.25*
pH	2.4	2.72	–	2.9	2.5	2.1	–	2.8 – 3.8
LHV (MJ/kg)	17.2	19.5^H	–	16	17^H	17.6^H	18.2	$16 – 19^H$
C (wt-% daf)	57.4	48.69	25.83	46	56.4	54	49.0	55 – 65
H (wt-% daf)	6.6	6.97	9.43	7	6.2	6.8	6.0	5 – 7
O (wt-% daf)^D	35.9	43.8	64.13	47	37.1	39.2	44.1	35 – 40
N (wt-% daf)	< 0.1	< 0.5	0.62	–	–	–	–	0.1 – 0.4
S (wt-% daf)	0.0046	< 0.08	–	–	–	–	–	0 – 0.05

^{D} by difference; – not reported; ^{H} HHV reported; * Correction of [109].

According to the latest National Forest Inventory, the most frequently occurring tree species in Dutch forests are pine (majority species in 28.0% of forest areas) and oak (17.9%) [111]. Considering that these two are also the only *genera* of tree of which Table 3.1 contains complete analyses, it will be assumed that the pyrolysis oil is a 50/50 blend of pine [69] and oak [98] wood, the average composition of which is

shown in Table 3.2. This mathematical composite is in reasonable agreement with the ranges given for unspecified wood in Table 3.1.

Table 3.2: Calculated Proximate and Ultimate Analysis of a 50/50 pine/oak Pyrolysis Oil.

Water (wt-% ar)	Ash (wt-% dry)	ρ (kg/L)	pH	LHV (MJ/kg)
18.6	0.30	1.2	2.6	16.8
C (wt-% daf)	**H (wt-% daf)**	**O (wt-% daf)**	**N (wt-% daf)**	**S (wt-% daf)**
53.1	6.8	39.9	0.2	0.04

3.3. Gasifier

In the bio-pyroil gasification unit, employing an Entrained Flow reactor is the obvious choice, as outlined in Section 2.2.1 and Table 2.4. As gasifying agents, a mixture of steam and oxygen will be used; no air, to avoid significant nitrogen content [68]. The oxygen is produced by the electrolyzer, and heat recovered during gas cleaning may be used to make steam from excess water produced by the electrolyzer.

In Section 3.2.1, it was estimated that the volume of pyrolysis oil available amounts to 180 thousand tons a year, equivalent to a continuous mass flow of 5.7 kg/s. In order to allow downtime for maintenance, the gasifier-methanator subsystem will be designed to process an input of $\dot{m}_{bio}^{gasf} = 6.0$ kg/s (21.6 t/h), operating at a system pressure of 50 bar.

An important parameter in gasification is the *Stoichiometric Oxygen Ratio* λ, (the inverse of) which is sometimes called the *Equivalence Ratio*, ER. λ is defined as the fraction of oxygen needed for complete combustion [25, 58]:

$$\lambda = \frac{\dot{m}_{O_2}^{gasf}}{\dot{m}_{O_2}^{comb}} \tag{3.1}$$

Therefore, $\lambda \geq 1$ represents combustion, $0 < \lambda < 1$ indicates gasification, and $\lambda = 0$ means pyrolysis. Typically, lower λ values are preferred because they produce higher concentrations of H_2 and CO; however, if λ is too low, the reactor temperature will drop due to increasing prevalence of endothermal reactions [25]. Typical values for λ in bio-oil gasification range from 0.2 to 0.5 [46, 68, 69].

The oxygen flow needed for complete combustion $\dot{m}_{O_2}^{comb}$, which is the denominator of Equation 3.1, is calculated as

$$\dot{m}_{O_2}^{comb} = \frac{M_{CO_2} - M_C}{M_C}\,\dot{m}_C^{bio} + \frac{M_{H_2O} - M_{H_2}}{M_{H_2}}\,\dot{m}_H^{bio} + \frac{M_{SO_2} - M_S}{M_S}\,\dot{m}_S^{bio} - \dot{m}_O^{bio} \tag{3.2}$$

which results in $\dot{m}_{O_2}^{comb} = 7.6$ kg/s, assuming that nitrogen is inert. This calculation is worked out in Appendix A.1.

Another significant parameter for syngas quality is the *Steam-to-Biomass Ratio*, SBR [25, 58], the quotient of the masses of steam and biomass supplied to the gasifier:

$$\text{SBR} = \frac{m_{H_2O}^{gasf}}{m_{bio}^{gasf}} \tag{3.3}$$

The influence of both λ and the SBR will be evaluated in the modeling calculations.

3.3.1. Gas Cleaning Strategy

Considering the temperatures in EF gasification (1200 – 1500°C) and methanation (250 – 500°C), a hot gas cleaning strategy is the thermodynamically most logical option. Therefore, the gas cleaning sequence will start with ceramic filtration candles to catch entrained dust and char particles, at temperatures around 800 – 900°C. These candles will be regularly cleaned by steam back-pulses.

Next, a nickel-based bed or catalytic filter will be employed to convert NH_3 & HCN into N_2 and COS into H_2S, as well as crack any tar that might have formed and come through the filter. Subsequently, an adsorption-desorption pairing of ZnO beds (about 500°C) will remove the sulfur species and the occasional chlorine compound from the gas flow; additional steam shall be used for regeneration of the ZnO. Finally, a secondary set of filtration candles is to be used, filtering particles from the ZnO bed; again, regular steam back-pulses will be employed to clean the filters.

3.3.2. Cross-Stream Estimations

In order to estimate the amount of ash, char and filter cake produced by the gasifier, it will be assumed that all ash content of the pyroil is collected at either the bottom of the gasifier or the first filtration candelabra. Based on the 6.0 kg/s feed rate, this combined ash stream amounts to 52.7 kg/h.

All sulfur should be adsorbed in the zinc bed, for a total flow of 7.01 kg/h of sulfur. This flow rate, equivalent to 7.45 kg/h H_2S, is too small to justify the construction of a private Claus process unit; therefore, it shall be supplied to the Claus process facility of a nearby oil refinery. By the time that fossil fuel extraction and refinement ceases, a single Claus facility might remain operational to process the collective sulfur waste streams of multiple biorefineries.

For regeneration of the ZnO beds, a mole-equivalent steam flow will be applied. The amount of steam required equals 3.94 kg/h.

3.4. Methanator

For the methanation unit, a reactor system of coupled fluidized beds is to be devised in accordance with the conclusions from Section 2.1.2. In order to minimize the attrition forces on the catalytic bed particles, the gas velocities will need to be kept low; therefore, both the adsorption and desorption columns shall resemble Bubbling Fluidized Beds.

As a catalyst-sorbent particle, Ni-loaded zeolite 13X will be used, having proven its high activity and selectivity [33, 34, 38, 44]. The possibility of ceria-promotion [35] will not be pursued here, but could be considered a future upgrade if the economic constraints allow for it.

Assuming that 100% carbon conversion efficiency can be achieved, the maximum methane yield from the 21.6 t/h pyroil feed totals 12.4 t/h CH_4. Also, all the nitrogen content of the bio-oil should exit here, as molecular nitrogen; this flow amounts to 35.1 kg/h. Therefore, the optimal methane purity obtainable – assuming that the methane contains no carbon oxides – is 99.7%.

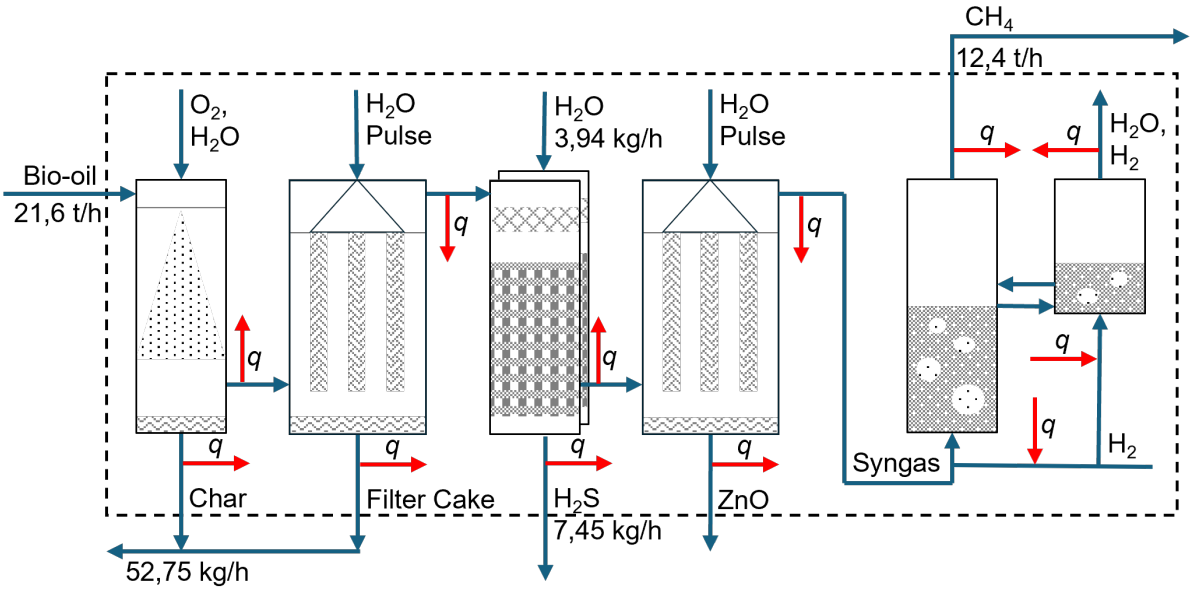

Figure 3.2: Gasification-Methanation subprocess flowsheet.

Figure 3.2 shows the flowsheet for the continuous gasification-methanation subprocess; featuring from left to right: EF gasifier (Section 3.3), dust & tar filter candles, an sulfur adsorption-desorption couple of vessels with a Ni mesh before a ZnO bed, secondary particulate filter candles (Section 3.3.1), DIFB methanator with water adsorption-desorption cycle (Section 3.4). Also indicated are the places and streams where heat (q) can be recovered and reused.

3.5. Post-processing

For customers within the Port of Rotterdam, injection into the high-calorific gas grid (H-grid) suffices. Accounting for the trace of nitrogen, the product gas should have a Wobbe index W = 53.2 MJ/m³, well within the quality requirements. A cryogenic liquefaction unit is required to cool the SNG down to LNG, after which it may leave the factory.

3.5.1. LNG Market

The global market for LNG traded 404 Mt in 2023, and demand is expected have grown by over 50% by 2040 [112]. Most of this is currently fossil methane, exported by traditional fossil fuel extractors like Qatar and the US. Nevertheless, the growing market has caused significant investment in LNG infrastructure, which is completely compatible with synthetic LNG made from biomass.

In the Netherlands specifically, import capacity has grown to 24 billion Nm³ (19.9 Mt [113]) over 2022, with expansions planned at both the Eemshaven and Rotterdam terminals [114]. Actual imports amounted to 24.8 BCM (20.5 Mt) in 2023, and 21 BCM (17.5 Mt) in 2024 [115, 116]. As of now, this LNG is regasified and distributed by the grid; considering, however, that efforts to minimize the domestic use of natural gas by 2050 are being made [117], mobility – in particular heavy transport – is likely a more promising market. In 2024, Dutch road traffic consumed 377.5 PJ, only 8.1% of which was derived from sustainable sources and electricity [118].

The Gate Terminal in Rotterdam, a joint venture between Gasunie and Vopak, is of particular interest, considering its location. They would make an excellent partner for the storage and distribution of bio-LNG.

3.6. Electrolyzer

As stated in Sections 2.3.2 and 2.4.1, the electrolysis subunit will consist of an alkaline Battolyser and a SeaHydrogen desalinator. The storage functionality of the Battolyser is not taken into consideration in this thesis. The desalination unit will have both the Membrane Distillation (MD) and Membrane Distillation Crystallization (MDC) functions, because no brine is produced in this way. Figure 3.3 shows the resulting flowsheet for the intermittent desalination-electrolysis subprocess.

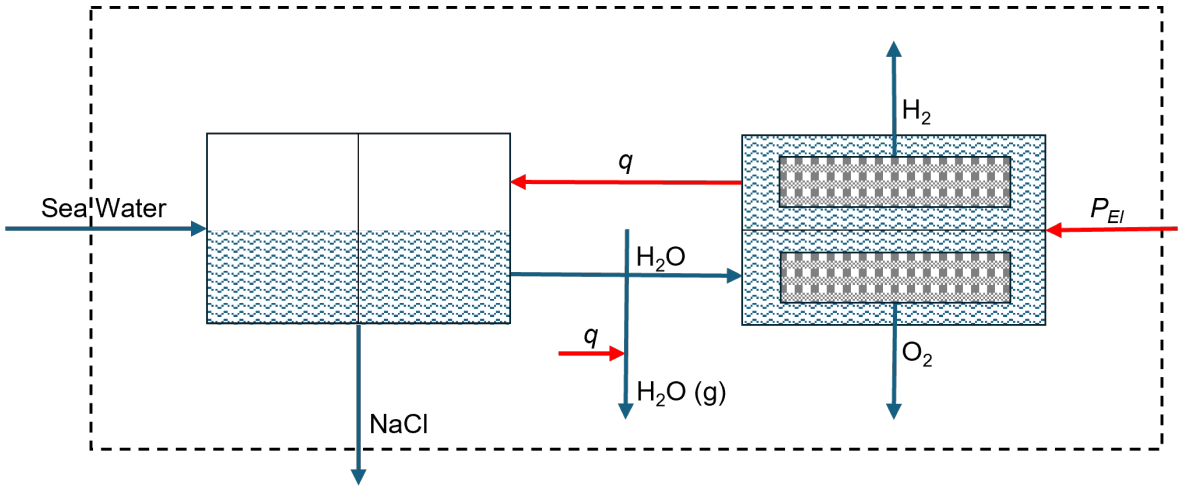

Figure 3.3: Desalination-Electrolysis subprocess flowsheet.

3.6.1. Sizing Estimates

Under the assumed conditions, the amount of hydrogen that the electrolysis subunit has to provide must be sufficient to convert all of the carbon from the biomass into methane, and all oxygen – both from the biomass and that used as gasifying agent – into water. Therefore, the hydrogen mass balance is as follows:

$$\dot{m}_{H_2}^{el} = \frac{M_{CH_4} - M_C}{M_C}\,\dot{m}_C^{bio} + \frac{M_{H_2O} - M_O}{M_O}\left(\dot{m}_O^{bio} + \dot{m}_{O_2}^{gasf}\right) - \dot{m}_H^{bio} \tag{3.4}$$

which can be simplified to $\dot{m}_{H_2}^{el} = 0.782 + 0.9545\lambda$ kg/s, as detailed in Appendix A.2. Considering typical values $0.2 < \lambda < 0.5$, the limits for $\dot{m}_{H_2}^{el}$ will be $0.974 < \dot{m}_{H_2}^{el} < 1.26$ kg/s. The equivalent total yearly hydrogen production is around 30.7 – 39.8 million kg H_2.

Battolysers reportedly have a Specific Energy Consumption (SEC) of 49 kWh/kg hydrogen [89], which is an excellent stack efficiency for an alkaline electrolyzer (Table 2.5). For the annual hydrogen production, 1505 – 1949 GWh of electricity is required.

On the North Sea, a capacity factor of 0.5 is a safe assumption for wind energy [119], which means that a wind park with a nominal power rating of 340 – 450 MW is required to supply the necessary electricity. This is equal to about 23 – 30 turbines of a modern off-shore type like the *Vestas V236-15.0 MW* [120].

The heat production associated with electrolysis is proportional to the overpotential applied over the thermoneutral water splitting potential of $E_{cell}^0 = -1.48$ V [121]. If the electrolyzer is 80% efficient, like Kuipers & van Medevoort assume, that means that 34 – 45 MW of heat is provided to the desalinator, which yields roughly 1.15 – 1.52 million m³ of drinking water per year [91]. About 24% of that is needed for the production of hydrogen within this process, another part will provide water for the steam that is injected in gasification and gas cleaning, and the remainder can be sold as drinking water.

As of April 2024, the 28-day average chlorinity in Hoek van Holland at –2.5 m NAP was calculated to be 5987 mg/L [100], which equates to a salt concentration of 10.65 kg/m³. Thus, the total salt production is estimated to be 24.5 – 32.4 thousand tons annually.

3.7. Selection of Key Performance Indicators

Table 3.3 contains the selection of Key Performance Indicators (KPIs) that will be calculated to characterize the proposed production process. Note that, where applicable, these indicators are relative to the main product (LNG) only. All definitions of the KPIs are given in Appendix A.3.

Table 3.3: Techno-economic Key Performance Indicators (KPIs) calculated in this thesis.

KPI	Name	Unit
$\dot{m}_{LNG}$	Produced LNG mass flow	t/h
LHV_{LNG}	Lower Heating Value of LNG produced	MJ/kg
EY	Energy Yield	%
CCE	Carbon Conversion Efficiency	%
CAPEX	Capital Expenditure	M€, M€/MW_{bio}
OPEX	Operational Expenditure	M€/y, €/MWh_{bio}
LCOM	Levelized Costs of Manufacturing	
– (m)	– per unit mass	€/kg
– (V)	– per unit volume	€/L
– (E)	– per unit energy	€/MWh

4

Base Model and Results

On the basis of design established in Chapter 3, this chapter builds the *Aspen Plus* model. Section 4.1 reports the making of the model unit by unit. Section 4.2 optimizes this model and performs a sensitivity analysis on the mass-flow model.

4.1. Building the Model

Section 4.1.1 explains the mathematical methods and components considered in the model. Section 4.1.2 details the implementation of the gasifier, and Section 4.1.3 the following syngas cleaning sequence. Then, Section 4.1.4 reports the development of the methanator model, and Section 4.1.5 implements the subsequent cryogenic liquefaction of the produced methane. Section 4.1.6 finally discusses the implementation of the desalinator-electrolyzer subsystem.

4.1.1. Model Set-Up

The model employs the Redlich-Kwong-Soave equation of state as base method, with Boston-Mathias modifications (RKS-BM). This is similar to both the fixed-bed methanation model by Er-rbib and Bouallou, who use the RKS with modified Huron-Vidal mixing rules (RKSMHV2) [122], and to the FB biomass gasification modeling by Abdul-Azeez *et al.*, who employ the Peng-Robinson equation of state with the BM alpha function (PR-BM) [123]. These RKS and PR cubic equations of state are both base models that *Aspen Plus* recommends for synthetic fuel applications.

The model considers the components listed in Table 4.1. All these are modeled as conventional, except C, Pyroil and the Other-column. Both Ni/13X zeolites, carbon, NaCl, ZnO and ZnS are conventional solids, and both the pyroil and ash are non-conventional components. The stream class is set to MIXCINC, as it contains mixed, conventional solid, and non-conventional solid substreams, but no particle size distribution.

Table 4.1: Components considered in the *Aspen Plus* simulation.

C/H/O species		N species	S species	Other
C	O_2	N_2	S	Ni/13X
CH_4	H_2	NH_3	H_2S	Ni/13X·70 H_2O
C_2H_4	H_2O	HCN	COS	ZnO
C_2H_6	CO	NO	SO_2	ZnS
$iso{-}C_4H_{10}$	CO_2	NO_2	SO_3	NaCl
Pyroil				Ash

Components representing tar (like BTX or naphthalene) are absent from Table 4.1, because EF gasifiers are known to produce virtually none [48]. Any hydrocarbon higher than methane that might form is represented by ethene (C_2H_4), the production of which turned out so minimal that such assumption was considered justified. The absence of chlorine species was explained in Section 3.2.3.

Properties
Properties estimations for pyrolysis oil and ash are performed by the HCOALGEN and DCOALIGT models. These allow an input in terms of proximate and ultimate analysis, which PO had been given in Table 3.2. Because, however, these analyses as required by *Aspen Plus* were intended for coal and are not ash-free, some assumptions and composition readjustments were made; the resulting proximate and ultimate analyses (PROXANAL and ULTANAL, respectively) are given in Table 4.2. The primary assumptions are that most of the compounds are volatile after pyrolysis, and that all sulfur is held by organic matter (SULFANAL input). The combustion enthalpy ΔH^0_{comb} of PO (LHV as reported in Table 4.2) was also fed to the model calculations. Ash composition was set to 100% ash.

Table 4.2: Proximate and Ultimate Analyses input for Pyrolysis Oil as implemented in *Aspen Plus*.

Moisture (% ar)	FC (%)	VM (%)	Ash (%)	LHV (MJ/kg)
18.6	3.7	96	0.3	16.8
C (%)	**H (%)**	**O (%)**	**N (%)**	**S (%)**
52.94	6.78	39.74	0.20	0.04

All percentages are weight-percent dry (except where indicated otherwise).
FC = fixed carbon; VM = volatile matter.

Implementation of Ni/13X is discussed under the methanator design in Section 4.1.4. Properties for all other components were provided by the *Aspen Plus* library.

4.1.2. Gasification Modeling
The gasifying agent is prepared by preheating a water and an oxygen stream to 1000°C, and combining them in a Mixer block. A Calculator block was successfully implemented to control the steam flow rate by setting the SBR. The gasifier operates autothermally, with no external heat input. As such, the quality of the syngas solely depends on the composition of the gasifying agent. The initial value for λ was set such that the gasifier temperature would reach at least 1200°C, which came out to be slightly outside the projected range, at λ = 0.556.

The gasifier is modeled in two blocks, both at 50 bar. First, a RYield block decomposes the pyrolysis oil into its moisture, ash, and C, H, O, N, and S contents. A Calculator block is attached to this step to control the decomposition. Second, a RGibbs block, which is fed the decomposed pyroil with its generated heat and the oxygen/steam mixture, calculates the equilibrium composition of the producer gas.

Immediately after the gasifier, a SSplit block is used to represent the collection of solids from the ash tray at the bottom of the gasifier and from the first filter candelabra. A screenshot of the *Aspen Plus* implementation of the gasifier is provided in Figure 4.1.

4.1.3. Gas Cleaning Modeling
Following a heat exchanger to bring the temperature down to 800°C, a RStoic block is used as the nickel mesh, converting all HCN, NO, NO_2, COS and NH_3 from the syngas into N_2, O_2, H_2, CO, CO_2. and H_2S. Another heat exchanger then cools the stream to 500°C.

For the zinc oxide desulfurization bed, the setup in the model is not exactly an alternating pair of fixed beds, which would require more control elements and dynamic programming; because it is not the main focus, the implementation of desulfurization was significantly simplified. Essentially, it is set up as a gas-solid scrubber, where ZnO reacts with all H_2S in the syngas, and is then regenerated with steam in a secondary reactor, releasing the hydrogen sulfide; the regenerated ZnO is subsequently fed back into the scrubber. Both the adsorption and desorption beds are represented by a RStoic block, followed by a SSplit separating the solid and gaseous phases.

As a final conditioning element, a water knockout was introduced to reduce the volume of water that the sorbent in the methanator has to process. The design of the gas cleaning in *Aspen Plus* is shown in Figure 4.2.

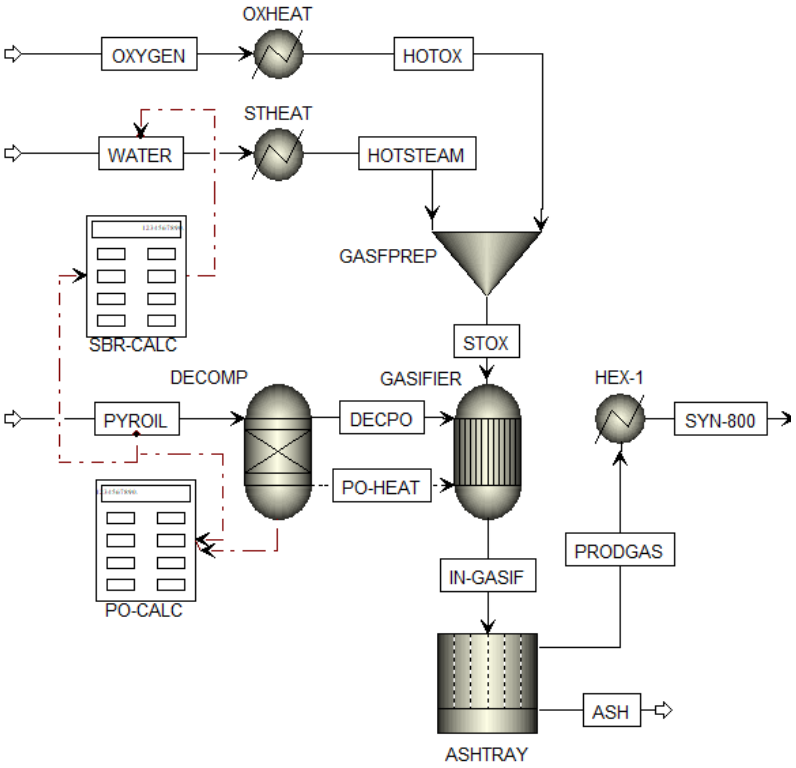

Figure 4.1: Initial implementation of the gasifier in *Aspen Plus*.

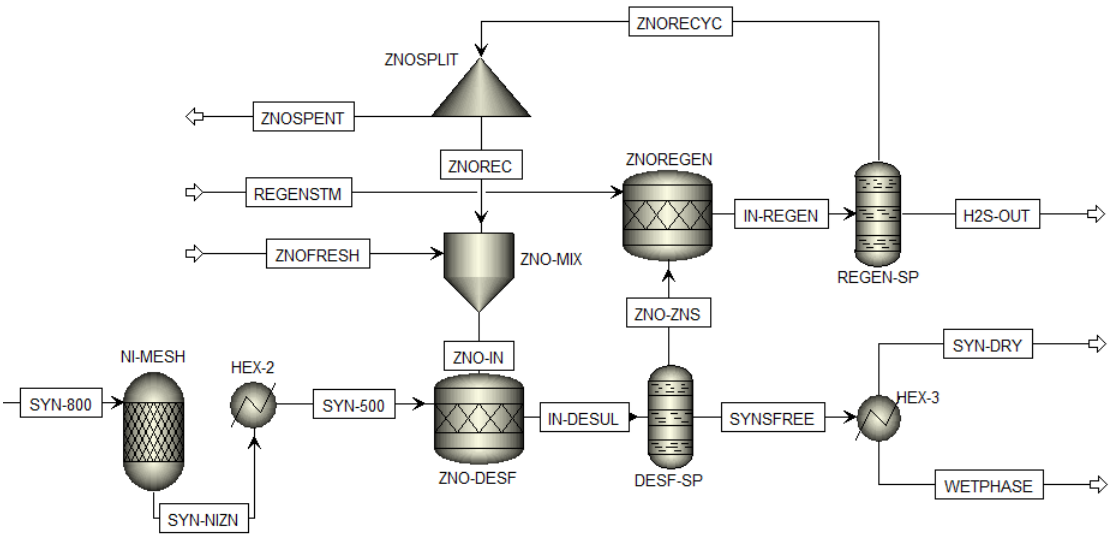

Figure 4.2: Implementation of the gas cleaning sequence in *Aspen Plus*.

4.1.4. Methanator Modeling

The methanator model starts with a conditioning step: a Mixer block combines the dried syngas stream with a preheated hydrogen flow. A Calculator is implemented to ensure that the H_2/C ratio is sufficient for full carbon conversion.

Modeling the reactor itself subsequently proved to be a challenge from several angles. Therefore, a sequence of increasingly accurate but complex models were devised in separate *Aspen Plus* files.

Base Case: CaO scrubber

The most basic design is similar in setup to the ZnO sulfur scrubber described in Section 4.1.3 and Figure 4.2: two sets of RStoic and SSplit blocks, one for the methanator and one for the desorber. Additionally, the sorbent is modeled as calcium oxide (CaO), because that and its hydrate (calcium hydroxide) are conventional solids found in the *Aspen Plus* database. This initial implementation is pictured in Figure 4.3.

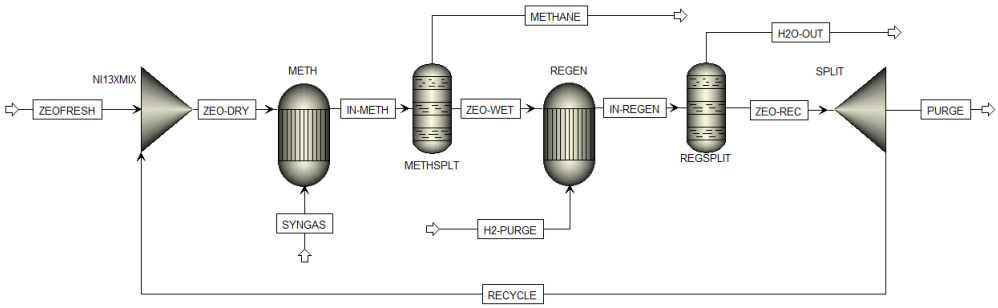

Figure 4.3: Sorbent-scrubber methanator design in *Aspen Plus*.

In this separate simulation, the reactor is fed 6 kg/s syngas with a molar composition of 10% CO, 10% CO_2, 70% H_2 and 10% water. The methanator is set to operate at 250°C, and the regenerator at 350°C. The CaO sorbent is provided to the methanator at 15 kg/s, of which 95% by mass is recycled. The hydrogen purge is set to 0.7 kg/s.

Literature Case: CaO Fluidized Bed

As an example of a coupled Fluidized Bed methanator, an attempt was initiated to reproduce the model by Coppola *et al.* [37]; the flow scheme is shown in Figure 4.4. A couple of necessary modeling details were unfortunately missing from their article; hence, those need to be discussed before the implementation of their model could commence.

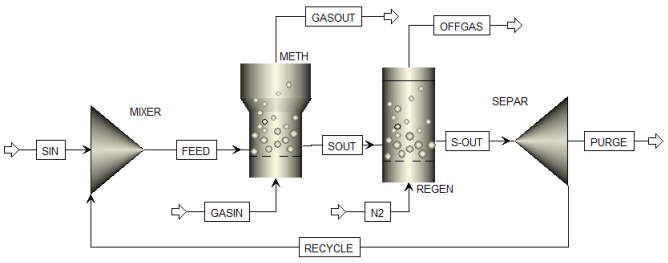

Figure 4.4: Fluidized Bed methanator design in *Aspen Plus*, reproduction from Coppola *et al.* [37].

Firstly, they failed to mention which property method is employed in *Aspen Plus* for their calculations. Considering their model operates at (near) atmospheric temperature, IDEAL would not be illogical; in order to keep consistency with other parts of the model under construction in this work, however, RKS-BM would have been used here for the reproduction.

Secondly, their article contains not a single word regarding the design of the distributor plates in both fluidized beds. This omission severely hindered reproduction, and proved a critical factor in the decision to abort and focus efforts elsewhere.

From this excursion, two important notes were taken. Firstly, the flowsheet (Figure 4.4) is a workable model representation of a DIFB methanator, and a logical evolution of the simplified setup in Figure 4.3. Secondly, in order to use the FLUIDBED blocks, *Aspen Plus* necessitates the inclusion of a particle size distribution (PSD) for the bed. Therefore, in the fluidized bed models, the stream class was upgraded to MIXCIPSD for the standalone gasifier models, and to MCINCPSD for the overall model.

Implementing Zeolite Sorbents
The first attempt at implementation of the zeolite catalyst-sorbent particle considered the Ni/13X to be a *non-conventional component*. Its properties estimation models were set to be HCOALGEN and DCHARIGT, so that the solid would have a moisture content statistic in its proximate analysis; the mineral part was interpreted as ash.

It is possible to change the composition of non-conventional components in a number of *Aspen Plus* blocks, as illustrated by the *Coal Drying* tutorial – elaborations on which are numerous online. Unfortunately, however, the calculations governing the adsorption and desorption of water from the zeolite were never perfected, and severe errors were reported by *Aspen Plus* due to problems with closing the mass balance.

The next approach taken was considering the Ni/13X a *conventional solid*. As there is no specific catalyst-sorbent material in the *Aspen Plus* database, it had to be defined specifically for this model. So, a 'molecular' formula was devised. Wei [33] reports SEM-EDX measurements of the elemental composition of his 5%Ni/13X catalyst/sorbent, which were used to compose a reasonable approximation for a molecular formula. The result was a 2381 atom compound with a molecular mass of 50264.81 g/mol:

$$Ni_{47}\left((Al_2O_3)_7(SiO_2)_{23}\right)_{18}(Na_2O)_{120}(MgO)_{37}(CaO)_7(Fe_3O_4)_2$$

which was entered in *Aspen Plus* under the name and alias Ni13X, and assigned several necessary properties. A material density of 1470 kg/m³ is given by Kim *et al.* [124, 125]; to obtain particle density, a measure of porosity is needed. Pore volumes in the 0.23 – 0.28 cm³/g range are reported for pure 13X [124, 126], and 0.21 – 0.22 cm³/g for Ni/13X [33, 127]; from the middle of the latter range, a particle density of 1117 kg/m³ was calculated. A heat capacity of 943 J/(kg K) was measured on pure 13X by Scuiller *et al.* [126]; the contribution of nickel to the heat capacity is assumed negligible. A formation enthalpy ΔH_f of –682.503 MJ/mol was estimated based on Mathieu and Vieillard [128] and Petrović and Navrotsky [129].

For the hydrated zeolite, a single, fully loaded 'particle' of Ni/13X·70 H_2O was devised and given its necessary thermodynamic properties. A heat capacity of 993.13 J/(kg K) was estimated, as well as a formation enthalpy ΔH_f of –707.483 MJ/mol, accounting for the water present and the adsorption enthalpy of –3.942 kJ/g [126].

Once all issues that *Aspen Plus* expressed with this approach were resolved by explicitly entering constants in the correlations for CPSPO1 and VSPOLY (solid molar heat capacity and solid molar volume, respectively), a working simulation was obtained. A zeolite sorbent flow of 175 kg/s proved necessary to adsorb all water, all other parameters being equal to the CaO scrubber setup (Figure 4.3).

4.1.5. Cryogenic Liquefaction Modeling

Cryogenic liquefaction can be carried out in a couple two ways: a cascade cooling process, with either a pure or mixture refrigerant; and an expansion-based process [130]. Within either, it is possible to include purification steps such as distillation to remove the last traces of contamination [131].

Capra *et al.* conducted a techno-economic comparison of five liquefaction technologies [132]: a reverse Brayton cylce, a reverse Rankine cycle with mixed refrigerant, an open Claude cycle, a reverse Stirling machine, and a base case of liquid nitrogen vaporization. From their analysis, the Rankine cycle (RC-MR) emerges as the most energy-efficient and most economic option, even becoming more convenient with larger plant size.

Therefore, a RC-MR cryogenic liquefaction cycle was set up in *Aspen Plus* based on the flowsheet and thermodynamic data given by Capra *et al.* [132], as shown in Figure 4.5. In this figure, the streams numbered 1 – 5 constitute the methane being cooled to –152.5°C at 2 bar, and streams 6 – 20 make up the mixed refrigerant cycle. The refrigerant consists of methane (42.3% molar), ethane (20.8%), isobutane (36.6%) and nitrogen (0.3%).

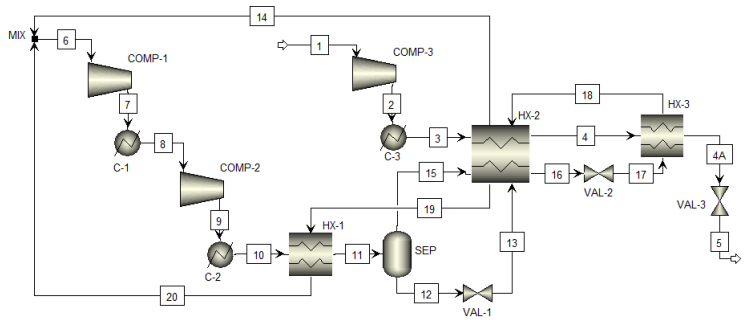

Figure 4.5: Flow sheet for cryogenic liquefaction implemented in *Aspen Plus*, based on Capra *et al.* [132].

4.1.6. The Desalination-Electrolysis Subsystem

The currently most recent edition of the *Aspen Plus* software, version 12, does not feature dedicated blocks for electrolysis or membrane distillation, and attempts at creating a working flowsheet using the blocks available (a Filter as membrane distiller, and RStoic with Flash2 blocks in per half reaction electrolysis) did not yield satisfactory results. Modeling literature on electrolyzers does exist, but typically employs heavily customized blocks or different software altogether [133, 134, 135, 136]; which this project had no time available to develop. Therefore, subject to optimization, a coarser analysis had to be performed.

With the λ estimate of 0.556 as given in Section 4.1.2, equivalent to $\dot{m}_{O_2}^{gasf}$ = 4.2 kg/s, Equation 3.1 returns a demand for hydrogen gas of $\dot{m}_{H_2}^{el}$ = 1.31 kg/s, or 41.3 thousand tons of H_2 per year. The largest module that *Battolyser Systems* currently has on offer online, rated at 25 MW_e, features a system-based electrolysis efficiency of 50.1 kWh/kg hydrogen; the annual electricity use thus equals 2067 GWh, as a continuous power consumption rated 236 MW.

Taking into account that North Sea wind energy has a capacity factor around 0.5, this means that 19 to 20 Battolyser modules rated 25 MW (totalling 475 – 500 MW) are needed to produce the necessary hydrogen on purely renewable electricity. The required 472 MW of electrical energy can be supplied by 32 15 MW offshore wind turbines.

Keeping with the estimate that 20% of the rated power can be recovered as heat, some 47.2 MW_{th} is available to the desalinator. That suffices to produce at least 182 m³/h of water alongside 6.6 ton/h of salt. However, considering the significantly lower salinity in the Rhine delta as compared to open ocean, less salt and more water can be produced from sea water at Hoek van Holland. From the salinity of 10.65 kg/m³, almost a factor 4 lower than in [91]'s calculations, the amount of salt obtainable is limited to 3.4 ton/h, which allows the desalinated water production to rise to 653 m³/h. Just over 42 ton/h (6.45%) of this stream is required to feed the electrolyzer, with the remainder available for ZnO regeneration in the gas cleaning, heating and cooling duties, and eventually discharge as drinking water.

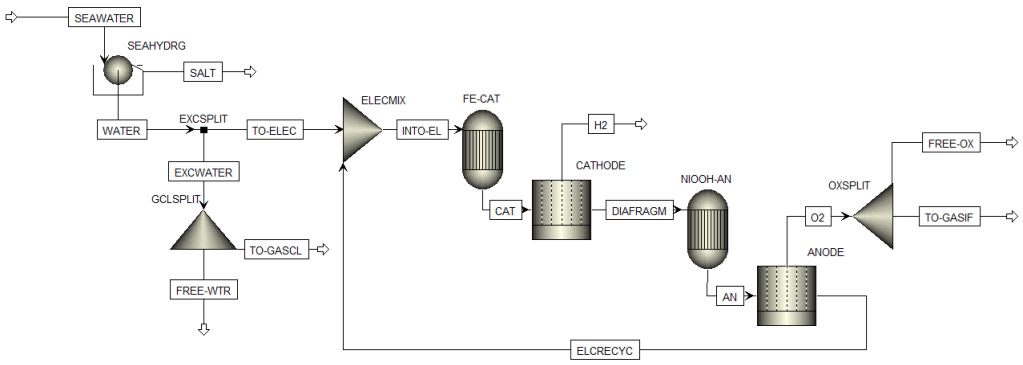

Figure 4.6: Flow sheet for implementation of desalination and electrolysis in *Aspen Plus*.

A *Aspen Plus* flowsheet for desalination and electrolysis is provided in Figure 4.6. Note however that this model does not accurately calculate heat and energy balances.

4.2. Model Optimization & Sensitivity Analysis

Having built a first iteration of the model, the design will now be refined and its most important parts subjected to sensitivity analysis. Section 4.2.1 explores the influence of the gasifying agent on the gasifier, and Section 4.2.2 updates the gasifier design accordingly. Section 4.2.3 tests the efficiency of water removal at the end of the gas cleaning sequence. …

4.2.1. Composition of the Gasifying Agent

As discussed in Section 3.3, there are two adjustable process parameters that impact the quality of the syngas produced by the gasifier: the λ and the SBR. A concise sensitivity analysis was performed to assess the impact of these parameters in the model. Afterwards, a third parameter is evaluated: the temperature of the gasifying agent when it enters the gasifier.

Stoichiometric Oxygen Ratio λ

In order to investigate λ in isolation, SBR was set to zero. The correlation between the oxygen feed as indicated by λ and the resulting gasifier temperature is graphed in Figure 4.7a. Within the typical temperature range for EF gasification (1200 – 1500°C), the relation is nearly linear, albeit at λ values outside of the typical range for gasification (0.2 – 0.5).

The gasifier temperature in turn affects the composition and quality of the produced syngas. Figure 4.7b shows the calculated mole fractions of the five most important components of synthesis gas: CO, CO_2, H_2, methane, and water. The high CO_2 content is exceptional for EF gasification, however, but not surprising considering there is ample oxygen available.

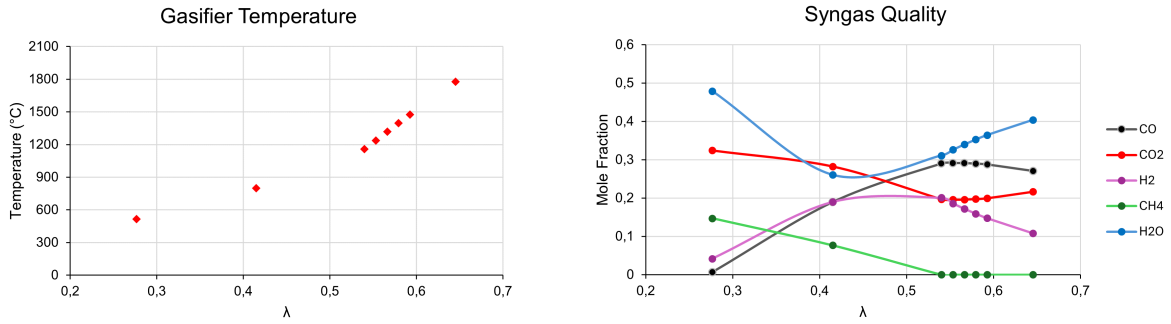

(a) Gasifier temperature.

(b) Composition of the produced syngas.

Figure 4.7: Influence of λ on the gasifier temperature and resulting syngas quality; SBR = 0.

It is also clear from Figure 4.7b that no gasification takes place when the temperatures are too low. Because the main components of the gas are CO_2 and water – full combustion products of hydrocarbons – what probably happens here is complete oxidation of a fraction of the carbon. Indeed, a significant amount of elementary carbon is found in the gasifier. In a real reactor, tar would likely form under these conditions; however, there is none reported as the model does not account for tar.

The oxygen stream fed to the gasifier $\dot{m}_{O_2}^{gas}$ = 4.2 kg/s, equivalent to λ = 0.556, was set against the background of these data points. In the model, it appears to be the lowest λ value that brings the reactor temperature within the range typically associated with EF gasification, and it is close to the maximum yields for CO and H_2.

Steam-to-Biomass Ratio

With the value for λ set, the influence of SBR on the gasifier temperature and syngas quality was also analyzed. Figure 4.8a shows the negative temperature effect of steam as calculated by the model. The resulting syngas quality as measured by the mass fractions of its most important constituents is displayed in Figure 4.8b. The share of H_2 in the syngas does increase as promised with rising SBR; however, the effect is minimal and barely significant.

This finding cannot be taken as a refutation of Bareschino [53]: the decisive difference is the amount of water already present in the biomass. In their study, Bareschino *et al.* use spruce wood pellets with a

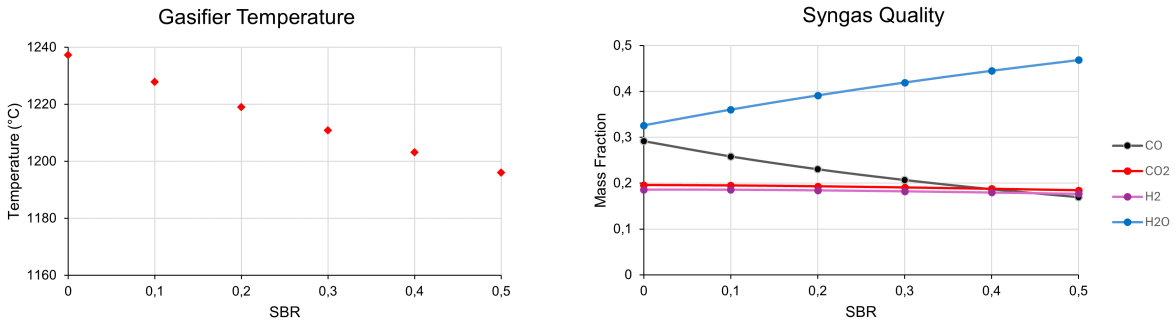

(a) Gasifier temperature.

(b) Composition of the produced syngas.

Figure 4.8: Influence of SBR on the gasifier temperature and resulting syngas quality; λ = 0.556.

moisture content of 8.5% (ar), whereas this thesis gasifies a liquid bio-oil containing over double as much water at 18.6% (ar).

This result is nevertheless dissonant with Zheng *et al.*, who, like this thesis, use a bio-oil and an EF gasifier [68]. Their oil, only given as empirical formula ($C_{3.48}H_{4.9}O_{1.74} \cdot 1.4\,H_2O$), is wetter at 25.2%; yet they reported no water in their syngas. Upon closer inspection of their setup, it appeared that their tar sampling setup was kept at 0°C for four steps and –15°C for the final two, which also condenses all the water – how much is not disclosed in the paper. In conclusion, their setup will never be compatible with immediate processing of the produced syngas in a thermodynamically sensible way.

In conclusion, the results given in Figure 4.8b indicate that pyrolysis oil contains sufficient water to harness the benefits of steam gasification without any additional steam being fed to the gasifier. Therefore, the value for SBR in this model was set to zero, and thus the blocks and streams introducing steam to the gasifier were deleted.

Inlet Gas Temperature
In Figure 4.7a, a break in continuity is apparent around the gas entrance temperature set at 1000°C. A short calculation, reported in Table 4.3, confirmed the significance of the gas temperature: at T_{gas} = 1250°C, the reactor reaches 1200°C at a lower λ, while more CO and less CO_2 is generated than in both reference cases taken from Figure 4.7. Therefore, it might be worth investigating whether it is feasible to preheat the oxygen stream beyond 1000°C, if there are materials available that can safely contain such a highly oxydizing stream.

Table 4.3: Influence of Inlet Gas Temperature on Syngas Quality.

T_{gas} (°C)	λ	T_{gasf} (°C)	y_{CO}	y_{CO_2}	y_{H_2}	y_{H_2O}
1000	0.556	1237	0.291	0.196	0.186	0.326
1250	0.543	1214	0.296	0.191	0.195	0.317
1000	0.543	1158	0.290	0.197	0.201	0.311

4.2.2. Gasifier Redesign

To implement the findings of Section 4.2.1, the gasifier design was updated. Because no benefit was found in the addition of steam, the blocks and streams adding steam were removed. Also, a HeatX countercurrent heat exchanger was inserted so that the first syngas cooling step now preheats the oxygen for the gasifier. The resulting flow chart is shown in Figure 4.9.

As shown in Table 4.3, a hotter oxygen stream fed to the gasifier results in higher quality syngas while less oxygen is required. The new setup as presented in Figure 4.9 allows for the oxygen to be heated to nearly gasifier temperature (a minimum ΔT of 5°C was observed) by cooling the produced syngas.

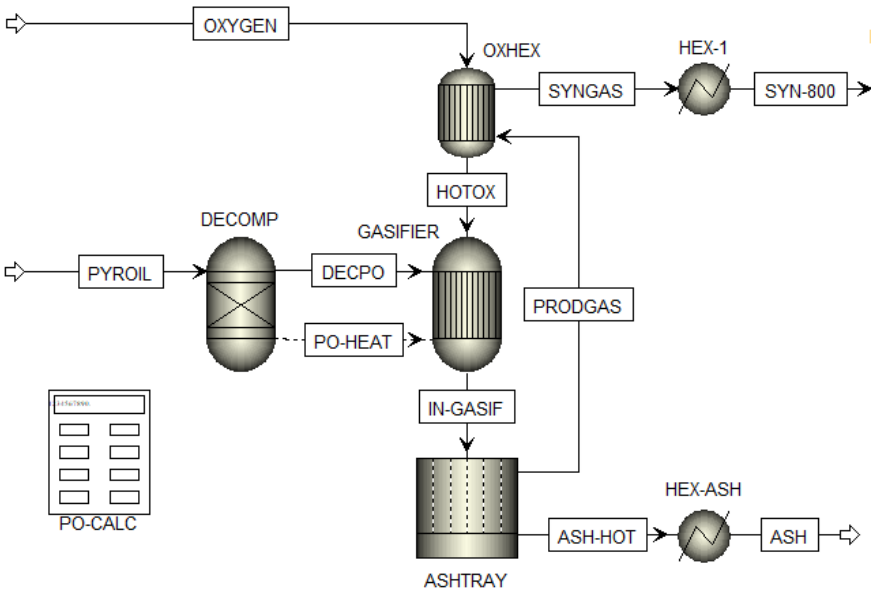

Figure 4.9: Final implementation of the gasifier in *Aspen Plus*. Stream conditions are included in Table B.3.

As a result, a new correlation between λ and the gasifier temperature is obtained, given in Figure 4.10a; the corresponding syngas compositions are displayed in Figure 4.10b. In this configuration, the lowest value for λ that induces a gasifier temperature in excess of 1200°C is λ = 0.543, equivalent to 4.1 kg/s, resulting in T_{gasf} = 1202.2°C.

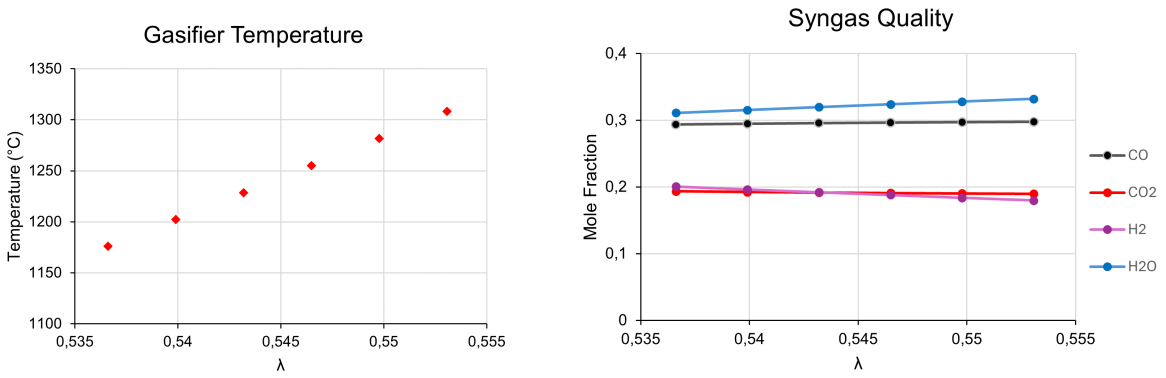

(a) Gasifier temperature.

(b) Composition of the produced syngas.

Figure 4.10: Influence of λ on the gasifier temperature and resulting syngas quality in the redesigned gasifier.

4.2.3. Water Removal Efficiency

In Section 4.1.2, one additional element was appended to the gas cleaning sequence as described in Section 3.3.1 to condensate and remove water from the gas stream, labeled HEX-3 in the flowsheet in Figure 4.2. Its effectiveness as a function of its target temperature is shown in Table 4.4.

As expected, larger portions of the water condensate at lower temperatures; however, cooling the syngas too far unnecessarily increases the heat duty of the methanator. Therefore, the cooling temperature for condensation was limited to 175°C, removing 46% of the water from the syngas stream.

Table 4.4: Water Removal Efficiency at HEX-3 by Temperature.

T_{cool} (°C)	$\dot{m}_{H_2O}$ (kg/s) remains	$\dot{m}_{H_2O}$ (kg/s) removed	Removal Efficiency (%)
200	2.511	0	0
195	2.393	0.117	4.68
190	2.068	0.443	17.63
185	1.791	0.720	28.67
180	1.553	0.958	38.15
175	1.348	1.163	46.31

4.2.4. Methanator Adaptation

Because rather large temperature drops have proven necessary to dry gas streams, the original setup of the sorbent regenerator was amended accordingly. In this updated design, shown in Figure 4.11, the hydrogen is not used as purge gas anymore, but it is instead pre-heated by the gas stream leaving the regenerator.

As the new purge gas, pure, pressurized nitrogen is used, as it is both affordable and inert. Its non-reactive nature is important, because some purge gas might leak into the methanator column of the interconnected BFB reactor, where it cannot cause any chemical reactions. Being inert, it will leave in the methane stream, and can be separated from the methane in liquefaction.

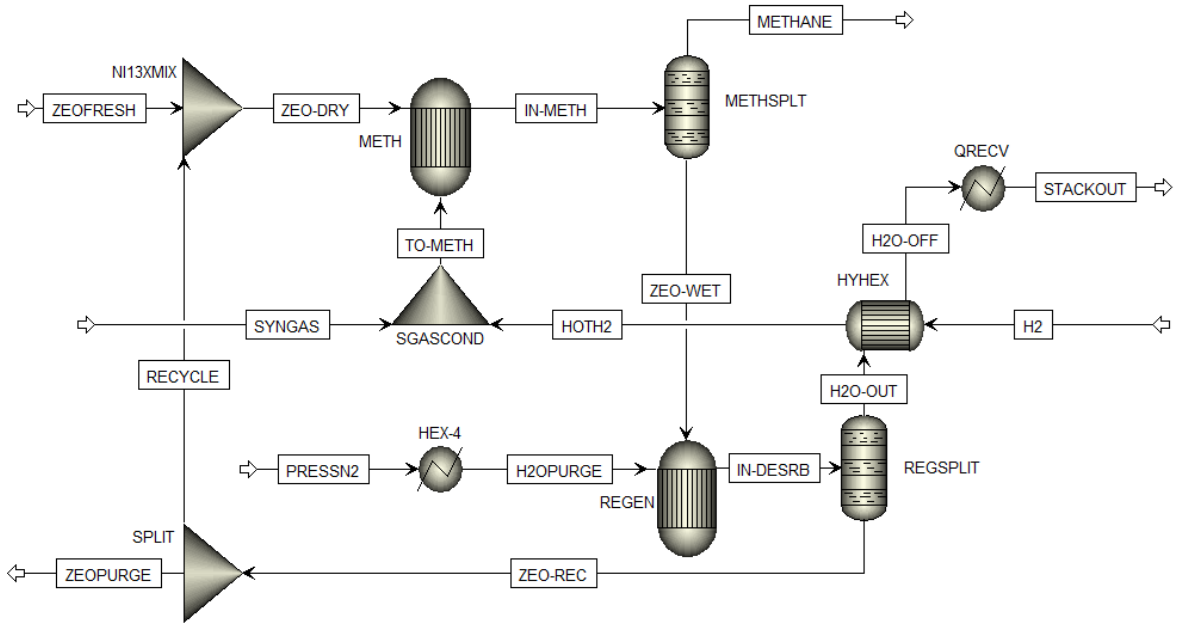

Figure 4.11: Implementation of the methanator in *Aspen Plus*.

5

Energy Performance Analysis

Having the mass flow sheet finalized, this chapter reports on the improvements on the design implemented to achieve a better energetic efficiency. Section 5.1 explains the basics of Pinch Analysis, which is then applied to the process in Section 5.2. Its findings are then used to improve the process flow sheet in Section 5.3. Finally, Section 5.4 discusses the resulting energy performance metrics.

5.1. Pinch Analysis

The research field of what is now called *Pinch Analysis* was born from *A User Guide on Process Integration for the Efficient Use of Energy* by Linnhoff *et al.*, published in 1982 [137]. Originally focusing on energy integration, it has grown to encompass energy supply, carbon footprint, and non-energy pinches [138].

In essence, Pinch Analysis is a thermodynamic method to minimize the utility load of the heat exchanger network, saving energy costs as well as often capital costs by reducing the number of units in the network. Its analysis yields *energy targets*, which represent the thermodynamic minimum of exchanger duties, and as such are a guide to finding the heat exchanger network that achieves this minimum [138].

5.1.1. Pinch Analysis in *Aspen Plus*

The software package of *Aspen Plus* includes a pinch analysis program, called *Aspen Energy Analyzer*. This program will be used to calculate the energy targets achievable. For consistency, only the continuous part of the flowsheet (gasification to liquefaction) will be subjected to pinch analysis, because none of the streams in the intermittent part (desalination and electrolysis) are constant, and thus cannot be relied upon to provide or be provided with a constant heat flow. While the gases (both H_2 and O_2) and water it produces can be stored, heat cannot effectively be shelved for later use.

Four utilities were defined to be used: cooling water and high-, medium-, and low-pressure steam. The cooling water (COOLANT) is given inlet and outlet temperatures of 12°C and 17°C, and is cooled by seawater. All steam is raised from water produced by the desalinator, and as such has an inlet temperature of 60°C and pressure of 30 bar. Per *Aspen Plus*'s definition, outlet conditions are 250°C for HP-STEAM, 175°C for MP-STEAM, and 125°C for LP-STEAM, all at a vapor fraction of 1. This makes for steam pressures of approximately 40 bar, 10 bar, and 2.4 bar, respectively.

5.2. Full SEM Heat Integration

In order to obtain insight in where in the process heat and work streams are created and needed, the overview in Table B.1 was compiled, and shown in Appendix B.1. Like the process, it is split into a continuous and an intermittent section. The data in Table B.1 indicates that the plant design is net exothermic (–81 MW), which suggests that external supply of additional heat ideally is not necessary.

5.2.1. Full SEM Pinch Analysis

Pinch Analysis was performed on this model by the *Aspen Energy Analyzer*, which returned the results presented in Table 5.1. As the calculated target indicates, it is not possible in this flowsheet to eliminate external heating, not even most of it. This heating duty essentially necessitates a flowsheet redesign.

Table 5.1: Energy Analysis of the Full SEM flowsheet by *Aspen Energy Analyzer*.

Utility	Current (MW)	Target (MW)	Pot. Savings (MW)
Fired Heat	56.54	41.63	14.91
Total Heating	**56.54**	**41.63**	**14.91**
Coolant	32.26	8.096	24.17
LP-Steam	102	0	102
MP-Steam	0	113.4	–113.4
HP-Steam	7.373	0	7.373
Total Cooling	**141.7**	**121.5**	**20.21**

5.2.2. Manual optimization

First, a couple of simple optimization steps were taken manually. The heat duties of blocks NI-MESH and ZNO-DESF are so small, that both reactors were converted into adiabatic reactors, inducing small temperature effects on the gas stream. This approach did unfortunately not work for the desorber ZNOREGEN. Therefore, a small heat exchanger (4.75 kW) was added to the syngas stream after NI-MESH to supply the necessary heat duty to the desorber.

Then, the heaters PO-HEX and METHEX were combined into a single heat exchanger (POMETHEX), the hot outlet stream of which was specified to 28°C, as required in the liquefaction process. As a result, the pyrolysis oil is heated slightly further, to 74°C). Also, heater ZNOREGST was converted into a heat exchanger, the hot side of which is the syngas stream between the NI-MESH and HEX-2 blocks. A cooler (SULFHEX) was added to recover heat from the H_2S stream from the gas cleaning process.

The primary consumer of heat is the catalyst regenerator for the methanator, with 53.4 MW. In terms of thermal power, there is sufficient heat available from the methanator itself to provide that heat (94.3 MW); however, the quality of that heat is not sufficient, because the methanator – as typical for adsorption-desorption processes – runs at a lower temperature than the regenerator, so it cannot be used. According to the pinch analysis results in Table 5.1, nowhere else in the flowsheet is sufficient heat of sufficient quality available.

A similar imbalance occurs in the desalinator-electrolyzer subsystem, where SEAHYDRG operates at 80°C, whereas the necessary heat provided by the electrolyzer, although sufficient in thermal power, is provided at the Battolyser operating temperature of 60°C. Here, the more sensible solution is to lower the operating temperature of the desalinator to the level of its heat supply.

5.3. Two-Stage Methanation

The methanator flowsheet needs to be redesigned to eliminate the necessity of external heat supply; Figure 5.1 shows a two-stage methanator design. After conditioning (SGASCOND), the syngas is first fed to a conventional fixed-bed methanator (CONVMETH), modeled as a RGibbs block. This methanator will need to be cooled anyway because of the exothermic nature of the methanation reaction; this heat can now be acquired at temperatures in the 400 – 500°C range, which then can satisfy the heat demand of a 300°C catalyst regenerator. The methanator temperature was limited to 420°C.

Subsequently, the partially converted syngas is cooled to knock out a part of the water formed in a Flash2 block (SRP-COOL), before it is fed to the sorption-enhanced methanator (SRP-METH). Because it is now only the second stage of methanation, the regenerator (REGEN) does not provide sufficient steam anymore to heat up the incoming hydrogen gas. Instead, both the hydrogen (HYDHEX) and nitrogen (NITHEX) streams are preheated by the partially converted syngas leaving the fixed-bed methanator.

The cooling temperatures of heat exchangers SULFHEX and QRECV were limited to 140°C, so they can be used to raise steam, but do not require additional cooling water.

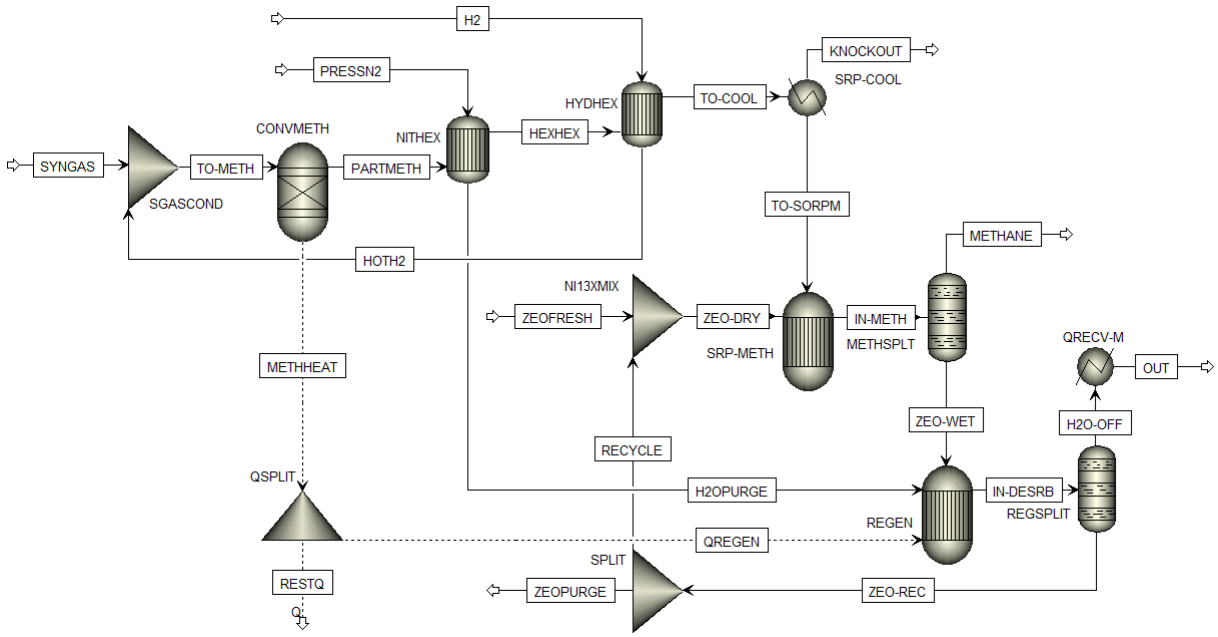

Figure 5.1: Mass flow sheet for a two-stage methanator in *Aspen Plus*. Stream conditions are included in Table B.3.

In addition to the energetic advantages that induced its adoption, this two-stage methanator design has an additional economic benefit. The extra water knockout at SRP-COOL decreases the amount of water that the zeolite catalyst particles have to adsorb; as a result of which less total zeolite mass is required, reducing the investment needed to acquire such a specialized material. The sorbent flow rate needed in the setup of Figure 5.1 is below 250 t/h (69.4 kg/s), a reduction of 60.3% as compared to 175 kg/s in the Full SEM design (see Section 4.1.4). Table B.2, shown in Appendix B.1, contains an overview of heat and work streams generated and consumed in the two-stage setup.

5.3.1. Flow Sheet Adjustments

The recycle rates for ZnO and Ni/13X have been lowered in anticipation of their economic impact. For Ni/13X, the refresh rate was reduced to 0.4% (1000 kg/h); the ZnO refresh rate was adjusted to 0.1% (0.225 mol/h).

At the very end of the process flow sheet, an adiabatic Flash2 block was appended in order to purge the gas from the LNG stream. The purge gas is 92.6% methane, 5.9% hydrogen and 1.5% nitrogen, and has a flow rate of 556 kg/h. As a result, the LNG is purified to 99.895% methane, with a flow rate of 11.9 t/h.

5.3.2. Computational Optimization

Pinch Analysis by *Aspen Plus* on this redesigned and optimized flowsheet yields the results shown in Table 5.2. Compared to the results of the Full SEM flowsheet in Table 5.1, external heating demand has been eliminated, and the total cooling utility load is more than halved. Additionally, the heat exchanger network design is very close to optimal, with just a 3% improvement still obtainable.

The specific network design of the thermodynamic target cooling lays beyond the scope of this thesis; as the latest design is reasonably close, it will be regarded as the final flowsheet design. This decision implies that the capital investment needed – as will be calculated in the next chapter – will be slightly overestimated and the steam raised might be undervalued in comparison with the optimal scenario. The impact of these deviations, however, is expected not to be significant in the economic evaluation.

Table 5.2: Energy Analysis of the Two-Stage flowsheet by *Aspen Energy Analyzer*.

Utility	Current (MW)	Target (MW)	Pot. Savings (MW)
Coolant	11.68	5.64	6.035
LP-Steam	30.67	0	30.67
MP-Steam	0	42.71	–42.71
HP-Steam	7.49	0	7.49
Total Cooling	**49.83**	**48.35**	**1.483**

5.4. Final Flowsheet Performance

Thus, having finalized the mass and energy flow sheets, the mass and energy performance of this process design are shown. Also, the technical Key Performance Indicators (KPIs) are quantified for comparison with competing processes.

5.4.1. Mass Flowsheet

An overview of the mass flows into and out of the process is given in Table 5.3, and the complete flowsheet itself is appended in Figure B.1. The methanation process has a carbon conversion efficiency (CCE) towards methane of 99.869%, and the methane stream produced is 99.555% (molar) pure. After cryogenic liquefaction, the LNG purity improves to 99.895%.

Table 5.3: Mass input and output of the final methanation process design.

Inflows			Outflows		
Pyrolysis Oil	21.6	t/h	LNG (99.895%)	11.9	t/h
Seawater	457.9	t/h	Methane (92.6%)	556	kg/h
Nitrogen	21.0	t/h	Sea salt	6.4	t/h
ZnO	0.09	kg/h	ZnO	0.09	kg/h
Ni/13X	1	t/h	Ni/13X	1	t/h
			Offgas	24.3	t/h
			Drinking water	409	t/h
			Process water	25.3	t/h
			H_2S	7.52	kg/h
			Hydrogen (excess)	58.7	kg/h
			Oxygen (excess)	22.8	t/h
			Ash	52.7	kg/h

5.4.2. Energy Performance

The complete methanation process costs 244.46 MW_e and results in a LNG production of 3.30 kg/s, giving a specific energy consumption (SEC) of 74.08 MJ_e/kg (20.6 kWh/kg). The lower heating value (LHV) of the produced LNG equals 49.9 MJ/kg, so the SEC per unit energy is 1.48 MJ_e/MJ.

The methane in the impurities-enriched degas stream might still be of sufficiently high quality that it could be injected into the gas grid, if the hydrogen contents are not too high. It could also be reliquefied while purging hydrogen and nitrogen, although that would be a possibly too capital-intensive process. Alternatively, it can be used as fuel at the plant, assisting in providing for the electricity demand of the production process.

In addition to methane, 15.415 kg/s (equal to 55.5 t/h) steam is produced, of which 2.94 kg/s (10.6 t/h) high-pressure steam and 12.474 kg/s (44.9 t/h) low-pressure steam, for a total ΔH_{vap} of 32.337 MW (5.043 MW HP, 27.294 MW LP). The discrepancy between these numbers and those given in Table 5.2 represents the heat capacity of the water, as the steam was raised from 60°C liquid water, produced by the desalinator.

Also, the use of self-made water to raise steam is not accounted for in Table 5.3. Ideally, as it is available at 175 °C, the mass output labeled *Process Water* is used first, because it might not meet the quality standards for drinking water. With HP-steam raised from the conditions of the dewatering streams WETPHASE, KNOCKOUT and OFFWATER, the optimized situation changes as shown in Table 5.4.

Table 5.4: Energy Analysis of the Two-Stage flowsheet by *Aspen Energy Analyzer*, with HP-steam raised from process water (175°C, 50 bar).

Utility	Current (MW)	Target (MW)	Pot. Savings (MW)
Coolant	11.68	7.688	3.987
LP-Steam	31.48	0.0590	31.42
HP-Steam	7.49	41.41	–33.92
Total Cooling	**50.64**	**49.16**	**1.483**

In this situation, the flow rate of high-pressure steam produced equals 13.1 t/h, which is entirely available; for the optimized scenario, 72.4 t/h is needed, which exceeds the availability of process water by a factor of three. Given that constrained availability of 175°C water, the exactly optimal allocation of cooling utilities is somewhere in between; the total cooling duty of the process water stream was calculated to amount to 24.52 MW. As before, the optimization potential is too insignificant to fully work out at this stage of the design process.

This supplementary analysis has shown that it is possible to use all process water to make high-pressure steam, while saving potable-quality water to be sold as drinking water. Returning this information to Table 5.3, the combined input-output analysis of process and utility streams is given in Table 5.5. This material balance sheet underlies the material cost estimations performed in Chapter 6.

Table 5.5: Input-output analysis of Process and Utility mass flows in the final methanation process design.

Inflows			Outflows		
Pyrolysis Oil	21.6	t/h	LNG (99.895%)	11.9	t/h
Seawater	457.9	t/h	Methane (92.6%)	556	kg/h
Nitrogen	21.0	t/h	Sea salt	6.4	t/h
ZnO	0.09	kg/h	ZnO	0.09	kg/h
Ni/13X	1	t/h	Ni/13X	1	t/h
			Offgas	24.3	t/h
			Drinking water	373.2	t/h
			H_2S	7.52	kg/h
			Hydrogen (excess)	58.7	kg/h
			Oxygen (excess)	22.8	t/h
			Ash	52.7	kg/h
			Steam, HP	25.3	t/h
			Steam, LP	35.9	t/h

5.4.3. Technical Key Performance Indicators

Table 5.6 shows an overview of the technical KPIs of the process flow sheet. The EY is fairly average for biomass-derived fuels: it is higher than those for FT or ammonia synthesis, but lower than the yields achieved by DME, MeOH or SNG production [139]; compared to SNG specifically, the lower energy yield is likely attributable to the inclusion of electrolysis in this process design. Also consistent with literature (see [26, 27, 28, 29]) is the practically full conversion of all fed carbon to methane, which demonstrates the working principle of sorption-enhancement.

Table 5.6: Technical Key Performance Indicators (KPIs) of the proposed production process.

KPI	Value	
$\dot{m}_{LNG}$	11.9	t/h
LHV_{LNG}	49.95	MJ/kg
EY	47.8	%
CCE (CH_4)	99.9	%
CCE (LNG)	95.6	%

6

Economic Analysis

To survive in a market economy, an industrial project needs to prove itself financially self-sufficient. To that end, this chapter performs a rudimentary economic analysis on the production process. Section 6.1 estimates the capital expenditure required to construct the facility. Section 6.2 provides an indication for operational costs to run the process. Section 6.3 assesses the potential sales value of the products. Section 6.4 summarizes the results of this economic analysis. Finally, Section 6.5 performs a sensitivity analysis on the impact of the most important money streams.

6.1. Capital Costs

Methods for estimating capital costs of proposed chemical process plants are described in textbooks like *Chemical Design Engineering* by Towler and Sinnott [140], and *Analysis, Synthesis and Design of Chemical Processes* by Turton *et al.*[141]. The final estimate will be an order of magnitude estimate, largely based on reported costs of facilities that use similar technologies.

Rough cost estimates are typically scaled across production capacity according to the formula

$$\frac{C_2}{C_1} = \left(\frac{S_2}{S_1}\right)^n \tag{6.1}$$

where C_i is the cost estimate at size S_i, and the exponent n typically varies from 0.4 – 0.5 for specialty chemicals and pharmaceuticals, to about 0.7 for petrochemical processes, up to between 0.8 – 0.9 for processes that use much mechanical work. The industry-wide average is approximately 0.6, why this relationship is commonly known as the *six-tenths rule* [140].

In order to account for the variability of prices over time, the estimates are subsequently indexed by the *Chemical Engineering Plant Cost Index* (CEPCI) to June 2024 [142].

6.1.1. Gasification

Dieterich *et al.* [139, 143, 144, 145] report capital costs for biomass EF gasification mostly lying between 10 – 20 M€ per 100 MW. Assuming similar expenditure for pyrolysis oil gasification, scaling down to 72 MW from the upper end of that range estimates the 2019 gasifier cost at €16.4 million, which equals €21.6 million in June 2024 [142].

6.1.2. Methanation

As mentioned in Section 2.1.2, SEM technology is about a decade old, as a result of which not many economic studies have been performed on SEM yet. Most of the literature reporting techno-economic evaluations of methanation processes considers variations of the traditional catalytic methanator setup: a sequence of multiple (typically 3 – 4) reactors with intercoolers in between.

Literature gives a wide capital cost range for methanation, from €130 up to €1500 per kW HHV of the methane produced; system boundaries in these are ill-defined, which contributes to the sizable uncertainty [146]. Specifically in the context of water electrolysis for CO_2 methanation, this range narrows down to about €450 [147] to €650 [148] per kW_{SNG}. Scaling up from the higher end of this range yields a CAPEX estimation worth €91.3 million in 2018, which equals €121 million in 2024. The resulting production cost for methane is €628/kW.

6.1.3. Cryogenic Liquefaction

According to the assessment of Capra *et al.* [132], capital investment for the RC-MR cryogenic liquefaction subprocess is estimated at €0.89 million, normalized to a methane stream of 4.6 t/d. Scaling that up to 12.5 t/h yields a CAPEX approximation valued at €10.9 million (2019), which puts the 2024 cost estimation at €14.4 million.

6.1.4. Desalination & Electrolysis

Because the selected technologies for desalination and electrolysis are still in their experimental phases or only very recently commercialized, thorough economic analysis on the exact technology or system design is not available. Therefore, estimations are partially based on similar technologies and designs for which techno-economic analysis was available.

SeaHydrogen Desalination

No economic studies have yet been performed on the SeaHydrogen concept, as it is still in the experimental stage of its development. For Membrane Distillation (MD) in general, Usman *et al.* [149] calculated that, when fully powered by waste heat, the water price (which contains both CAPEX and OPEX) can be reduced to \$1.6 per m³. For the system under design, that equals \$68 million (2024). The exchange rate is €0.96 to a dollar as of January of 2025 [150], which finalizes the desalination cost estimation at €70.8 million.

Battolysers

The 25 MW *Battolyser* units, 20 of which are provided for in the process design, are yet to be commercialized, which is planned for the third quarter of 2026 [89]. Generally, however, literature provides estimations for the order of magnitude of the CAPEX of an electrolyzer. Park *et al.* [151] assume \$880 per kW (PEM) in Korea, Gorre *et al.* [147] cite €650 per kW (AE), and Witte *et al.* [146] quote €930 per kW (AE). On the optimistic end, Iaquaniello *et al.* [148] believe that AE CAPEX by 2030 will be brought down to €500 – €600 per kW (paper reads ”per kWh”, likely mistaken) due to increased research, development, and deployment (RD&D) funding, based on an expert survey [152].

Considering these numbers, as well as the novelty of the *Battolyser* appliances, a conservative estimate was made for this work amounting to €1000 per kW (1 M€/MW installed), which makes the entire electrolysis stack cost €500 million.

6.1.5. Total Capital Costs

The five primary process units thus sum to a capital cost estimate of €727.8 million. To finalize the CAPEX estimation, a substantial margin was added to account for the gas cleaning equipment, storage tanks, engineering costs and contingency charges; the final total CAPEX estimate is worth €1000 million. Figure 6.1 visualizes the makeup of this guesstimate.

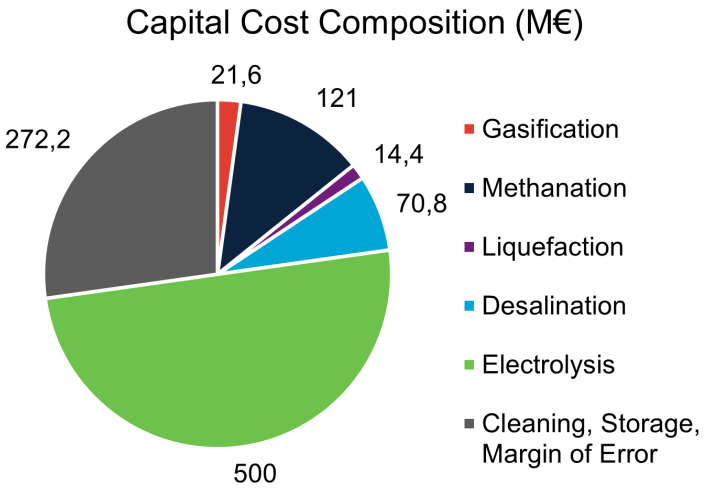

Figure 6.1: Composition of the CAPEX estimation. Total CAPEX equals €1000 million.

6.2. Operational Costs

Operational costs are subdivided into 3 categories: expenses for operation and maintenance, acquisition costs for the materials and utilities required, and salaries for the labor operating the facility. Operation and maintenance (O&M) costs are touched upon in Section 6.2.1, material and utility costs are estimated in Section 6.2.2, and labor costs are discussed in Section 6.2.3.

6.2.1. Operation and Maintenance Costs

Annual O&M cost estimates are typically formulated as a fraction of the cost of the plant itself, typically 3% for plants that handle gases and liquids, and around 5% for plants that work solids and significant mechanical equipment [140]. Observing some margin for error, the yearly O&M expenses will be estimated at 3% of CAPEX, which equals €30 million annually.

6.2.2. Materials and Utilities Costs

Material Costs

Estimations for material costs are made as follows:

- For pyrolysis oil, a price around €200 per ton is assumed. This is slightly lower than the €300 per ton mentioned in a 2012 symposium presentation by BTG [153], but well within the limits reported by the European Biomass Industry Association (EUBIA) [154];
- The catalytic sorbent Ni/13X particles will have to be custom-made, either in-house or by a as of now non-existent supplier; as such, its acquisition price is estimated to be in the order of €1000 per ton;
- For the nitrogen supply, a cost rate of €20 per ton is assumed, noting that a cryogenic air separation unit on site might be an economically better decision [155, 156];
- It will be assumed that seawater can be used without compensation, and that ZnO is unlikely to have a significant impact on the cost rate.

Utilities Costs

Electricity is needed primarily in two places: some 236 MW is used for electrolysis alone (as shown in Table B.2), and cryogenic liquefaction demands 10.6 MW at 0.85 kWh/kg methane [132]; the gasification and methanation processes require almost none. Additionally accounting for control and safety equipment, the plant electricity demand is estimated to be 250 MW.

The costs of electricity acquired from offshore wind parks *Hollandse Kust* (north, south, and west) were modeled to range from €61 – €66 per MWh [157], so €64/MWh was assumed.

The total cost rate based on these estimations is given in Table 6.1.

Table 6.1: Price estimations of Material and Utility Inputs.

Inflows	Unit	Consumption (units/h)	Unit Price (€/unit)	Cost Rate (€/h)
Pyrolysis Oil	t	21.6	200	4320
Seawater	t	457.9	0	0
Ni13X	t	1.0	1000	1000
Nitrogen	t	21.0	20	420
Electricity	MWh	250	64	16000
Total Costs	**€/h**			**21750**

As shown in Table 6.1, electricity is the most expensive input of the process, at some three quarters of the total material cost rate. Over an operational year of 8400 hours, the annual costs amount to €182.7 million.

6.2.3. Labor Costs

The plant is assumed to require 24 full-time positions (four shifts of 5 – 6 operators), whose salary estimate amounts to €60,000 per year per FTE [132], for a total of €1.44 million annually. An extra €60,000 is added for supervision and management, which rounds the total labor cost estimate at €1.5 million per year.

6.2.4. Total Operational Costs

The total OPEX estimate thus is €214.1 million annually. Figure 6.2 shows the breakdown of the estimated OPEX, from which it is clear that the proposed production process is heavily capital-intensive, with labor accounting for only 0.7% of operational expenses.

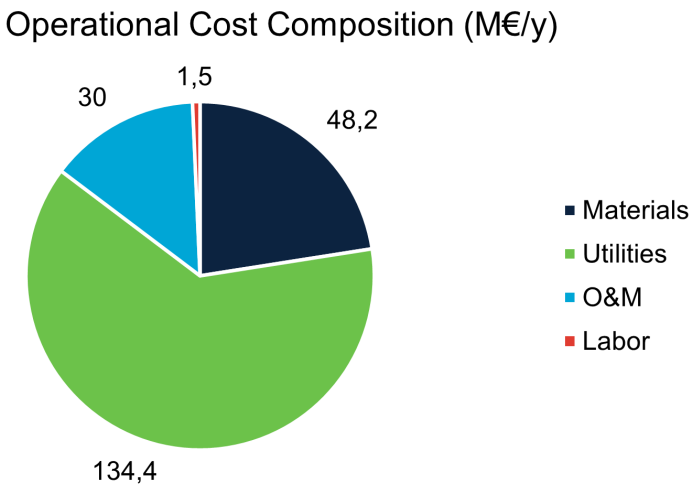

Figure 6.2: Composition of the OPEX estimation. Total OPEX equals €214.1 million annually.

6.3. Revenues

As of November 2024, Bio-LNG retails for €2.179 per liter in the Netherlands [158]; excluding taxes [159], actual sales revenues amount to €1.61 per liter. The mass density of LNG was calculated to be 410 kg/m³. The methane-rich off-gas separated from the cryogenic liquefaction unit is valued for now at the natural gas market price of €0.48 per cubic meter [160], even though it might be too hydrogen-rich for injection into the gas grid.

Price estimations for the minor products were made as follows:

- For sea salt, bulk prices about €250 per ton were found online for applications like road salt and animal feed. Culinary sea salt may have stricter quality requirements, but is also significantly more valuable with bulk prices close to €1/kg [161, 162]. Based on these prices, an overall sales price of €300 per ton salt is assumed;
- Drinking water in and around Rotterdam is quoted at €0.95 per m³ [163];
- In a report by CE Delft, potential buyers for green hydrogen are cited as expecting a price range of €8 – €15 per kg for the 2027 – 2030 period [164]; from the middle of that range, €12 per kg was assumed reasonable;
- Steam prices found vary in the range of €30 – €40 per ton [165, 166, 167, 168], within which high-pressure steam represents more value than low-pressure steam;
- The sale of any H_2S is unlikely to significantly impact the resulting figures and will be ignored.

Table 6.2 contains an overview of the income streams resulting from these price estimations. It appears that 67.5% of income is generated by the sale of the primary LNG product; as a result, the plant revenue is highly sensitive to fluctuations in the liquid gas price. For this base scenario, in an 8400 hour operational year, the annual revenue amounts to €581.7 million.

Table 6.2: Price estimations of Material and Utility Outputs.

Outflows	Unit	Production (units/h)	Unit Price (€/unit)	Revenue (€/h)
LNG (99.895%)	kg	11900	3.93	46750
Methane (92.6%)	m³	171	0.48	82
Sea salt	t	6.42	300	19250
Drinking water	t	373	0.95	354
Hydrogen (excess)	kg	58.7	12	704
Steam, HP	t	25.3	38	960
Steam, LP	t	35.9	32	1150
Total Revenue	**€/h**			**69250**

6.4. Economic Results

Considering that operational expenses were estimated at €214.1 million a year as per Section 6.2.4 and revenues at €581.7 million annually according to Section 6.3, the proposed project would run an annual operational profit of €367.6 million. The fact that this number is positive indicates that the project is likely economically feasible.

Amortizing the €1 billion CAPEX (Section 6.1.5) over a period of 20 years yields €50 million per year, which totals the average cost of the plant at €264.1 million annually. Figure 6.3 visualizes the contributions of each class of expenses to this yearly sum.

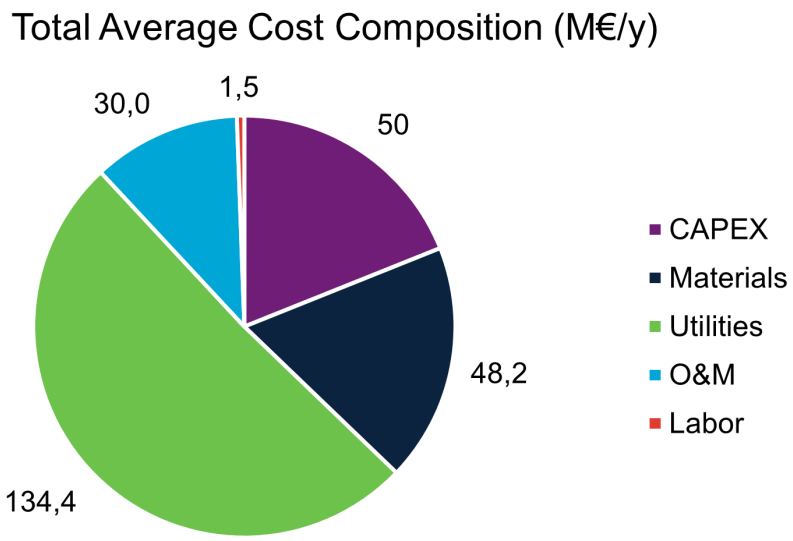

Figure 6.3: Composition of the Total Annual Cost estimation. Total AC equals €264.1 million annually.

With the interest rate set at 4% and the project life time at 20 years, the **NPV** of the project proposal was calculated to be **€3995.6 million**, and the **IRR** equal to **36.7%**. In summary, these key economic indicators are positive about the prospects of the proposed production process plant.

6.4.1. Economic Key Performance Indicators

Table 6.3 contains an overview of the economic KPIs of the proposed process, and contrasts them with four other biomass-to-X processes evaluated by Dieterich *et al.* [139]: SNG, FT-fuel, DME, and MeOH.

Both CAPEX and OPEX are significantly higher for LNG in this thesis than any of the four biofuels in [139]; OPEX is just over three times larger, CAPEX even over five times. This reflects the cost of including electrolysis for additional hydrogen: [139] never considered introducing hydrogen into their process designs, evidenced by the fact that hydrogen is omitted from their cost estimations for raw materials.

Even so, the LCOM of bio-LNG in this thesis are generally lower than all biofuels analyzed by [139]. The mass-specific LCOM is marginally higher than that of DME, the volume-specific LCOM is the lowest of all liquids, and the energy-specific LCOM is the least of all alternatives.

Table 6.3: Economic Key Performance Indicators (KPIs) of the proposed LNG production process, compared to four biofuels analyzed by Dieterich *et al.* [139].

KPI		Unit	LNG	SNG	FT	DME	MeOH
CAPEX		M€	1000				
		M€/MW$_{bio}$	9.92	1.58	1.72	1.82	1.73
OPEX		M€/y	214.1				
		€/MWh$_{bio}$	252.9	70.45	73.65	76.40	70.49
LCOM	(m)	€/kg	2.64	3.55	4.05	2.37	1.56
	(V)	€/L	1.08	0.07	3.21	1.56	1.24
	(E)	€/MWh	190.4	282.4	421.9	296.7	283.5

6.5. Sensitivity Analysis

The NPV and IRR of this project proposal, as calculated in Section 6.4, were subsequently subjected to sensitivity analysis with respect to the five variables that are deemed most likely to significantly impact the results:

1. CAPEX;
2. Acquisition price of pyrolysis oil;
3. Price of electricity;
4. Catalyst costs;
5. LNG sales price.

The values of these parameters were varied from –50% to +50%, and the resulting impact on both NPV and IRR was tabulated. CAPEX was only assessed to –20%, as further reduction is considered unrealistic. Figure 6.4 shows the sensitivity of the NPV to the five selected variables, and Figure 6.5 that of the IRR.

It is apparent from both these figures, and most clearly from the NPV sensitivity graph, that the projected income (the sales price of LNG) is the most impactful parameter of the five. Yet, even when the income from LNG sales is halved, both NPV and IRR remain positive, at €1327.1 million and 16.3%, respectively.

Electrolysis still shows to be the economically most important subprocess, with CAPEX and electrical energy as the next two most important parameters. The electrolyzers make up 50% of the CAPEX (Figure 6.3), while the electricity runs those electrolyzers.

Because the LNG market price cannot be controlled, electrolysis is the section of the process where the most effective financial improvements can be made. It would be beneficial for both NPV and especially IRR if the construction and installation of electrolysis units turns out closer to the €500 – €600 per kW of Iaquaniello *et al.* [148] than to the €1000 per kW used in this work.

Compared to the other three parameters, the pyrolysis oil and catalyst costs have a relatively minimal impact on the final economic results.

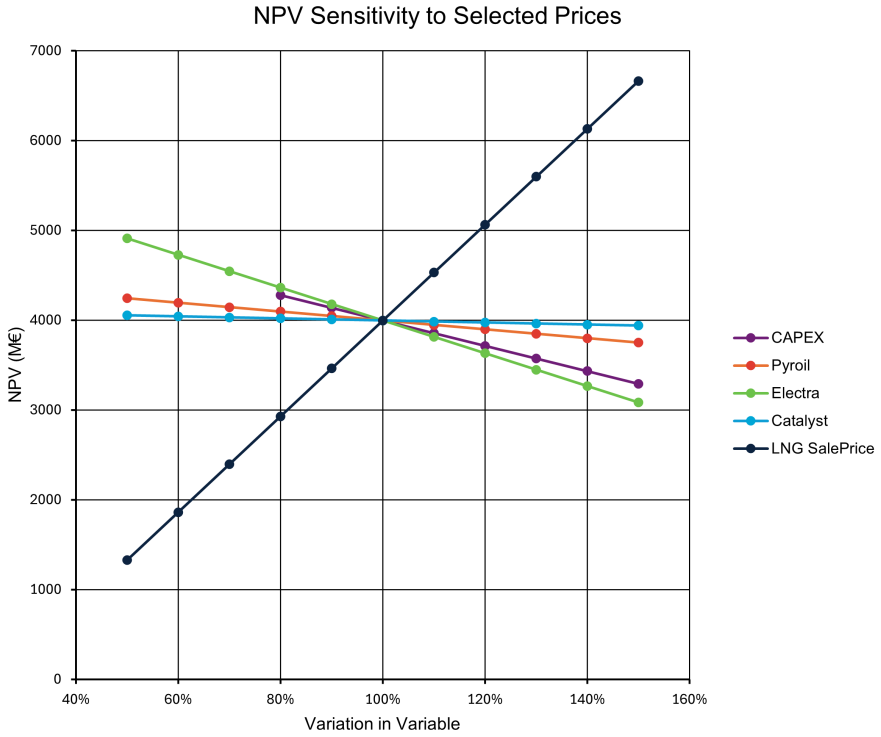

Figure 6.4: NPV Sensitivity to the five selected parameters.

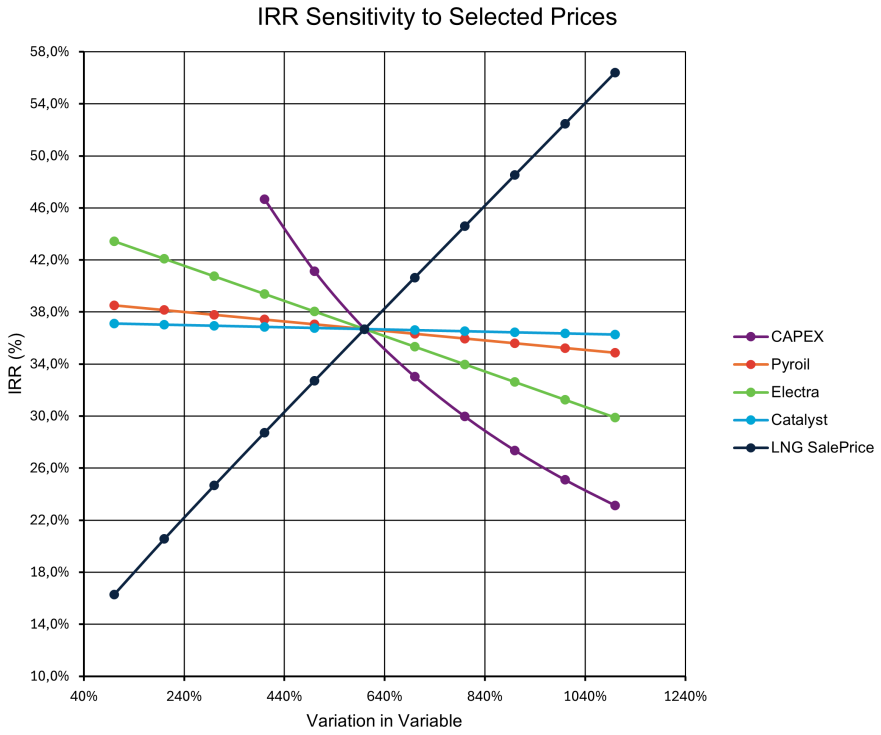

Figure 6.5: IRR Sensitivity to the five selected parameters.

7

Conclusion & Recommendations

7.1. Conclusion

In this thesis, a production process was designed and evaluated for the synthesis of Liquid Natural Gas from pyrolysis oil derived from Dutch domestic biomass sources. Based on the acquisition of 6 kg/s (21.6 t/h) biomass pyrolysis oil, 11.9 t/h LNG is produced at 99.9% purity, in addition to over 6 t/h of salt, 373 m³/h of drinking water, and various minor byproducts. The process flow sheet is attached as Appendix B.2.

Subsequent economic evaluation of the proposed production process indicates that the project NPV is worth just under €4 billion given an interest rate of 4%, and the IRR equals 36.7%. Sensitivity analysis performed on five variables shows that the LNG sales price is the most important variable in these results, followed by the capital costs and electricity acquisition price.

The techno-economic Key Performance Indicators (KPIs) given in Tables 5.6 and 6.3 are combined into a single overview in Table 7.1. Technically, the EY is comparable to other biomass-derived fuels, while the exceptional CCE is the signature characteristic of sorption-enhancement. Economically, even though both the CAPEX and OPEX are considerable, the LCOM compare favorably to other biomass-to-X processes.

Table 7.1: Techno-economic Key Performance Indicators (KPIs) of the proposed production process.

Technical KPI	Value		Economic KPI		Value	
$\dot{m}_{LNG}$	11.9	t/h	CAPEX		1000	M€
LHV_{LNG}	49.95	MJ/kg			9.92	M€/MW_{bio}
EY	47.8	%	OPEX		214.1	M€/y
CCE (CH_4)	99.9	%			252.9	€/MWh_{bio}
CCE (LNG)	95.6	%	LCOM	(m)	2.64	€/kg_{LNG}
				(V)	1.08	€/L_{LNG}
				(E)	190.4	€/MWh_{LNG}

The projected LNG production equals about 0.1 Mt a year (4.99 PJ), which equals around 0.75% by LHV of the Dutch LNG imports in 2024. Alternatively, if applied only to mobility, it covers 1.32% of the energy use of Dutch road traffic. Because the assumed size of the facility is based on 10% of Dutch woody biomass, the ultimate consequence is that a maximum of approximately 13% of road traffic could be fueled by fully domestically produced biomethane; realistically, 10% of road-going traffic is highly ambitious.

This scenario highlights that the Netherlands is a very energy-intensive country, unlikely to ever achieve full energy independence. Yet, in combination with other renewable resources and supplies from trusted foreign trading partners, domestic biomass can absolutely contribute to sustained energy security.

7.2. Recommendations

Firstly, a Sorption-Enhanced Methanator should be applied as a final unit in a methanation process. A single-step, full-SEM process is technically feasible, but its heat input requirements are so high that it is energetically inferior to a two-stage setup; on top of that, the financial burden of the extra needed catalyst suggests that even from a purely economical point of view, a design with a SEM final stage is the more sensible idea.

Additional research is required to verify the results as described, preferably employing other software like *Aspen Adsorption*, followed by potential experimental work. Part of those experiments needs to be an investigation into the attrition and abrasion suffered by the zeolite particles when subjected to a Fluidized Bed regime.

Also, in the general interest of modeling studies into sorption processes, a more intuitive implementation of zeolites in *Aspen Plus* would be highly appreciated. Ideally, zeolites should be a separate class of unconventional solids within *Aspen Plus*, with their thermodynamic and kinetic behavior under sorption for at least H_2O and CO_2 preprogrammed, and the sorbent loading as an output parameter.

Then, in order to take advantage of the fluctuations in electricity prices and the battery function of the Battolyser, it may well be worth to store cheap wind energy to be sold when electricity supply is low. This could provide additional income, although it would need corresponding investment in the most expensive part of the design. If the capital costs for electrolysis actually are lower than the €1000 per kW assumed in this thesis, that extra capacity may well be affordable.

On a system level, it might be worth to look into the potential of harder-to-use waste streams like demolition wood. These types of biomass may require additional pretreatment and potentially extra syngas cleaning subunits; therefore, this investment will have to be justified by the additional revenue it provides.

Another such avenue for expansion could be the use of hydrothermal liquefaction (HTL) for wet feedstocks that are not suited for pyrolysis, like manure, as it yields a similar oil. Currently, the best method to valorize excess manure is fermentation, which produces a biogas that is about equal parts methane and CO_2 and needs to be upgraded. Such process would, however, only need significantly smaller-scale methanation and electrolysis units.

References

[1] "KNMI: 2023 natste en warmste jaar sinds begin metingen". In: *NOS.nl* (Dec. 29, 2023). URL: https://nos.nl/collectie/13871/artikel/2503101-knmi-2023-natste-en-warmste-jaar-sinds-begin-metingen (visited on 04/22/2024).

[2] K. van der Wiel. "Klimaatstreepjescode 1901-2023". In: *KNMI* (Dec. 27, 2023). URL: https://www.knmi.nl/over-het-knmi/nieuws/klimaatstreepjescode-1901-2023 (visited on 04/22/2024).

[3] K. van der Wiel. "Van blauw naar rood: klimaatverandering in beeld". In: *KNMI* (Dec. 20, 2024). URL: https://www.knmi.nl/over-het-knmi/nieuws/klimaatstreepjescode-2024 (visited on 01/09/2025).

[4] E. van den Besselaar, G. van der Schrier, and T. Vlemmix. "Europa was in 2023 uitzonderlijk warm en nat". In: *KNMI* (Apr. 22, 2024). URL: https://www.knmi.nl/over-het-knmi/nieuws/europa-was-in-2023-uitzonderlijk-warm-en-nat (visited on 04/22/2024).

[5] *European State of the Climate – Report 2023*. Tech. rep. Copernicus Climate Change Service (C3S) and World Meteorological Organization (WMO), 2024. URL: https://climate.copernicus.eu/esotc/2023 (visited on 04/22/2024).

[6] IPCC. *Climate Change 2023: Synthesis Report*. Contribution of Working Groups I, II and III to the Sixth Assessment Report of the Intergovernmental Panel on Climate Change [Core Writing Team, H. Lee and J. Romero (eds.)] Geneva, Switzerland: IPCC, 2023. DOI: 10.59327/IPCC/AR6-9789291691647.

[7] IOR Energy. *Engineering Conversion Factors*. 2010. URL: https://web.archive.org/web/20100825042309/http://www.ior.com.au:80/ecflist.html (visited on 08/25/2010).

[8] B.R. Cooper and W.A. Ellingson. *The Science and Technology of Coal and Coal Utilization*. Boston, MA: Springer US, 1984. DOI: 10.1007/978-1-4684-4580-0_1.

[9] *Handbook of Chemistry and Physics*. 8th Ed. CRC, 1920.

[10] Panasonic. *Lithium Ion NCR18650B*. 2015. URL: https://web.archive.org/web/20150722042425/http://industrial.panasonic.com/lecs/www-data/pdf2/ACA4000/ACA4000CE417.pdf (visited on 07/22/2015).

[11] *The Coal Resource: A comprehensive overview of coal*. Original Title: Coal - Power for Progress. London, UK: World Coal Institute (now FutureCoal), 2009.

[12] *Statistical Review of World Energy*. Tech. rep. Energy Institute, 2023. URL: https://www.energyinst.org/statistical-review (visited on 04/24/2024).

[13] Our World in Data. *Years of Fossil Fuel Reserves Left, 2020*. 2023. URL: https://ourworldindata.org/grapher/years-of-fossil-fuel-reserves-left (visited on 04/24/2024).

[14] R. Koster. "CO_2 van industrie wordt afgevangen en opgeslagen onder Noordzee". In: *NOS.nl* (Apr. 13, 2024). URL: https://nos.nl/artikel/2516624-co2-van-industrie-wordt-afgevangen-en-opgeslagen-onder-noordzee (visited on 04/25/2024).

[15] *Port of Rotterdam*. 2024. URL: https://www.portofrotterdam.com/en/ (visited on 03/06/2024).

[16] *Porthos*. 2023. URL: https://www.porthosco2.nl/en/ (visited on 04/25/2024).

[17] S.P. Lynch. "2 - Hydrogen embrittlement (HE) phenomena and mechanisms". In: *Stress Corrosion Cracking*. Ed. by V.S. Raja and T. Shoji. Woodhead Publishing Series in Metals and Surface Engineering. Woodhead Publishing, 2011, pp. 90–130. DOI: 10.1533/9780857093769.1.90.

[18] N. Klopčič, I. Grimmer, F. Winkler, M. Sartory, and A. Trattner. “A review on metal hydride materials for hydrogen storage”. In: *Journal of Energy Storage* 72 (2023), p. 108456. DOI: 10.1016/j.est.2023.108456.

[19] RVO. *Wat is netcongestie en wat betekent dit voor uw bedrijf?* July 15, 2024. URL: https://www.rvo.nl/onderwerpen/netcongestie/wat-netcongestie (visited on 02/18/2025).

[20] Ministerie van Klimaat en Groene Groei. *Kamerbrief Stand van Zaken Netcongestie*. Nov. 21, 2024. URL: https://www.rijksoverheid.nl/documenten/kamerstukken/2024/11/21/kamerbrief-netcongestie (visited on 02/18/2025).

[21] Netbeheer Nederland. *Capaciteitskaart elektriciteitsnet*. URL: https://capaciteitskaart.netbeheernederland.nl/ (visited on 02/18/2025).

[22] J.M. Douglas. “A Hierarchical Decision Procedure for Process Synthesis”. In: *AIChE Journal* 31.3 (1985), pp. 353–362. DOI: 10.1002/aic.690310302.

[23] P. Sabatier and J.B. Senderens. “New methane synthesis”. In: *CR de l’Académie des Sciences à Paris* 134 (1902), pp. 514–516.

[24] J. Kopyscinski, T.J. Schildhauer, and S.M.A. Biollaz. “Production of synthetic natural gas (SNG) from coal and dry biomass – A technology review from 1950 to 2009”. In: *Fuel* 89.8 (2010), pp. 1763–1783. DOI: 10.1016/j.fuel.2010.01.027.

[25] W. de Jong and J.R. van Ommen. *Biomass as a Sustainable Energy Source for the Future*. Wiley, 2015.

[26] A. Borgschulte et al. “Sorption enhanced CO_2 methanation”. In: *Physical Chemistry Chemical Physics* 15 (2013), pp. 9620–9625. DOI: 10.1039/C3CP51408K.

[27] S. Walspurger, W.G. Haije, and B. Louis. “CO_2 Reduction to Substitute Natural Gas: Toward a Global Low Carbon Energy System”. In: *Israel Journal of Chemistry* 54.10 (2014), pp. 1432–1442. DOI: 10.1002/ijch.201300135.

[28] S. Walspurger, G.D. Elzinga, J.W. Dijkstra, M. Sarić, and W.G. Haije. “Sorption enhanced methanation for substitute natural gas production: Experimental results and thermodynamic considerations”. In: *Chemical Engineering Journal* 242 (2014), pp. 379–386. DOI: 10.1016/j.cej.2013.12.045.

[29] A. Catarina Faria, C.V. Miguel, and L.M. Madeira. “Thermodynamic analysis of the CO_2 methanation reaction with in situ water removal for biogas upgrading”. In: *Journal of CO_2 Utilization* 26 (2018), pp. 271–280. DOI: 10.1016/j.jcou.2018.05.005.

[30] L.P.L.M. Rabou and M.H.F. Overwijk. “The Alkmaar 4 MW bio-SNG demo project”. In: *3rd International Conference on Renewable Energy Gas Technology*. Malmö, Sweden: ECN, Mar. 2016. URL: http://resolver.tudelft.nl/uuid:debdb363-11a2-4ee3-a80f-2aa18402ff7b.

[31] U. Zuberbühler. “Adjusting methanation stoichiometry via AER process”. In: *BioSNG 09 – International conference on advanced biomass-to-SNG technologies and their market implementation*. Zürich, Switzerland, 2009.

[32] B.T. Carvill, J.R. Hufton, M. Anand, and S. Sircar. “Sorption-enhanced reaction process”. In: *AIChE Journal* 42.10 (1996), pp. 2765–2772. DOI: 10.1002/aic.690421008.

[33] Wei L. “Sorption Enhanced CO_2 methanation for large scale energy storage”. PhD thesis. Delft University of Technology, 2022.

[34] Wei L. et al. “Can bi-functional nickel modified 13X and 5A zeolite catalysts for CO_2 methanation be improved by introducing ruthenium?” In: *Molecular Catalysis* 494 (2020), p. 111115. DOI: 10.1016/j.mcat.2020.111115.

[35] Wei L. et al. “Sub-nanometer ceria-promoted Ni 13X zeolite catalyst for CO_2 methanation”. In: *Applied Catalysis A: General* 612 (2021), p. 118012. DOI: 10.1016/j.apcata.2021.118012.

[36] L. Gómez, I. Martínez, M.V. Navarro, T. García, and R. Murillo. “Sorption-enhanced CO and CO_2 methanation (SEM) for the production of high purity methane”. In: *Chemical Engineering Journal* 440 (2022), p. 135842. DOI: 10.1016/j.cej.2022.135842.

[37] A. Coppola, F. Massa, and F. Scala. “Simulation of a sorption-enhanced methanation process with CaO in a dual interconnected fluidized bed system”. In: *Fuel* 339 (2023), p. 127374. DOI: 10.1016/j.fuel.2022.127374.

[38] P. Bareschino, G. Piso, F. Pepe, C. Tregambi, and E. Mancusi. “Numerical modelling of a sorption-enhanced methanation system”. In: *Chemical Engineering Science* 277 (2023), p. 118876. DOI: 10.1016/j.ces.2023.118876.

[39] A. Cañada-Barcala, M. Larriba, V.I. Águeda Maté, and J.A. Delgado Dobladez. “Synthetic natural gas production through biogas methanation using a sorption-enhanced reaction process”. In: *Separation & Purification Technology* 331 (2024), p. 125714. DOI: 10.1016/j.seppur.2023.125714.

[40] R. Delmelle et al. “Development of improved nickel catalysts for sorption enhanced CO_2 methanation”. In: *International Journal of Hydrogen Energy* 41.44 (2016), pp. 20185–20191. DOI: 10.1016/j.ijhydene.2016.09.045.

[41] F. Massa, A. Coppola, and F. Scala. “A thermodynamic study of sorption-enhanced CO_2 methanation at low pressure”. In: *Journal of CO_2 Utilization* 35 (2020), pp. 176–184. DOI: 10.1016/j.jcou.2019.09.014.

[42] A. Coppola, F. Massa, P. Salatino, and F. Scala. “Fluidized bed CaO hydration-dehydration cycles for application to sorption-enhanced methanation”. In: *Combustion Science & Technology* 191.9 (2019), pp. 1724–1733. DOI: 10.1080/00102202.2019.1640689.

[43] A. Coppola, F. Massa, P. Salatino, and F. Scala. “Evaluation of two sorbents for the sorption-enhanced methanation in a dual fluidized bed system”. In: *Biomass Conversion & Biorefinery* 11 (2021), pp. 111–119. DOI: 10.1007/s13399-020-00829-4.

[44] Wei L. et al. “Influence of nickel precursors on the properties en performance of Ni-impregnated zeolite 5A and 13X catalysts in CO_2 methanation”. In: *Catalysis Today* 362 (2021). 1st International Conference on Unconventional Catalysis, Reactors and Applications: Catalysis Beyond the Reactor, pp. 35–46. DOI: 10.1016/j.cattod.2020.05.025.

[45] DNV GL. *Requirements for gas quality and gas appliances*. Tech. rep. Report No. 74106553.01b. Groningen, 2015.

[46] Zheng J., Zhu Y., Zhu M., Kang K., and Sun R. “A review of gasification of bio-oil for gas production”. In: *Sustainable Energy Fuels* 3 (2019), pp. 1600–1622. DOI: 10.1039/C8SE00553B.

[47] N. Dahmen et al. “State of the art of the bioliq® process for synthetic biofuels production”. In: *Environmental Progress & Sustainable Energy* 31.2 (2012), pp. 176–181. DOI: 10.1002/ep.10624.

[48] Q. Fradet, M. Braun-Unkhoff, and U. Riedel. “Parametrization of a Sectional Approach for the Entrained-Flow Gasification of Biomass Char”. In: *Energy Fuels* 35.19 (2021), pp. 15752–15769. DOI: 10.1021/acs.energyfuels.1c01946.

[49] M. Cortazar et al. “Syngas production by bio-oil steam gasification in a fountain confined conical spouted bed reactor”. In: *Fuel* 345 (2023), p. 128228. DOI: 10.1016/j.fuel.2023.128228.

[50] A. Buelvas et al. “Gasification of solid biomass or fast pyrolysis bio-oil: Comparative energy and exergy analyses using AspenPlus®”. In: *Engineering Reports* (2024), e12825. DOI: 10.1002/eng2.12825.

[51] M. Pozzo, A. Lanzini, and M. Santarelli. “Enhanced biomass-to-liquid (BTL) conversion process through high temperature co-electrolysis in a solid oxide electrolysis cell (SOEC)”. In: *Fuel* 145 (2015), pp. 39–49. DOI: 10.1016/j.fuel.2014.12.066.

[52] R. Anghilante et al. “Innovative power-to-gas plant concepts for upgrading of gasification bio-syngas through steam electrolysis and catalytic methanation”. In: *Energy Conversion & Management* 183 (2019), pp. 462–473. DOI: 10.1016/j.enconman.2018.12.101.

[53] P. Bareschino et al. “Integration of biomasses gasification and renewable-energies-driven water electrolysis for methane production”. In: *Energy* 230 (2021), p. 120863. DOI: 10.1016/j.energy.2021.120863.

[54] F. Miccio, A. Picarelli, and G. Ruoppolo. “Increasing tar and hydrocarbons conversion by catalysis in bubbling fluidized bed gasifiers”. In: *Fuel Processing Technology* 141 (2016), pp. 31–37. DOI: 10.1016/j.fuproc.2015.06.007.

[55] F. Miccio, B. Piriou, G. Ruoppolo, and R. Chirone. “Biomass gasification in a catalytic fluidized reactor with beds of different materials”. In: *Chemical Engineering Journal* 154.1 (2009). XVIII International Conference on Chemical Reactors - CHEMREACTOR -18 (September 29 - October 3, 2008, Malta), pp. 369–374. DOI: 10.1016/j.cej.2009.04.002.

[56] I. Martínez, M.S. Callén, G. Grasa, J.M. López, and R. Murillo. “Sorption-enhanced gasification (SEG) of agroforestry residues: Influence of feedstock and main operating variables on product gas quality”. In: *Fuel Processing Technology* 226 (2022), p. 107074. DOI: 10.1016/j.fuproc.2021.107074.

[57] E. Kurkela, M. Kurkela, and I. Hiltunen. “Steam–oxygen gasification of forest residues and bark followed by hot gas filtration and catalytic reforming of tars: Results of an extended time test”. In: *Fuel Processing Technology* 141 (2016), pp. 148–158. DOI: 10.1016/j.fuproc.2015.06.005.

[58] E. Giglio, G. Vitale, A. Lanzini, and M. Santarelli. “Integration between biomass gasification and high-temperature electrolysis for synthetic methane production”. In: *Biomass and Bioenergy* 148 (2021), p. 106017. DOI: 10.1016/j.biombioe.2021.106017.

[59] I. Martínez and M.C. Romano. “Flexible sorption enhanced gasification (SEG) of biomass for the production of synthetic natural gas (SNG) and liquid biofuels: Process assessment of stand-alone and power-to-gas plant schemes for SNG production”. In: *Energy* 113 (2016), pp. 615–630. DOI: 10.1016/j.energy.2016.07.026.

[60] H. Hofbauer, R. Rauch, K. Bosch, R. Koch, and C. Aichernig. “Biomass CHP Plant Güssing – a success story”. In: *Proceedings of the Expert Meeting on Pyrolysis and Gasification of Biomass and Waste, Strasbourg, France*. Vol. 30. 2002.

[61] M. Gassner and F. Maréchal. “Thermo-economic optimisation of the polygeneration of synthetic natural gas (SNG), power and heat from lignocellulosic biomass by gasification and methanation”. In: *Energy & Environmental Science* 5 (2012), pp. 5768–5789. DOI: 10.1039/C1EE02867G.

[62] Q. Bernical et al. “Integrated Design of High Temperature Steam Electrolysis and Biomass to Liquid Fuel Process”. In: *11th International Symposium on Process Systems Engineering*. Ed. by I.A. Karimi and R. Srinivasan. Vol. 31. Computer Aided Chemical Engineering. Elsevier, 2012, pp. 865–869. DOI: 10.1016/B978-0-444-59506-5.50004-3.

[63] M. Gassner and F. Maréchal. “Thermo-economic optimisation of the integration of electrolysis in synthetic natural gas production from wood”. In: *Energy* 33.2 (2008). 19th International Conference on Efficiency, Cost, Optimization, Simulation and Environmental Impact of Energy Systems, pp. 189–198. DOI: 10.1016/j.energy.2007.09.010.

[64] M. Gassner and F. Maréchal. “Thermo-economic process model for thermochemical production of Synthetic Natural Gas (SNG) from lignocellulosic biomass”. In: *Biomass & Bioenergy* 33.11 (2009), pp. 1587–1604. DOI: 10.1016/j.biombioe.2009.08.004.

[65] L. Gómez, G. Grasa, I. Martínez, and R. Murillo. “Performance study of a methanation process for a syngas obtained from a sorption enhanced gasification process”. In: *Chemical Engineering Science* 267 (2023), p. 118291. DOI: 10.1016/j.ces.2022.118291.

[66] M. Latifi, F. Berruti, and C. Briens. “Thermal and catalytic gasification of bio-oils in the Jiggle Bed Reactor for syngas production”. In: *International Journal of Hydrogen Energy* 40.17 (2015), pp. 5856–5868. DOI: 10.1016/j.ijhydene.2015.02.088.

[67] M.H. Ghezelchi and Wu H. “Modelling of bio-oil steam gasification in a fluidized bed reactor”. In: *Fuel* 220 (2018), pp. 575–585. DOI: 10.1016/j.fuel.2018.02.036.

[68] Zheng J., Zhu Y., Zhu M., Wu H., and Sun R. “Bio-oil gasification using air - Steam as gasifying agents in an entrained flow gasifier”. In: *Energy* 142 (2018), pp. 426–435. DOI: 10.1016/j.energy.2017.10.031.

[69] E.J. Leijenhorst et al. “Entrained flow gasification of straw- and wood-derived pyrolysis oil in a pressurized oxygen blown gasifier”. In: *Biomass & Bioenergy* 79 (2015). The 22nd European Biomass Conference and Exhibition held in Hamburg, June 2014, pp. 166–176. DOI: 10.1016/j.biombioe.2014.11.020.

[70] D.C. de Oliveira, E.E.S. Lora, O.J. Venturini, D.M.Y. Maya, and M. Garcia-Pérez. “Gas cleaning systems for integrating biomass gasification with Fischer-Tropsch synthesis - A review of impurity removal processes and their sequences”. In: *Renewable & Sustainable Energy Reviews* 172 (2023), p. 113047. DOI: 10.1016/j.rser.2022.113047.

[71] Prabhansu, M.Kr. Karmakar, P. Chandra, and P.Kr. Chatterjee. “A review on the fuel gas cleaning technologies in gasification process”. In: *Journal of Environmental Chemical Engineering* 3.2 (2015), pp. 689–702. DOI: 10.1016/j.jece.2015.02.011.

[72] M. Asadullah. “Biomass gasification gas cleaning for downstream applications: A comparative critical review”. In: *Renewable & Sustainable Energy Reviews* 40 (2014), pp. 118–132. DOI: 10.1016/j.rser.2014.07.132.

[73] S. Heidenreich. “Hot gas filtration – A review”. In: *Fuel* 104 (2013). 10th Japan/China Symposium on Coal and C1 Chemistry, pp. 83–94. DOI: 10.1016/j.fuel.2012.07.059.

[74] S. Bengtsson. “The CHRISGAS project”. In: *Biomass & Bioenergy* 35 (2011). CHRISGAS, S2–S7. DOI: 10.1016/j.biombioe.2011.08.012.

[75] S. Bengtsson. “VVBGC demonstration plant activities at Värnamo”. In: *Biomass & Bioenergy* 35 (2011). CHRISGAS, S16–S20. DOI: 10.1016/j.biombioe.2011.03.034.

[76] S. Heidenreich et al. “Hot gas filtration for syngas cleaning in biomass gasification; [Heißgasfiltration zur synthesegasreinigung in der biomassevergasung]”. In: *Gefahrstoffe Reinhaltung der Luft* 71.6 (2011), pp. 281–285.

[77] E. Simeone, M. Siedlecki, M. Nacken, S. Heidenreich, and W. de Jong. “High temperature gas filtration with ceramic candles and ashes characterisation during steam-oxygen blown gasification of biomass”. In: *Fuel* 108 (2013), pp. 99–111. DOI: 10.1016/j.fuel.2011.10.030.

[78] M. Stemmler and M. Müller. “Chemical hot gas cleaning concept for the ”CHRISGAS” process”. In: *Biomass & Bioenergy* 35 (2011), S105–S115. DOI: 10.1016/j.biombioe.2011.03.044.

[79] Wang Y. et al. “Carbonyl sulfur removal from blast furnace gas: Recent progress, application status and future development”. In: *Chemosphere* 307 (2022), p. 136090. DOI: 10.1016/j.chemosphere.2022.136090.

[80] W. Torres, S.S. Pansare, and J.G. Goodwin Jr. “Hot Gas Removal of Tars, Ammonia, and Hydrogen Sulfide from Biomass Gasification Gas”. In: *Catalysis Reviews* 49.4 (2007), pp. 407–456. DOI: 10.1080/01614940701375134.

[81] J.M. Sánchez, E. Ruiz, and J. Otero. “Selective Removal of Hydrogen Sulfide from Gaseous Streams Using a Zinc-Based Sorbent”. In: *Industrial & Engineering Chemistry Research* 44.2 (2005), pp. 241–249. DOI: 10.1021/ie0497902.

[82] Jung S.Y., Lee S.J., Lee T.J., Ryu C.K., and Kim J.C. “H2S removal and regeneration properties of Zn-Al-based sorbents promoted with various promoters”. In: *Catalysis Today* 111.3 (2006). ”Advances in Catalysis and Catalytic Materials for Energy and Environmental Protection”, pp. 217–222. DOI: 10.1016/j.cattod.2005.10.029.

[83] Park N.K. et al. “Two-stage desulfurization process for hot gas ultra cleanup in IGCC”. In: *Fuel* 85.2 (2006). Special Issue: The 21st Annual International Pittsburgh Coal Conference, pp. 227–234. DOI: 10.1016/j.fuel.2005.04.033.

[84] O.A. Sofekun and L.K. Doraiswamy. “High-Temperature Oxidation of Zinc Sulfide: Kinetic Modeling under Conditions of Strict Kinetic Control”. In: *Industrial & Engineering Chemistry Research* 35.9 (1996), pp. 3163–3170. DOI: 10.1021/ie960013e.

[85] I. Dincer and C. Zamfirescu. “Chapter 3 - Hydrogen Production by Electrical Energy”. In: *Sustainable Hydrogen Production*. Ed. by I. Dincer and C. Zamfirescu. Elsevier, 2016, pp. 99–161. DOI: 10.1016/B978-0-12-801563-6.00003-0.

[86] L.R. Clausen. “Energy efficient thermochemical conversion of very wet biomass to biofuels by integration of steam drying, steam electrolysis and gasification”. In: *Energy* 125 (2017), pp. 327–336. DOI: 10.1016/j.energy.2017.02.132.

[87] L.R. Clausen, N. Houbak, and B. Elmegaard. “Technoeconomic analysis of a methanol plant based on gasification of biomass and electrolysis of water”. In: *Energy* 35.5 (2010), pp. 2338–2347. DOI: 10.1016/j.energy.2010.02.034.

[88] F.M. Mulder, B.M.H. Weninger, J. Middelkoop, F.G.B. Ooms, and H. Schreuders. “Efficient electricity storage with a battolyser, an integrated Ni–Fe battery and electrolyser”. In: *Energy & Environmental Science* 10 (2017), pp. 756–764. DOI: 10.1039/C6EE02923J.

[89] *Battolyser Systems*. 2023. URL: https://www.battolysersystems.com/ (visited on 02/13/2024).

[90] European Investment Bank. *Netherlands: €40 million European backing for Dutch hydrogen innovator Battolyser Systems*. Oct. 2023. URL: https://www.eib.org/en/press/all/2023-370-eur40-million-european-backing-for-dutch-hydrogen-innovator-battolyser-systems (visited on 02/13/2024).

[91] N.J.M. Kuipers and J. van Medevoort. *SeaHydrogen: Position paper: Integral Nexus Approach for the Production of Hydrogen at Sea*. Tech. rep. Wageningen Food & Biobased Research, 2023. DOI: 10.18174/644081.

[92] A. Weiß et al. “Impact of Intermittent Operation on Lifetime and Performance of a PEM Water Electrolyzer”. In: *Journal of the Electrochemical Society* 166.8 (2019), F487. DOI: 10.1149/2.0421908jes.

[93] E. Kuhnert et al. “Impact of intermittent operation on photovoltaic-PEM electrolyzer systems: A degradation study based on accelerated stress testing”. In: *International Journal of Hydrogen Energy* 55 (2024), pp. 683–695. DOI: 10.1016/j.ijhydene.2023.11.249.

[94] C. Leguijt et al. *Bio-Scope: Toepassingen en beschikbaarheid van duurzame biomassa [Bio-scope: Applications and availability of sustainable biomass]*. Tech. rep. Delft: CE Delft & Royal Haskoning DHV, 2020.

[95] B. Strengers and H. Elzenga. *Availability and applications of sustainable biomass: Report on a search for shared facts and views*. The Hague: PBL, 2020.

[96] D. Corbey and B. van Asselt. *Routekaart Nationale Biogrondstoffen: Naar een groter aanbod en betere benutting [Roadmap National Bioresources: Towards a larger supply and better use]*. The Hague: RVO, 2020. URL: https://www.klimaatakkoord.nl/documenten/publicaties/2020/06/29/routekaart-nationale-biogrondstoffen.

[97] SER. *Biomassa in balans: Een duurzaamheidskader voor hoogwaardige inzet van biogrondstoffen [Balanced Biomass: A sustainability framework for high-value use of bioresources]*. The Hague, 2020.

[98] E.B. Hassan, H. Abou-Yousef, P. Steele, and E. El-Giar. “Characterization of bio-oils from the fast pyrolysis of white oak and sweetgum”. In: *Energy Sources, Part A: Recovery, Utilization, and Environmental Effects* 38.1 (2016), pp. 43–50. DOI: 10.1080/15567036.2011.649338.

[99] C. Blom, R. Delahaye, R. Mosterd, F. Prins, and S. Schenau. *Collecting and assessing data on the provisioning and use of wood biomass for energy purposes*. PR001858 2021 European Green Deal Regulation (EU) No 691/2011. CBS [Statistics Netherlands], 2023.

[100] Rijkswaterstaat Waterinfo. URL: https://waterinfo.rws.nl/#/publiek/zouten (visited on 04/09/2024).

[101] Oxford University Press. *Oxford Reference*. URL: https://www.oxfordreference.com/display/10.1093/oi/authority.20110810104609306# (visited on 03/27/2024).

[102] E.J. Leijenhorst. "Biomass Gasification via Fast Pyrolysis". PhD thesis. Ghent University, 2016.

[103] E. Björkman and B. Strömberg. "Release of Chlorine from Biomass at Pyrolysis and Gasification Conditions". In: *Energy & Fuels* 11.5 (1997), pp. 1026–1032. DOI: 10.1021/ef970031o.

[104] J.M. Johansen, J.G. Jakobsen, F.J. Frandsen, and P. Glarborg. "Release of K, Cl, and S during Pyrolysis and Combustion of High-Chlorine Biomass". In: *Energy & Fuels* 25.11 (2011), pp. 4961–4971. DOI: 10.1021/ef201098n.

[105] M.U. Rahimand, Gao X., M. García-Pérez, Li Y., and Wu H. "Release of Chlorine during Mallee Bark Pyrolysis". In: *Energy & Fuels* 27.1 (2013), pp. 310–317. DOI: 10.1021/ef3018157.

[106] S.B. Saleh et al. "Release of Chlorine and Sulfur during Biomass Torrefaction and Pyrolysis". In: *Energy & Fuels* 28.6 (2014), pp. 3738–3746. DOI: 10.1021/ef4021262.

[107] Du S. et al. "Releasing behavior of chlorine and fluorine during agricultural waste pyrolysis". In: *Energy* 74 (2014), pp. 295–300. DOI: 10.1016/j.energy.2014.01.012.

[108] H. Braidy, S. Valin, and F. Patisson. "Characterization of sulfur and chlorine behavior during pyrolysis of biomass and waste". In: *Sustainable Energy Fuels* 7 (2023), pp. 3067–3076. DOI: 10.1039/D3SE00263B.

[109] R.H. Venderbosch and W. Prins. "Fast pyrolysis technology development". In: *Biofuels, Bioproducts & Biorefining* 4 (2010), pp. 178–208. DOI: 10.1002/bbb.205.

[110] S. Czernik and A.V. Bridgwater. "Overview of Applications of Biomass Fast Pyrolysis Oil". In: *Energy & Fuels* 18.2 (2004), pp. 590–598. DOI: 10.1021/ef034067u.

[111] M.J. Schelhaas et al. *Zevende Nederlandse Bosinventarisatie [Seventh National Forest Inventory of the Netherlands]*. Wettelijke Onderzoekstaken Natuur & Milieu, WOt-rapport 142. Wageningen Environmental Research, 2022. DOI: 10.18174/571720.

[112] *LNG Outlook 2024*. Tech. rep. Shell, 2024. URL: https://www.shell.com/what-we-do/oil-and-natural-gas/liquefied-natural-gas-lng/lng-outlook-2024.html (visited on 01/21/2025).

[113] CBS [Statistics Netherlands]. *Gewichtseenheden energie*. URL: https://www.cbs.nl/nl-nl/onze-diensten/methoden/begrippen/gewichtseenheden-energie (visited on 01/23/2025).

[114] Rijksoverheid. *Maatregelen om tekort aan gas te voorkomen*. URL: https://www.rijksoverheid.nl/onderwerpen/gas/minder-afhankelijk-worden-van-rusland (visited on 01/23/2025).

[115] L. van Putten. "Gasverbruik Nederland opnieuw lager". In: *CBS [Statistics Netherlands]* (2024). URL: https://www.cbs.nl/nl-nl/nieuws/2024/07/gasverbruik-nederland-opnieuw-lager (visited on 01/23/2025).

[116] CBS [Statistics Netherlands]. *Aardgasbalans; aanbod en verbruik*. URL: https://opendata.cbs.nl/#/CBS/nl/dataset/00372/table (visited on 01/23/2025).

[117] Rijksoverheid. *Hoe lang kan ik nog koken en stoken op gas?* URL: https://www.rijksoverheid.nl/onderwerpen/duurzame-energie/vraag-en-antwoord/hoe-lang-kan-ik-nog-koken-op-gas (visited on 01/29/2025).

[118] CBS [Statistics Netherlands]. *Energiebalans; aanbod, omzetting en verbruik*. Nov. 15, 2024. URL: https://opendata.cbs.nl/#/CBS/nl/dataset/83140NED/table?ts=1737462147527 (visited on 01/29/2025).

[119] M. Hjelmeland and J.K. Nøland. "Correlation challenges for North Sea offshore wind power: a Norwegian case study". In: *Scientific Reports* 13 (2023), p. 18670. DOI: 10.1038/s41598-023-45829-2.

[120] Vestas. *V236-15.0 MW™*. 2024. URL: https://www.vestas.com/en/products/offshore/V236-15MW (visited on 04/09/2024).

[121] A. Mangel Raventos. “Towards upscaling the Battolyser - An Integrated Ni-Fe Alkaline Battery and Electrolyser: A combined modeling and experimental study”. PhD thesis. TU Delft, 2023. DOI: 10.4233/uuid:b980646c-b40f-48f1-977e-9ccb4a86bcab.

[122] H. Er-rbib and C. Bouallou. “Modeling and simulation of CO methanation process for renewable electricity storage”. In: *Energy* 75 (2014), pp. 81–88. DOI: 10.1016/j.energy.2014.05.115.

[123] K.T. Abdul-Azeez, P. Suraj, C. Muraleedharan, and P. Arun. “Aspen Plus Simulation of Biomass Gasification: a Comprehensive Model Incorporating Reaction Kinetics, Hydrodynamics and Tar Production”. In: *Process Integration and Optimization for Sustainability* 7 (2023), pp. 255–268. DOI: 10.1007/s41660-022-00291-x.

[124] Kim H., Yang S., S. Narayanan, I. McKay, and E.N. Wang. “Experimental Characterization of Adsorption and Transport Properties for Advanced Thermo-Adsorptive Batteries”. In: *Proceedings of the ASME 2013 International Mechanical Engineering Congress and Exposition, Volume 8C: Heat Transfer and Thermal Engineering*. San Diego, CA, USA, Nov. 2013. DOI: 10.1115/IMECE2013-65490.

[125] S. Sircar and A.L. Myers. “Gas separation by zeolites”. In: *Handbook of Zeolite Science and Technology*. CRC Press, 2003, pp. 1063–1105.

[126] E. Scuiller, P. Dutournié, M. Zbair, and S. Bennici. “New Approach for Measuring the Specific Heat Capacity of Reactive Adsorbents Using Calorimetry”. In: *Journal of Chemical & Engineering Data* 68.8 (2023), pp. 1865–1871. DOI: 10.1021/acs.jced.3c00121.

[127] Wei L., H. Azad, W.G. Haije, H. Grénman, and W. de Jong. “Pure methane from CO_2 hydrogenation using a sorption enhanced process with catalyst/zeolite bifunctional materials”. In: *Applied Catalysis B: Environmental* 297 (2021), p. 120399. DOI: 10.1016/j.apcatb.2021.120399.

[128] R. Mathieu and Ph. Vieillard. “A predictive model for the enthalpies of formation of zeolites”. In: *Microporous and Mesoporous Materials* 132.3 (2010), pp. 335–351. DOI: 10.1016/j.micromeso.2010.03.011.

[129] I. Petrović and A. Navrotsky. “Thermochemistry of Na-faujasites with varying Si/Al ratios”. In: *Microporous Materials* 9.1 (1997), pp. 1–12. DOI: 10.1016/S0927-6513(96)00060-0.

[130] L.A. Pellegrini, G. de Guido, and S. Langé. “Biogas to liquefied biomethane via cryogenic upgrading technologies”. In: *Renewable Energy* 124 (2018). SI: Waste Biomass to Biofuel, pp. 75–83. DOI: 10.1016/j.renene.2017.08.007.

[131] G. Bassioni and H. Klein. “Liquefaction of natural gas and simulated process optimization - A review”. In: *Ain Shams Engineering Journal* 15.2 (2024), p. 102431. DOI: 10.1016/j.asej.2023.102431.

[132] F. Capra, F. Magli, and M. Gatti. “Biomethane liquefaction: A systematic comparative analysis of refrigeration technologies”. In: *Applied Thermal Engineering* 158 (2019), p. 113815. DOI: 10.1016/j.applthermaleng.2019.113815.

[133] Jang D., Cho H., and Kang S. “Numerical modeling and analysis of the effect of pressure on the performance of an alkaline water electrolysis system”. In: *Applied Energy* 287 (2021), p. 116554. DOI: 10.1016/j.apenergy.2021.116554.

[134] M. Sánchez, E. Amores, D. Abad, L. Rodríguez, and C. Clemente-Jul. “Aspen Plus model of an alkaline electrolysis system for hydrogen production”. In: *International Journal of Hydrogen Energy* 45.7 (2020), pp. 3916–3929. DOI: 10.1016/j.ijhydene.2019.12.027.

[135] R. Rivera-Tinoco et al. “Investigation of power-to-methanol processes coupling electrolytic hydrogen production and catalytic CO2 reduction”. In: *International Journal of Hydrogen Energy* 41.8 (2016), pp. 4546–4559. DOI: 10.1016/j.ijhydene.2016.01.059.

[136] Koh J.H., Yoon D.J., and Oh C.H. “Simple Electrolyzer Model Development for High-Temperature Electrolysis System Analysis Using Solid Oxide Electrolysis Cell”. In: *Journal of Nuclear Science and Technology* 47.7 (2010), pp. 599–607. DOI: 10.1080/18811248.2010.9720957.

[137] B. Linnhoff et al. *A User Guide on Process Integration for the Efficient Use of Energy*. First Ed. IChemE, Rugby, UK, 1982.

[138] I.C. Kemp and Lim J.S. *Pinch Analysis for Energy and Carbon Footprint Reduction*. Third Ed. Butterworth-Heinemann (Elsevier), 2020.

[139] V. Dieterich, A. Hanel, S. Bastek, H. Spliethoff, and S. Fendt. “Entrained flow gasification-based biomass-to-X processes: A techno-economic assessment”. In: *Energy Conversion and Management* 301 (2024), p. 118061. DOI: 10.1016/j.enconman.2024.118061.

[140] G. Towler and R. Sinnott. *Chemical Engineering Design. Principles, Practice and Economics of Plant and Process Design*. Third ed. Butterworth-Heinemann (Elsevier), 2022.

[141] R. Turton, R.C. Bailie, W.B. Whiting, J.A. Shaeiwitz, and D. Bhattacharyya. *Analysis, synthesis, and design of chemical processes*. Fourth ed. Pearson, 2012.

[142] C. Maxwell. *Cost Indices*. URL: https://toweringskills.com/financial-analysis/cost-indices/ (visited on 11/28/2024).

[143] J. Andersson, J. Lundgren, and M. Marklund. “Methanol production via pressurized entrained flow biomass gasification - Techno-economic comparison of integrated vs. stand-alone production”. In: *Biomass and Bioenergy* 64 (2014), pp. 256–268. DOI: 10.1016/j.biombioe.2014.03.063.

[144] R.M. Swanson, A. Platon, J.A. Satrio, R.C. Brown, and Hsu D.D. “Techno-Economic Analysis of Biofuels Production Based on Gasification”. In: (Nov. 2010). DOI: 10.2172/994017. URL: https://www.osti.gov/biblio/994017.

[145] A.L. Villanueva Perales, C. Reyes Valle, P. Ollero, and A. Gómez-Barea. “Technoeconomic assessment of ethanol production via thermochemical conversion of biomass by entrained flow gasification”. In: *Energy* 36.7 (2011), pp. 4097–4108. DOI: 10.1016/j.energy.2011.04.037.

[146] J. Witte, A. Kunz, S.M.A. Biollaz, and T.J. Schildhauer. “Direct catalytic methanation of biogas - Part II: Techno-economic process assessment and feasibility reflections”. In: *Energy Conversion and Management* 178 (2018), pp. 26–43. DOI: 10.1016/j.enconman.2018.09.079.

[147] J. Gorre, F. Ruoss, H. Karjunen, J. Schaffert, and T. Tynjälä. “Cost benefits of optimizing hydrogen storage and methanation capacities for Power-to-Gas plants in dynamic operation”. In: *Applied Energy* 257 (2020), p. 113967. DOI: 10.1016/j.apenergy.2019.113967.

[148] G. Iaquaniello, S. Setini, A. Salladini, and M. De Falco. “CO_2 valorization through direct methanation of flue gas and renewable hydrogen: A technical and economic assessment”. In: *International Journal of Hydrogen Energy* 43.36 (2018), pp. 17069–17081. DOI: 10.1016/j.ijhydene.2018.07.099.

[149] H.S. Usman, K. Touati, and M.S. Rahaman. “An economic evaluation of renewable energy-powered membrane distillation for desalination of brackish water”. In: *Renewable Energy* 169 (2021), pp. 1294–1304. DOI: 10.1016/j.renene.2021.01.087.

[150] Wisselkoers.nl. URL: https://www.wisselkoers.nl/dollar-euro (visited on 01/07/2025).

[151] Park S. et al. “Techno-economic analysis of adiabatic four-stage CO_2 methanation process for optimization and evaluation of power-to-gas technology”. In: *International Journal of Hydrogen Energy* 46.41 (2021), pp. 21303–21317. DOI: 10.1016/j.ijhydene.2021.04.015.

[152] O. Schmidt et al. “Future cost and performance of water electrolysis: An expert elicitation study”. In: *International Journal of Hydrogen Energy* 42.52 (2017), pp. 30470–30492. DOI: 10.1016/j.ijhydene.2017.10.045.

[153] BTG. *EMPYRO – Fast Pyrolysis Demonstration Plant*. Sept. 27, 2012. URL: https://www.ieabioenergy.com/wp-content/uploads/2015/02/XII3-vd-Beld-BTG_pyrolysis.pdf (visited on 02/12/2025).

[154] European Biomass Industry Association. “Pyrolysis”. In: (). URL: https://www.eubia.org/cms/wiki-biomass/pyrolysis-and-gasification/pyrolysis/# (visited on 02/12/2025).

[155] Thunder Said Energy. *Cryogenic Air Separation: costs and energy economics?* URL: https://thundersaidenergy.com/downloads/cryogenic-air-separation-the-economics/ (visited on 11/18/2024).

[156] Peak Scientific. *Nitrogen cylinder costs vs nitrogen generator costs*. URL: https://www.peakscientific.com/nitrogen-gas-costs-genius-xe/ (visited on 11/18/2024).

[157] S. Lensink and I. Pisca. *Costs of offshore wind energy 2018*. Tech. rep. The Hague: PBL, 2019.

[158] OG Clean Fuels. URL: https://ogcleanfuels.com/nl/onze-brandstoffen/bio-lng?_gl=1*1xpy3rb*_up*MQ..&gclid=Cj0KCQiAlsy5BhDeARIsABRc6ZuNg2ojoeBL8nFOc3qEdew-RU71Yiu9n0ibKGRCixT3CEIZskKcJSEaAh5HEALw_wcB (visited on 11/18/2024).

[159] ANWB. URL: https://www.anwb.nl/auto/autobelastingen/brandstofprijzen (visited on 12/02/2024).

[160] Energievergelijk.nl. *Gasprijs*. URL: https://www.energievergelijk.nl/energieprijzen/gasprijs (visited on 01/08/2025).

[161] Zoutvoordeel.nl. URL: https://www.zoutvoordeel.nl/nl/marselr-1-3-middelgrof-zeezout-52106-cps-0-1-1000-kg/ (visited on 11/18/2024).

[162] Zoutcentrum. URL: https://www.zoutcentrum.nl/strooizout-kopen/25kg-zak-strooizout (visited on 02/12/2025).

[163] Vitens. URL: https://www.vitens.nl/Tarieven-en-voorwaarden (visited on 11/18/2024).

[164] C. Leguijt et al. *Afnameverplichting Groene Waterstof*. Tech. rep. Report nr. 23.230209.150. CE Delft & TNO, 2023.

[165] Energik. “Stoom centraal op Pumps & Valves Antwerpen”. In: (June 3, 2024). URL: https://www.energik.be/nieuws-detail.php?blog_id=45&page_platform_id=0&page_categroy_id=0&page_year= (visited on 11/18/2024).

[166] Indea. *Rekentools stoom en energie*. URL: https://www.indea.be/rekentool-stoom-energie/ (visited on 11/18/2024).

[167] P. van den Brand. “Elektrische stoom wint terrein”. In: (2023). URL: https://fluidsprocessing.nl/artikel/elektrische-stoom-wint-terrein/ (visited on 11/18/2024).

[168] D. van Steeg. *Wat kost een ton stoom?* URL: https://nl.linkedin.com/pulse/wat-kost-een-ton-stoom-dick-van-steeg-r55ie# (visited on 11/18/2024).

A

Calculations & Definitions

A.1. Calculation of Oxygen needed

The amount of oxygen needed for the complete combustion of the bio-oil feed stream is given in Equation 3.2, repeated here:

$$\dot{m}_{O_2}^{comb} = \frac{M_{CO_2} - M_C}{M_C}\,\dot{m}_C^{bio} + \frac{M_{H_2O} - M_{H_2}}{M_{H_2}}\,\dot{m}_H^{bio} + \frac{M_{SO_2} - M_S}{M_S}\,\dot{m}_S^{bio} - \dot{m}_O^{bio} \tag{A.1}$$

The right-hand side of this oxygen balance has four terms, from left to right: **(1)** full combustion of the carbon content to CO_2, **(2)** full combustion of the hydrogen content to water, **(3)** combustion of the sulfur content to SO_2, and **(4)** the oxygen already present in the biomass. All factors $(M_{oxide} - M_i)/M_i$ calculate the amount of oxygen needed to form the oxide as a mass fraction of i. The moisture, ash, and nitrogen contents are considered not to have any calorific combustion value.

Each of the biomass component streams $\dot{m}_i^{bio}$ is calculated as its weight fraction of the total bio-oil intake $\dot{m}_{bio}^{gasf}$ of 6.0 kg s^{-1}, discounted by the moisture and ash contents:

$$\dot{m}_i^{bio} = \frac{\text{Mass-\% (daf) of } i}{100}\left(1 - \frac{\text{Moisture content (ar)}}{100}\right)\left(1 - \frac{\text{Ash content (dry)}}{100}\right)\dot{m}_{bio}^{gasf} \tag{A.2}$$

Filling in the data as given in Table 3.2 and the molecular and atomic weights M_i of all species and elements involved, gives $\dot{m}_{O_2}^{comb} = 7.575$ kg s^{-1}, rounding to 7.6 kg s^{-1}. Based on the model pyrolysis oil in Table 4.2, $\dot{m}_{O_2}^{comb} = 7.554$ kg s^{-1} is obtained.

A.2. Calculation of Hydrogen needed

The amount of hydrogen needed to achieve complete methanation in accordance with the Sabatier reactions (Equations 2.1 and 2.2) is calculated from the hydrogen mass balance as given in Equation 3.4, restated here:

$$\dot{m}_{H_2}^{el} = \frac{M_{CH_4} - M_C}{M_C}\,\dot{m}_C^{bio} + \frac{M_{H_2O} - M_O}{M_O}\left(\dot{m}_O^{bio} + \dot{m}_{O_2}^{gasf}\right) - \dot{m}_H^{bio} \tag{A.3}$$

which has three terms: **(1)** hydrogen needed to convert all carbon in the process to methane, **(2)** hydrogen needed to convert all oxygen to water, and **(3)** the hydrogen content of the pyrolysis oil. Parallel to the derivation above, the factors $(M_{hydrate} - M_i)/M_i$ calculate the hydrogen needed as a mass fraction of i, and the bio-oil component streams $\dot{m}_i^{bio}$ are computed by Equation A.2.

That leaves a single term yet to be examined: $\dot{m}_{O_2}^{gasf}$, the oxygen fed to the gasifier. The value of this variable is yet to be determined; however, it is possible to use Equation 3.1 to rephrase it in terms of process variable λ and $\dot{m}_{O_2}^{comb}$, which was calculated in Appendix Section A.1 above,

$$\dot{m}_{O_2}^{gasf} = \lambda\,\dot{m}_{O_2}^{comb} \tag{A.4}$$

Combining all these results in $\dot{m}_{H_2}^{el} = 0.782 + 0.9545\lambda$ kg s^{-1} using Table 3.2, or, when Table 4.2 is used, $\dot{m}_{H_2}^{el} = 0.779 + 0.9519\lambda$ kg s^{-1}.

A.3. Definitions of Key Performance Indicators

The selected Key Performance Indicators given in Section 3.7 are defined as follows. Where applicable, the conversion factor between per-year and per-hour figures is yearly operational hours.

Because electricity is one of the primary energy sources for this process, the Energy Yield (EY) is defined accordingly:

$$\text{EY} = \frac{\dot{E}_{LNG}}{\dot{E}_{fuel}} = \frac{\dot{m}_{LNG}\,\text{LHV}_{LNG}}{\dot{m}_{bio}\,\text{LHV}_{bio} \;+\; P_{El}} \tag{A.5}$$

Carbon Conversion Efficiency (CCE) is defined as

$$\text{CCE}\;(i) = \frac{\dot{n}_{CH4}\text{ in product stream } i}{\dot{n}_{C}\text{ in bio-oil feed stream}} \tag{A.6}$$

where i can refer to the 'gross' production of methane, or to the 'net' production of LNG specifically.

The CAPEX and OPEX relative to the biomass input are calculated as follows. Note that these are never explicitly called 'relative', but only bear the units M€/MW and €/MWh respectively.

$$\text{Relative CAPEX} \;=\; \frac{\text{CAPEX}}{\dot{m}_{bio}\,\text{LHV}_{bio}} \tag{A.7}$$

$$\text{Relative OPEX} \;=\; \frac{\text{OPEX}}{\dot{m}_{bio}\,\text{LHV}_{bio}} \tag{A.8}$$

The Levelized Costs of Manufacturing (LCOM) with respect to the product's mass, volume, and heating value are defined as follows:

$$\text{LCOM (m)} \;=\; \frac{\text{AC}}{\dot{m}_{LNG}} \tag{A.9}$$

$$\text{LCOM (V)} \;=\; \frac{\text{AC}}{\dot{m}_{LNG}/\rho_{LNG}} \tag{A.10}$$

$$\text{LCOM (E)} \;=\; \frac{\text{AC}}{\dot{m}_{LNG}\,\text{LHV}_{LNG}} \tag{A.11}$$

where the Average Cost (AC) is given by

$$\text{AC} \;=\; \text{OPEX} + \frac{\text{CAPEX}}{\text{Project Life Time}} \tag{A.12}$$

as shown in Figure 6.3 in Section 6.4.

B

Datasheets

B.1. EPA Data

Table B.1 contains the overview of heat and work streams in the Full SEM scenario.

Table B.1: Overview of energy inputs and outputs in the Full SEM flowsheet.

Block ID	Heat (MW_{th})	Work (MW_{el})	Temperature (°C)
PO-HEX	0.65818	0	15 – 64
DECOMP	71.105	0	1202.4
GASIFIER	–71.015	0	1202.4
HEX-1	–2.2121	0	923.4 – 800
NI-MESH	0.00010	0	800
HEX-2	–5.1614	0	800 – 500
ZNO-DESF	–0.00462	0	500
GCLPUMP	0	9.85E-6	80 – 81.5
ZNOREGST	0.00357	0	15 – 550
ZNOREGEN	0.00483	0	550
HEX-3	–7.6990	0	500 – 175
METH	–94.316	0	250
HEX-4	3.1078	0	15 – 500
REGEN	53.429	0	300
QRECV	–17.304	0	227.5 – 15
DECOMPR	0	-1.1765	250 – 123.4
METHEX	–0.79131	0	123.4 – 28
CCOMP1	0	4.3234	–11.3 – 90.5
C-1	–3.2965	0	90.5 – 20
CCOMP2	0	3.2463	20 – 102.8
C-2	–7.2978	0	102.8 – 37
Total continuous	**–80.879**	**6.393**	
SEAHYDRG	39.720	0	80
ELYSIS	-47.193	235.96	60
HYDCOMP	0	1.4104	60 – 133
HYDCOOL	-2.2509	0	133 – 15
OXCOMP	0	0.69144	60 – 130.6
OXCOOL	-1.2044	0	130.6 – 15
Total DESEL	**-10.928**	**238.064**	

Table B.2 contains the overview of heat and work streams in the Two-Stage Methanation scenario.

Table B.2: Overview of energy inputs and outputs in the Two-Stage flowsheet.

Block ID	Heat (MW_{th})	Work (MW_{el})	Temperature (°C)
DECOMP	70.962	0	1211.4
GASIFIER	–70.962	0	1211.4
HEX-1	–2.3338	0	923.4 – 800
NI-MESH	0	0	799.9
HEX-2	–5.1516	0	799.8 – 500
ZNO-DESF	0	0	500.3
GCLPUMP	0	9.69E-6	60 – 61.4
ZNOREGEN	0.00475	0	557.6
SULFHEX	–0.00110	0	557.6 – 140
HEX-3	–7.7036	0	500 – 175
CONVMETH	–37.983	0	420
SRP-COOL	–9.0534	0	223.0 – 175
SRP-METH	–13.640	0	250
REGEN	12.5	0	317.9
QRECV	–1.5381	0	318.0 – 140
DECOMPR	0	-1.1759	250 – 123.4
CCOMP1	0	4.3223	–11.3 – 90.5
C-1	–3.2927	0	90.5 – 20
CCOMP2	0	3.2463	20 – 102.8
C-2	–7.2978	0	102.8 – 37
Total continuous	**-75.490**	**6.3927**	
SEAHYDRG	27.611	0	60
ELYSIS	-47.193	235.96	60
HYDCOMP	0	1.4104	60 – 133
HYDCOOL	-2.2509	0	133 – 15
OXCOMP	0	0.69144	60 – 130.6
OXCOOL	-1.2044	0	130.6 – 15
Total DESEL	**-23.037**	**238.06**	

B.2. Final Design of the Mass Flow Sheet

Figure B.1 contains the final flow sheet design, sections of which have been shown in detail throughout this thesis: see figures 4.9 (gasifier), 4.2 (gas cleaning), 5.1 (methanator), 4.6 (desalination and electrlolysis), and 4.5 (cryogenic liquefaction), as well as their accompanying paragraphs for more details.
Table B.3 below contains the mass flow rates, temperatures and pressures of every mass stream in Figure B.1, as calculated by *Aspen Plus*.

Table B.3: Overview of all process mass flows, temperatures and pressures in the finalized version of the mass flow sheet, as shown in Figure B.1.

Stream Name	Mass Flow (kg/h)	Temperature (°C)	Pressure (bar)	Main component
PYROIL	21600	15	1	Pyroil
HOT-PO	21600	74.26	1	Pyroil
DECPO	21600	1250	50	Pyroil
HOTOX	14760	1206.4	50	O_2
IN-GASIF	36360	1211.4	50	Syngas
ASH	52.747	1211.4	50	Ash
PRODGAS	36307.25	1211.4	50	Syngas
SYNG-CL	36307.25	930.48	50	Syngas
SYN-800	36307.25	800	50	Syngas
SYN-STHX	36307.25	799.995	50	Syngas
SYN-HEXS	36307.25	799.772	50	Syngas
SYN-NIZN	36307.25	799.504	50	Syngas
SYN-500	36307.25	500	50	Syngas
ZNOFRESH	2.0347	15	50	ZnO
ZNO-IN	18.313	505.91	50	ZnO
IN-DESUL	36325.57	500.28	50	Syngas
ZNO-ZNS	21.836	500.28	50	ZnS
REGENSTM	4	600	50	H_2O
IN-REGEN	25.836	557.60	50	ZnS
H2S	7.5234	557.60	50	H_2S
H2S-COLD	7.5234	140	50	H_2S
ZNORECYC	18.313	557.60	50	ZnO
ZNOSPENT	2.0347	557.60	50	ZnO
ZNOREC	16.278	557.60	50	ZnO
SYNSFREE	36303.73	500.28	50	Syngas
WETPHASE	4237.975	175	50	H_2O
SYN-DRY	32065.75	175	50	Syngas
HOTH2	4675	322.02	50	H_2
TO-METH	36740.75	258.86	50	Syngas
PARTMETH	36740.75	420	50	H_2O, CH_4
PRESS-N2	21010.2	15	50	N_2
HEXHEX	36740.75	327.02	50	H_2O, CH_4
H2	4675	15	50	H_2
TO-COOL	36740.75	223.00	50	H_2O, CH_4
KNOCKOUT	19276.98	175	50	H_2O
TO-SORPM	17463.88	175	50	CH_4, H_2O

Table B.3 *(cont.)*

Stream Name	Mass Flow (kg/h)	Temperature (°C)	Pressure (bar)	Main component
ZEOFRESH	10000	15	50	Ni/13X
ZEO-DRY	249999.6	305.84	50	Ni/13X
IN-METH	267463.5	250	50	Ni/13X
ZEO-WET	255007.5	250	50	Ni/13X
H2OPURGE	21010.2	414.99	50	N_2
IN-DESRB	276017.7	317.96	50	Ni/13X
H2O-OUT	26018.11	317.96	50	N_2
OFFGAS	24266.91	175	50	N_2
OFFWATER	1751.20	175	50	H_2O
ZEO-REC	249999.6	317.96	50	Ni/13X
ZEOPURGE	9999.98	317.96	50	Ni/13X
RECYCLE	239999.6	317.96	50	Ni/13X
METHANE	12455.94	250	50	CH_4
SEAWATER	457852.98	15	1	H_2O
SALT	6421.62	60	31.013	NaCl
DESALD	451431.4	60	31.013	H_2O
TO-DRINK	409127.4	60	31.013	H_2O
TO-GASCL	4	60	31.013	H_2O
REGWATER	4	61.422	50	H_2O
TO-ELEC	42300	60	31.013	H_2O
TO-ELC	195966.5	60.016	30	Zn, H_2O
ON-CAT	195966.5	60	30	ZnO, H_2
CAT-HYD	4733.68	60	30	H_2
HYDR-P	4733.68	133.05	50	H_2
HYDR-PC	4733.68	15	50	H_2
TO-HSTOR	58.676	15	50	H_2
DIAFRAGM	191232.8	60	30	ZnO
ON-AN	191232.8	60	30	Zn, O_2
ELCRECYC	153666.5	60	30	Zn
AN-OX	37566.3	60	30	O_2
OX-P	37566.3	130.61	50	O_2
OX-PC	37566.3	15	50	O_2
FREE-OX	22806.3	15	50	O_2
OXYGEN	14760	15	50	O_2
2	12455.9	123.3	6.3	CH_4
3	12455.9	28	6.3	CH_4
4	12455.9	–150	6.3	CH_4
5	12455.9	–152.5	6.3	CH_4
6	85500	–11.48	1.03	Refrigerant
7	85500	90.411	6.9	Refrigerant
8	85500	20	6.9	Refrigerant
9	85500	102.82	28.6	Refrigerant
10	85500	37	28.6	Refrigerant
11	85500	28.1	28.6	Refrigerant

Table B.3 *(cont.)*

Stream Name	Mass Flow (kg/h)	Temperature (°C)	Pressure (bar)	Main component
12	59682.48	28.1	28.6	Refrigerant
13	59682.48	–40.17	1.03	Refrigerant
14	59682.48	10.7	1.03	Refrigerant
15	25817.52	28.1	28.6	Refrigerant
16	25817.52	–136.7	28.6	Refrigerant
17	25817.52	–154.13	1.03	Refrigerant
18	25817.52	–153.95	1.03	Refrigerant
19	25817.52	–79.70	1.03	Refrigerant
20	25817.52	–55.49	1.03	Refrigerant
LNG	12455.94	–154.74	2	CH_4
CL-GAS	556.04	–153.3	2	CH_4
LNG-OUT	11899.9	–153.3	2	CH_4

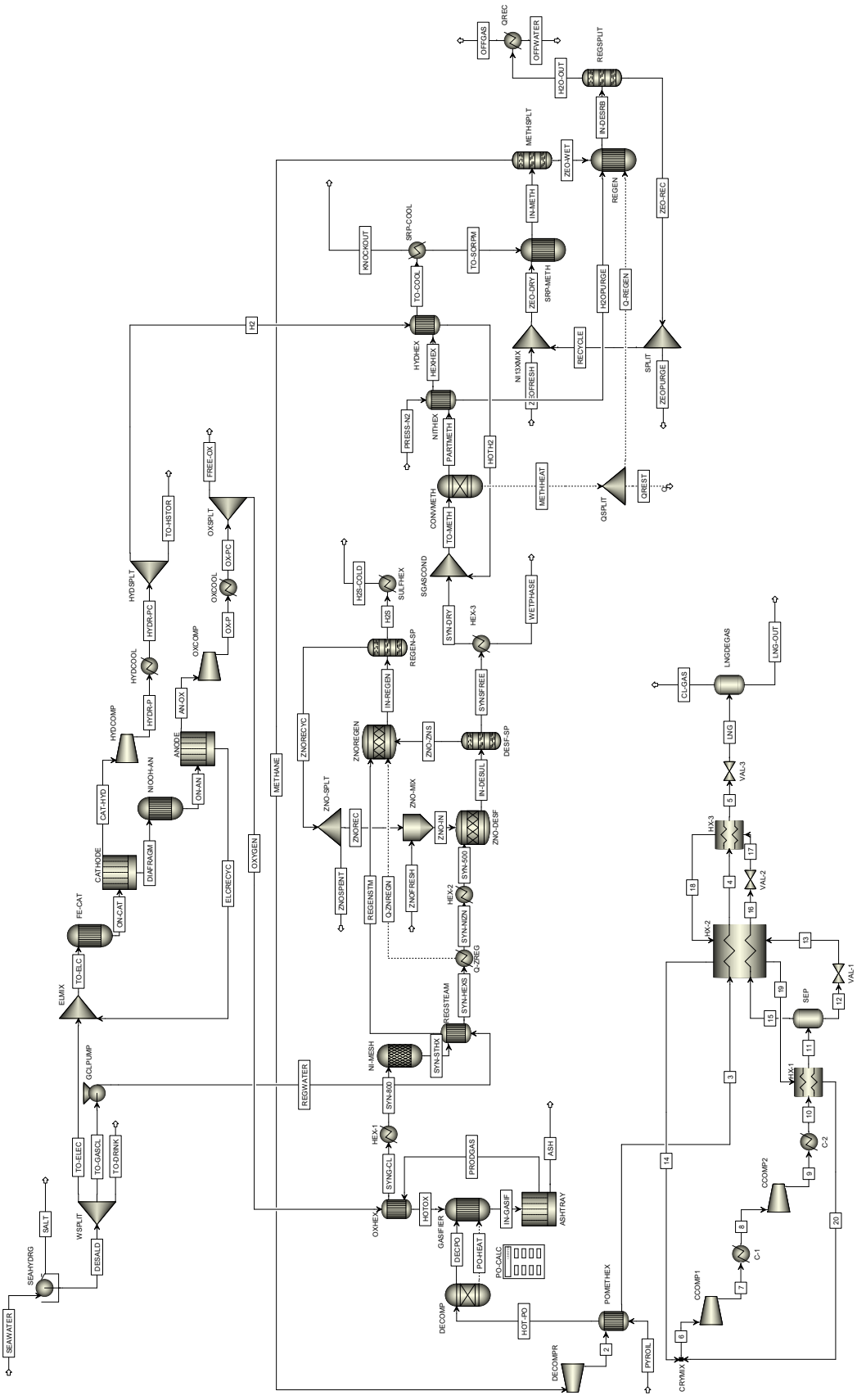

Figure B.1: Complete Process Flowsheet. Desalination and electrolysis at the top, gasification, gas cleaning and methanation in the middle, and cryogenic liquefaction at the bottom.